Nonlinear Oscillations in Continuous Crystallization Processes

Dissertation

zur Erlangung des akademischen Grades

Doktoringenieur
(Dr.-Ing.)

von M.Tech. Prasanna Kumar Pathath

geb. am 15. Mai 1975 in Visakhapatnam, Indien

genehmigt durch die Fakultät für Elektrotechnik und Informationstechnik
der Otto-von-Guericke-Universität Magdeburg

Gutachter: Prof. Dr.-Ing. Achim Kienle
Prof. Dr.-Ing. Andreas Seidel-Morgenstern

Promotionskolloquium am 10. Oktober 2006

Forschungsberichte aus dem Max-Planck-Institut
für Dynamik komplexer technischer Systeme

Band 16

Prasanna Kumar Pathath

Nonlinear Oscillations in Continuous Crystallization Processes

Acknowledgment

This thesis originated while I was working at the Max-Planck-Institut für Dynamik komplexer technischer Systeme (MPI), Magdeburg, Germany. Completing a Ph.D. is truly a marathon event, and I would not have been able to complete this journey without the aid and support of countless people over the past seven years. First of all I would like to thank Prof. Dr.-Ing. Ernst Dieter Gilles for giving me opportunity to work in this institute. I would like to thank Prof. Dr.-Ing. Achim Kienle for being a great advisor. He has given me room to think on my own and his ideas have tremendous impact on this thesis. Moreover, on the personal front I learnt a lot from him and I hope that in the near future I will be able to follow his foot steps.

I would like to extend my thanks to Dr. Heike Lorenz, Mr. Jan Portzmann and Ms. Anett Perlberg for helping me to do some experiments at the MPI. A special thanks to Dr.-Ing. Michael Mangold. He was patient enough to check my computer code and also in explaining some critical things in detail. I am grateful to share my office along with Dr.rer.nat. Klaus Peter Zeyer. The informal discussions that I had with him about German culture, Nonlinear dynamics etc. was helpful. I am also thankful to my former colleagues Dr.-Ing. Roland Waschler and Dr.-Ing. Malte Kaspereit for going through the draft version of my Ph.D. thesis and giving their valuable inputs. More on a personal note I would like to thank my friends Mr. Surasani Vikranth Kumar and Mr. Milind Joshi for making my stay at Magdeburg pleasant.

Finally I would like to thank my parents for their constant support and patience during my Ph.D. study. I feel that I am very fortunate to have wife like Dr. Sindhu. She was patient enough to wait for me when sometimes I return home at late night. Words are not adequate enough to thank her rather than hugging her to show my thanks as well my love to her.

October 11, 2006   Prasanna Kumar Pathath

To my wife Sindhu and to my parents

Contents

Notation

Please note that some of the units ● depend on the chosen coordinates.

A_D	surface area of dispersed phase	m^2
A_j	proportionality constant	-
a_{st}	number of stirrer blades	-
B	nucleation rate	$1/(m^3 s)$
B_{nuc}	total nucleation rate	$1/(m^3 s)$
B_{prim}	primary nucleation rate	$1/(m^3 s)$
B_S	surface based nucleation rate	$1/(m^3 s)$
b	nucleation rate exponent	-
b_{blade}	width of the stirrer blade	m
b_{edge}	width of the stirrer edge	m
c	concentration of solute	mol/m^3
c_{in}	concentration of solute going in	mol/m^3
c_{sat}	saturation concentration of solute	mol/m^3
$c_{sat,real}$	real saturation concentration of solute	mol/m^3
c_S	molar density of the solid phase	mol/m^3
C_{het}	heterogeneous nucleation factor	-
d	diameter	m
D_{AB}	diffusion coefficient	m^2/s
$\bar{e}$	external coordinate	●
E	efficiency factor	-
f	volume based number density function	$1/(m^3 m)$
$\dot{f}$	volume based number density flux	$1/(m^3 m\ s)$
F	number density function	$1/m$
$\dot{F}$	number density function flux	$1/(m\ s)$
G	growth rate	m/s
G_L	size dependent growth rate	m/s
g	growth rate exponent	-
H	Heavyside function	-
H_V	vickers hardness	-
h	step size	●

h_f	fines classification function	-
h_{fd}	non-ideal fines classification function	-
h_p	product classification function	-
I	intensity of diffraction pattern	lumens
$\bar{i}$	internal coordinate	•
k_b	nucleation rate constant	•
k_g	growth rate constant	•
k_v	volume shape factor	-
k_B	Boltzmann constant	J/K
k_d	mass transfer coefficient	m/s
k_{fd}	large crystal dissolution factor	-
k_v	volume shape factor	-
k_r	integration reaction coefficient	m^4/(mol s)
K_r	crack efficiency	-
L	crystal length	m
L_{crit}	critical nucleation length	m
L_f	fines removal cut size	m
L_{fd}	large crystal dissolution cut size	m
L_p	product classification cut size	m
L_0	length of crystal with zero growth rate	m
L_{50}	mass median crystal length	m
$\bar{L}$	mean crystal length	m
m_t	suspension density	kg/m^3
M	molar mass	kg/kmol
N	number of grid points	-
N_A	Avogadro number	1/mol
N_{frag}	number of fragments	-
N_{pump}	pump discharge coefficient	-
n	number of moles	mol
$\dot{n}$	molar flux	mol/s
n_{LS}	mass that is transfered from liquid to solid phase	-
p	number of particles	-
p	parameter	•
Q	flow rate of the streams	m^3/s
q	feed flow rate	m^3/s

q_f	fines removal rate	m^3/s
q_{prod}	flow rate from crystallizer to product classifier	m^3/s
R	ideal gas constant	J/(mol K)
R_1	fines removal recycle ratio	-
R_2	product removal recycle ratio	-
r	radial position of the stirrer	-
r	upwind ratio	-
S_{rat}	supersaturation	-
t	time	s
T	temperature	K
T	period	s
V	volume	m^3
$\dot{V}$	volumetric flux	m^3/s
v	velocity	m/s
w	weight fraction of solute	kg/kg
x	state variable	•
$x_{L,A}$	mole fraction of the solute	-
y	state variable	•

Greek letters

ρ	density	kg/m^3
ϵ	void fraction	-
μ	eigen value	-
β	pitch angle	°
β_{attr}	attrition rate	1/s
σ	source and sink	•
$\prod$	population phase space	•
Δ	difference	•
λ	wave length of light	n m
λ	limiter function	-
∇	Nabla operator	•
τ	residence time	s
α	diffraction angle	°
Γ	fracture resistance	J/m^2

Γ_S	surface related energy increase	J m/mol
γ_{LS}	surface tension	J/m^2
ω_{st}	rotational frequency of the stirrer	1/s
η_L	dynamic viscosity of the liquid phase	N s/m^2
μ_{shear}	shear modulus	N/m^2

Super and Subscripts

∞	maximum
$+$	source
$-$	sink
$\pm$	source and sink
0	initial
A	component A
$attr$	attrition
ax	axial
B	component B
$blade$	blade
$class$	classified
$diss$	dissolution
dt	draft tube
$edge$	edge
exp	experimental
f	fines
$feed$	feed
$frag$	fragments
gr	growth
H	hopf point
in	incoming
j	class j
k	k^{th} stream
k	k^{th} element
L	liquid phase
m	molecule
max	maximum

min	minimum
nuc	nucleation
out	outgoing
P	particle
p	classified product
p	predicted point
$prod$	product
$pump$	pump
$phen$	phenomena
S	solid phase
sat	saturation
st	stirrer
v	volume

Abbreviations

CLD	chord length distribution
CSD	crystal size distribution
CCD	charge couple device
CMSMPR	continuous mixed suspension mixed product removal
DSP	digital processing unit
DTB	draft tube baffled
FBRM	focused beam reflectance method
IPDE	integero-partial differential equation
MDD	mass density distribution
MOL	method of lines
ODE	ordinary differential equation
PBE	population balance equation
PDE	partial differential equation
DAE	differential algebraic equation

Kurzfassung

Kristallisation wird oft eher als Kunst, denn als Wissenschaft angesehen – vermutlich da sie eine der am schwierigsten zu verstehenden Grundoperationen darstellt. Die Kristallisation dient der Gewinnung von Feststoffen aus flüssigen Schmelzen oder Lösungen und wird in der chemischen Industrie als eines der effizientesten Trennverfahren bei der Produktion organischer und anorganischer Stoffe genutzt. Großtechnisch wird sie dabei als kontinuierliches Verfahren durchgeführt, im kleinen Maßstab wird sie im Batchbetrieb zur Produktion von hochreinen Substanzen angewandt. Trotz ihrer industriellen Bedeutung bereitet die Kristallisation nach wie vor eine Reihe von Problemen. Motivation für die vorliegende Arbeit sind solche Probleme, wie sie im praktischen Betrieb kontinuierlicher Kristallisatoren auftreten.

Die Kristallisation aus Lösungen ist durch das Entstehen eines mehr oder minder weiten Spektrums von Kristallen unterschiedlicher Größe gekennzeichnet. Die Partikelgrößenverteilung (*crystal size distribution*, CSD) ist daher ein wesentliches Charakteristikum eines jeden Kristallisationsprozesses und wird durch mehrere simultan stattfindende kinetische Prozesse beeinflusst. Die wichtigsten sind hierbei Keimbildung, anschließendes Kristallwachstum und Kristallbruch. Die Geschwindigkeitsansätze für diese Vorgänge sind meist nichtlinear. Diese Nichtlinearitäten können komplexes Prozessverhalten auslösen, wie z.B. Dauerschwingungen, welche wiederum schlechte Produktqualität, geringere Ausbeute und Reinheit, sowie weitere Probleme hinsichtlich der Weiterverarbeitung des Produktes zur Folge haben.

Aus vorangegangenen Studien sind zwei unterschiedliche Erklärungen für dieses Schwingungsverhalten bekannt: Schwingungen höherer und niedriger kinetischer Ordnung. Erstere werden durch nichtlineare Keimbildungsraten bei gleichzeitig hohen Keimbildungsexponenten verursacht. Schwingungen niedriger Ordnung treten auch bei niedrigen Keimbildungsexponenten auf, falls der Kristallisator mit klassierendem Produktabzug und Feinkornauflösung betrieben wird. Die Feinkornauflösung dient hierbei der Erzeugung größerer Kristalle und engerer CSD's, während der klassierende Produktabzug eingesetzt wird, um ein Produkt mit gewünschter Kristallgröße zu erlangen. Zielstellung dieser Arbeit ist es, mittels numerischer Bifurkations- und Stabilitätsanalyse Parameterbereiche für Betriebsbedingungen und physikalische Eigenschaften zu bestimmen, in welchen Instabilitäten auftreten.

Das für die Stabilitätsanalyse notwendige mathematische Modell eines speziellen Kristallisators (*draft tube baffle*, DTB) wird in Kapitel 2 hergeleitet. Das Modell berück-

sichtigt sowohl die disperse, als auch die kontinuierliche Phase. Um die Entwicklung der CSD in der dispersen Phase zu beschreiben, wird die Populationsbilanz nach Hulburt & Katz verwendet, während die kontinuierliche Phase durch eine Mengenbilanz modelliert wird. Drei unterschiedliche Modelle werden für die Stabilitätsanalysen genutzt: ein Modell mit einfacher Kinetik, idealer Feinkornauflösung und klassierendem Produktabzug (Modell 1), ein Modell mit komplexer Kinetik (inklusive Kristallbruch durch Abrieb) und idealer Feinkornauflösung (Modell 2), sowie ein Modell mit einfacher Kinetik, nichtidealer Feinkornauflösung und klassierendem Produktabzug (Modell 3).

Ein Überblick zur Kinetik von Kristallisationsprozessen wird ebenfalls in Kapitel 2 gegeben. Die notwendigen Beziehungen zur Berechnung der Keimbildungs- und Wachstumsraten, sowie des Partikelanzahlflusses durch Abrieb der Kristalle am Rührer werden angegeben und in das Populationsbilanzmodell integriert.

Für die Untersuchungen in dieser Arbeit werden zwei experimentelle Stoffsysteme betrachtet – Kaliumchlorid/Wasser und Ammoniumsulfat/Wasser. Beide Systeme wurden in der Vergangenheit intensiv untersucht und können als Standardsysteme in der Kristallisation angesehen werden. Da allerdings einige kinetische Parameter für das System Kaliumchlorid/Wasser nicht der Literatur entnommen werden konnten, wurden zu ihrer Bestimmung experimentelle Untersuchungen an einem kontinuierlichen 20l DTB-Kristallisator vorgenommen. Die entsprechenden Ergebnisse werden in Kapitel 3 zusammengefasst. Diese werden darüber hinaus zur Modellvalidierung genutzt.

In Kapitel 4 werden die Ergebnisse einer numerischen Bifurkations- und Stabilitätsanalyse von Kristallisationsprozessen mit Feinkornauflösung und klassierendem Produktabzug dargestellt. Im Vergleich zu früheren Untersuchungen wurde spezielles Augenmerk auf den Einfluss der Feinkornauflösung und des klassierenden Produktabzugs gelegt. Beide vorgenannten Stoffsysteme werden anhand der drei verschiedenen Modelle untersucht. Es wird gezeigt, daß die Stabilität stark von den Betriebsbedingungen und den physikalischen Parametern des jeweiligen Stoffsystems abhängt. Im Fall des Ammoniumsulfat-Systems zeigt sich überraschenderweise, daß detaillierte Angaben zur Kinetik keine wesentliche Rolle für die Vorhersage der Instabilitätsregion der Betriebsparameter spielen. Im Gegensatz hierzu wurden für das Kaliumchrolid-System starke Abweichungen zwischen den Modellen 1 und 2 gefunden. Eine detaillierte Analyse lässt den Schluss zu, daß die Parameter für Modell 1, welche der Literatur entnommen wurden, nicht geeignet sind, um die in dieser Arbeit betrachtete Situation zu beschreiben. Darüber hinaus wird gezeigt, daß eine nicht-ideale Feinkornauflösung (Modell 3) einen starken Einfluß auf Lage und Größe der Instabilitätsregionen und damit auf die einstellbaren Betriebsbedingungen hat.

Abstract

Crystallization is often viewed as an art not as a science, perhaps because it is one of the most difficult unit operations to understand. It is a technology used to isolate solids from liquid phase melts or solution. In chemical industry it is one of the most efficient separation processes for production of organic and inorganic chemicals. In bulk scale it is conducted in the form of continuous process and in small scale it is conducted in the form of batch process for production of high purity chemicals. Despite its importance, it still poses some problems. The work covered in this thesis is motivated from practical operational problems existing in industrial continuous crystallizers.

Crystallization from solution is characterized by the CSD (crystal size distribution), i.e. the generation of a wide spectrum of differently sized crystals. During crystallization processes, the CSD is mainly determined by a number of simultaneously occurring kinetic processes within the crystallizer. The main kinetic processes are nucleation of crystals, the subsequent growth of crystals as well as breakage of crystals. The rate equations of these kinetic processes are usually nonlinear. This nonlinearity can lead to complex dynamic behavior like self sustained oscillations. This will lead to poor product quality, yield loss, loss of purity as well as problems for further downstream processing of the product.

Analysis by previous researchers reveals two different explanations for this oscillating behavior, i.e high order cycling and low order cycling [72, 73]. High order cycling is induced due to the non-linearity of the nucleation rate at high nucleation exponents. Low order cycling occurs at low nucleation exponents when the crystallizer is operated with classified product removal and fines dissolution. Fines dissolution is employed to achieve coarser crystalline product and narrow CSD. In order to produce crystals of controlled size with a specific crystal length from the crystallizer, a product classifier is used. The goal of this thesis is to predict regions in the parameter space of the operating conditions and the physical properties where the instability occurs using numerical bifurcation and stability analysis.

For doing the stability analysis a model is necessary to describe the crystallization processes. A model is derived for a DTB (draft tube baffle) continuous crystallizer in Chapter 2 based on first principles. Crystallization process comprise a dispersed phase and a continuous phase. A PBE (population balance equation) introduced by Hulburt & Katz [25] is derived for describing the evolution of the CSD in the dispersed phase. A mass balance

equation is derived to describe the dynamics of the solute concentration in the continuous phase. In particular, three models will be used in this work to study the instability of the crystallization process. (i) A model with simple kinetics (model 1) and ideal fines classification and classified product removal, (ii) a model with complex kinetics involving breakage of crystals due to attrition and ideal fines classification and classified product removal (model 2), and (iii) a model with simple kinetics and non-ideal fines classification and classified product removal (model 3).

An overview of the kinetics of crystallization processes is given in Chapter 2. The expressions for the calculation of nucleation rate, growth rate and particular number flux due to attrition of crystals with the stirrer are given. These kinetics expressions are incorporated into the population balance model to describe the crystallization process.

For studying instabilities in the crystallization process, two well known chemical systems, i.e. KCl - $H_2 0$ (Potassium Chloride - Water) and $(NH_4)_2SO_4$ - $H_2 0$ (Ammonium Sulfate - Water) are considered. These systems have been studied intensively in the past and can be viewed as standard systems for crystallization processes. However, some of the kinetic parameters of the detailed kinetics are not available for the KCl - $H_2 0$ system in the literature. For this, experiments are conducted in a 20 litre DTB continuous crystallizer and experimental results are presented in Chapter 3. These experimental results are not only used for estimation of parameters but also for model validation.

In Chapter 4, results of a numerical bifurcation and stability analysis of continuous crystallization processes are presented. It is shown that crystallizer stability critically depends on operating conditions and the physical parameters of the system considered. Compared to previous studies, special emphasis was on the influence of fines dissolution and classified product removal. The stability of ammonium sulfate and potassium chloride crystallization with fines dissolution and classified product removal are studied by means of the three different models mentioned above. For the $(NH_4)_2SO_4$ - $H_2 0$ system it is shown that detailed kinetics is surprisingly not that important for the prediction of the instability region in the space of the adjustable operating parameters. In contrast to this, large deviations between model 1 and model 2 were found for the KCl - $H_2 0$ system. From a detailed analysis it is conjectured that the parameters of the simple model 1, which were taken from the literature, are not adequate to describe the situation considered in this work. Moreover, it is shown that non-ideal fines classification (model 3) has a large impact on the size and location of the instability regions in the space of the adjustable operating parameters.

List of Figures

Chapter 1

Introduction

Industrial crystallization operations [79] are still something of an art and their performance often depends to a considerable degree on the skill of the operator. The complex behavior of crystallization processes leads to significant control problems. The work covered in this thesis is motivated from operational problems existing in industrial crystallizers which have severe impact on product quality. Results of the stability analysis for different operational modes of continuous crystallization processes are presented.

1.1   Background

Crystallization is a well known and commonly used process in the chemical industries for separation and purification. It takes advantage of the solubility characteristics of certain materials in a particular solvent to produce crystalline particles of very high purity. The importance of continuous crystallization processes is evident from the vast amount of its application for the production of bulk agrochemicals like potassium chloride, ammonium sulfate, polymer intermediates like para-xylene [12] (a raw material for polyester) and dye stuffs etc. In comparison, batch crystallization processes are conducted in small scale for the production of high purity fine chemicals or pharmaceuticals such as aspartame (a sweetener), L-serine (an amino acid) and L-ascorbine (vitamin C).

Advantages of crystallization processes are high product purity, low temperature environment and relatively low capital and operating costs. Moreover, due to its moderate process and operating conditions it is attractive for a wide range of products, and in particular for temperature liable substances.

Crystallization is a technology used to isolate solid products from liquid phase melts and solutions. Crystallization from solution is a two step process [61]. The first step is the phase separation or birth of new crystals, where a solute is transfered from a continuous liquid phase to a dispersed solid phase. The second step is the growth of these crystals to larger sizes. These two processes are known as nucleation and crystal growth. More details pertaining to these phenomena are discussed in Chapter 2. When mass transfer is dominant in the process then it is referred to as suspension or solution crystallization. When heat transfer is dominant in the process then it is referred to as melt crystallization [61]. Melt crystallization is used when large single crystals are of prime interest. Focus of this work is on the continuous mixed suspension crystallizers where the product stream consists of slurry of crystals and solution.
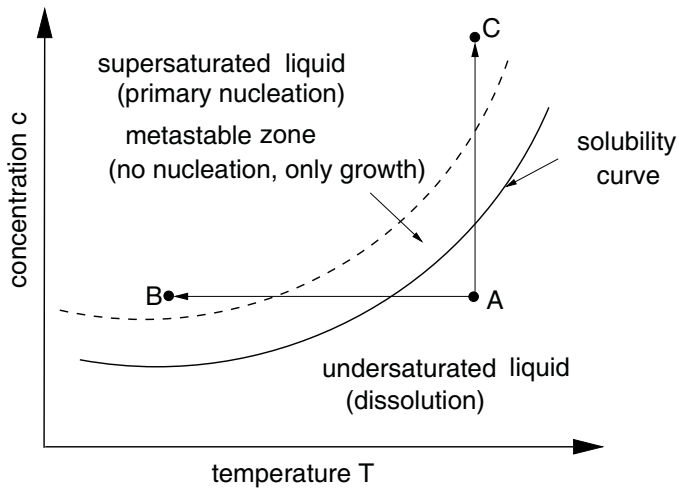
Figure 1.1: Solubility diagram.

The kinetic driving force [51] for the crystallization is the difference of the chemical potential between the continuous liquid phase and the dispersed solid phase. According to Mersmann [51], this driving force can in turn be transformed into supersaturation. Supersaturation of a liquid phase or mother liquor determines the rate at which the dissolved component can be crystallized. There are four main ways of creating supersaturation, i.e. cooling the solution, evaporation of the solvent, chemical reaction and changing the

solvent composition depending on the chemical system [56, 65, 61]. Supersaturation can be expressed either as a difference in concentration of solute in the liquid phase

$$\Delta c = c - c_{sat}(T) \quad , \tag{1.1}$$

or as relative supersaturation

$$S_{rat} = \frac{c}{c_{sat}(T)} \quad , \tag{1.2}$$

or

$$\sigma = \frac{\Delta c}{c_{sat}(T)} = S_{rat} - 1 \quad . \tag{1.3}$$

How to attain the supersaturation can be easily understood by referring to Fig. 1.1, which is the solubility diagram of concentration c versus temperature T. From Fig.1.1, the solubility line divides the supersaturated liquid and the undersaturated liquid. There are two ways of attaining supersaturation. They are i) if we start at point A and cool the solution to point B, then the solution becomes supersaturated. This is called cooling crystallization. ii) if we start at point A and increase the concentration to point C by evaporating the solvent, the solution is also supersaturated. This is called evaporative crystallization.

Supersaturated solutions exhibit a metastable zone in which nucleation is usually not spontaneous. The area between the dashed line and the solubility line depicted in Fig. 1.1, is called metastable zone. The dashed line represents the *metastable limit*. Beyond the metastable limit spontaneous nucleation occurs. Crystal growth is active mainly within the metastable zone. Knowledge about the width of the metastable zone is important in crystallization because it aids in understanding the nucleation behavior of each system. The measurement of effective metastable limits and a tabulation of the results for several inorganic species is found in Nyvlt et al. [66].

Crystallization from solution is characterized by the generation of a wide spectrum of differently sized crystals [20]. The quality of the product as well as down stream processing depends on the crystal size distribution (CSD). The CSD determines the washability, storage and transport behavior of the product as well as the separability from the solvent. Many products must be dissolved for subsequent use and a broad size range leads to variation in time necessary for dissolution of product crystals. Shape can be also important in applications such as pharmaceuticals where different crystal faces have different dissolution rates, leading to variation in bio availability for crystals of different shapes. Above all, often the customer specifies certain CSD characteristics such as average crystal size and spread around this size.

Typical crystallizer configurations are shown in Fig. 1.2. The externally forced - circulation crystallizer with suspension chamber (FCSC) [60] and the simple forced - circulation unit (FC) are typified by external recirculation. These are general purpose crystallizers that can be utilized for either evaporative or indirect cooling modes of operation. The draft tube baffle (DTB) crystallizer which is used frequently, is supplied with an internal baffle to facilitate fines removal. It has high internal recirculation and is suitable for adiabatic cooling, indirect cooling, and medium evaporative loads. Although there are many possible crystallizer geometries, the three types shown below have flow patterns which resemble the majority of commercial crystallizers. Focus in this study is on draft tube crystallizers.

Figure 1.2: Typical continuous crystallizer configurations according to Moyers & Randolph [60].

1.2 Motivation and Problem Formulation

Occurrence of slow CSD oscillations as shown in Fig. 1.3 is a major problem in many continuous industrial crystallization processes. Unstable CSD behavior is not a result of external disturbances but caused by interactions between nucleation rate, growth rate of crystals and process configurations. This results in the presence of an excessive number density of fine crystals in the product [12], which causes problems with solid-liquid separation in the downstream process. In addition to the above problems, cyclic behavior of CSD in crystallization processes can cause significant production losses and lowers the yield. With increasing material and energy costs, increasing environmental and product quality requirements evolving over the last 20 years, and the growing competition between large companies, industrial and academic researchers are paying increased attention to the operational problems arising in industrial crystallization processes.
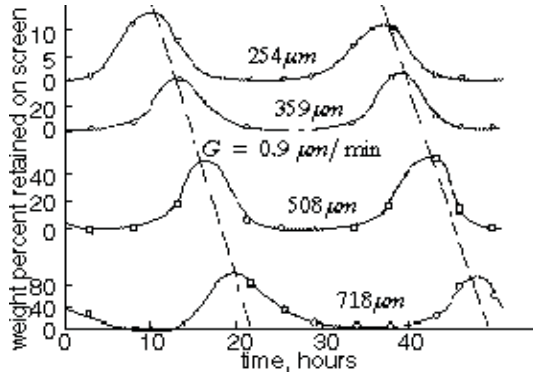
Figure 1.3: CSD limit cycles in an industrial KCl crystallizers according to Randolph [72].

Oscillations in particle size distribution and slurry density were reported for industrial KCl crystallizers (see e.g. Randolph & Larson [73] and references [74, 75, 79, 44, 28] therein). According to Yu & Douglas [92], the periodic behavior of the process is due to the competition between the nucleation and the growth rates. In other words, a small increase in concentration results in the formation of shower of nuclei. These nuclei then grow, supplying such a large area for the growth that the solute concentration decreases

significantly. The decrease in concentration causes the nucleation rate to decrease until the removal of crystals (and therefore area for growth) by the convective flow. Addition of more solute in the feed stream alters the conditions to a point another shower of nuclei occurs. Thus the system generates oscillations even when the feed conditions are maintained constant. These oscillations pose a grave practical problem leading to off-specification products. The subsequent analysis revealed two different explanations for this oscillatory behavior of crystallization processes, i.e. high order and low order cycling [72, 73].

High order cycling is induced by the nonlinearity of the nucleation rate and it occurs for high nucleation exponents. This type of instability can be observed for rather simple continuous mixed suspension mixed product removal (CMSMPR) crystallizers with or without fines dissolution. Without classified product removal and with a simple point fines trap, an analytical investigation of high order cycling is possible. Here, a point fines trap is defined as a fines-removal system in which the excess particles are segregated and removed at a size vanishingly small compared to the resultant product crystal size [73]. Analytical investigation can be made by reducing the population balance model, consisting of a partial differential equation for the dispersed phase and an integro-differential equation for the continuous phase, to a few ordinary differential equations by using the method of moments [26, 73, 42, 43].

In contrast to this, low order cycling occurs for low nucleation exponents, when classified product removal and fines dissolution are taken into account. This corresponds to the typical situation in practice. An analytical approach is not possible anymore because the moment equations do not close and one has to deal with the full blown population balance model. Therefore, only a numerical approach is possible. Initial work in this direction using dynamic simulation was done by Randolph & Larson [73], Kind & Nieken [34] and Kind & Lieb [31] among others. In this thesis, this work is extended by means of a numerical bifurcation analysis. This method allows the prediction of operating and parameter regions where instability occurs and therefore it gives further insight into the process behavior. This knowledge can be used for better design and control of continuous crystallizers in various ways.

1.3   Dissertation Overview

The first section of Chapter 2 describes the formulation of the general population balance equation (PBE) for a dispersed solid phase and its subsequent simplification for CSD modeling in a DTB continuous crystallization system. The corresponding mass balance for a continuous liquid phase is also presented. The three models that will be used in this work along with underlying assumptions are discussed in Section 2.3. The models are (i) a model with simple kinetics and ideal fines classification (model 1), (ii) a model with complex kinetics involving breakage of crystals due to attrition and ideal fines classification (model 2) and (iii) a model with simple kinetics and non-ideal fines classification (model 3).

In Section 2.4, an overview of the kinetics of crystallization processes is given. Rates of crystal growth, attrition and nucleation are given, which were used by a number of researchers to model crystal kinetics. These models are used together with the population balance to simulate the crystallizer CSD behavior.

Chapter 3 describes the experimental results. Experiments are conducted to determine the growth rate parameters of potassium chloride crystals used for model 2. These parameters are not available in the literature to the best of our knowledge. The equipment used for experimentation and the manner of operation of the equipment are described. The in-line and off-line instruments used in the analysis of the CSD and the fluid phase are also described along with the problems encountered in sampling of the suspension.

Chapter 4 deals with the analysis of the nonlinear behavior of crystallization processes. Two chemical systems are considered. One is KCl - H_20 (Potassium Chloride - Water) and the other is $(NH_4)_2SO_4$ - H_20 (Ammonium Sulfate - Water). These systems have been studied intensively in the past and can be viewed as standard systems for crystallization processes. For the nonlinear analysis, first, model 1 including fines dissolution and classified product removal is considered. Using methods from numerical bifurcation analysis, the stability of the system is investigated. An instability region is predicted for model 1 in the space of adjustable operating parameters like fines dissolution rate, classified product removal rate, fines cut size etc. For a finite number of operating points dynamic simulations are carried out with model 2. The results predicted by model 1 are compared those predicted by model 2 in terms of stability, evolution of mass density distribution (MDD) and the mass median crystal size L_{50}. The mass median crystal size L_{50} is defined as the characteristic length up to which half of the overall crystal mass is

reached. Finally the influence of non-ideal fines classification as proposed by Mitrović [57] is studied and conclusions are drawn.

Chapter 2

Modeling

A process model is a set of equations (including the necessary input data to solve the equations) that allows us to predict the behavior of a chemical process system [5]. A model is derived based on the fundamental knowledge of chemical-physical relationships. This includes the application of conservation of mass, energy and transport phenomena as well as thermodynamic relationships. For a given set of input data, the model can predict an output response. In addition to this, the model can be used for solving many problems. For example, it can be used for the design of the equipment, operation of the equipment, synthesis, control of the equipment etc. For particulate processes, besides the conservation laws of the fluid phase, an additional balance [84] is required to describe the changes in the particulate population during the processes. This balance is generally referred to as the population balance equation (PBE).

A crystallization process is composed of two phases. One is a dispersed solid phase consisting of crystals and the other is a continuous liquid phase containing a binary mixture of solute and solvent. The population balance equation is used to describe the evolution of the CSD in the dispersed phase and the mass balance equation is used to model the continuous phase. In Section 2.1 of this chapter, a general form of the PBE is derived and simplified to a DTB continuous crystallizer model. Based upon this model, different models are deduced with the corresponding assumptions in Section 2.3. The crystallization process is driven by the kinetic processes of crystal nucleation and growth. Different models of these kinetics and their mechanisms are given in Section 2.4.

2.1 Population Balance Model

Before going into the details of modeling crystallization processes, it is noteworthy to discuss the significance of population balance modeling and its evolution. In the early 1960's, population balance models were used to model biological populations. They were first introduced for engineering problems by Hulburt & Katz [25] and later formulated in detail in a book by Randolph & Larson [73]. Most recently, Ramkrishna [71] has presented a treatment of population balances covering various generic issues. Currently, population balances are most frequently used to model processes like granulation, crystallization, combustion, polymerization etc. Population balance modeling is not only confined to particulate processes, but it is also used to model dispersion processes. For example, it may be used to calculate the gas holdup of gas bubbles in a stirred tank reactor containing liquid, where gas is bubbled through the sparge at the bottom of the reactor. Another example is the determination of the drop size distribution for a liquid-liquid extraction in a stirred tank diameter [1].

The population balance of any system is used to account for the size, the number of particles and PSD (particle size distribution). The particles of interest are represented by internal coordinates $\bar{i}$ and external coordinates $\bar{e}$. The internal coordinates of particles [70] refer to those properties attached to each individual particle and that quantitatively measure its state, independent of its position. For example crystal size, particle age, volume of the particle etc. An external coordinate refers to the representation of the particle in the physical space. Both the internal and external coordinates are referred to as the particle state space which is defined as

$$\prod = [\bar{i}, \bar{e}] \quad . \tag{2.1}$$

The properties of the PSD can be characterized utilizing population density functions. The number density function is a function of the internal coordinates $\bar{i}$, the external coordinates $\bar{e}$ and time t. It is represented as

$$f = f(\bar{i}, \bar{e}, t) \quad , \tag{2.2}$$

and has dimensions

$$f(\bar{i}, \bar{e}, t) = \frac{1}{m^{3\bar{i}}} \quad . \tag{2.3}$$

The particle states vary with time. This could be an addition viz., birth or destruction of particles at a point in the internal particle state space. An addition or destruction of

particles can be termed as source and sink respectively. For example, in the crystalliza-
tion process, an addition of crystals can be due to nucleation or crystals formed due to
breakage. Destruction of particles can be due to attrition or breakage of crystals in the
crystallization process.

A particle changes its position in the particle state space. A gradual change in particle
state along the particle state space can be described as a convective process. This can be
termed as particle velocity along the external and internal coordinates. For example, in
the crystallization process, the growth rate of crystals is considered as a change in particle
state with time along the internal coordinate length L. The particle velocity along the
internal coordinate is represented as $v_{\bar{i}}$ and along the external coordinate as $v_{\bar{e}}$. The total
velocity in the whole particle state space is given by

$$v = v_{\bar{i}} + v_{\bar{e}} \quad . \tag{2.4}$$

Consider a region $V(\bar{i}, \bar{e})$ in the particle state space. The total population of particles in
that region is given by

$$\int_V f(\bar{i}, \bar{e}, t) dV \quad . \tag{2.5}$$

Let $\sigma(\bar{i}, \bar{e}, c, t)$ represent the net rate of particles per unit volume of the particle state space
due to birth and death rate of particles. The number conservation can be written as

$$\frac{d}{dt} \int_V f(\bar{i}, \bar{e}, t) dV = \int_V \sigma(\bar{i}, \bar{e}, t) dV \quad . \tag{2.6}$$

Using the Reynolds transport theorem [71], equation (2.6) can be rewritten as

$$\int_V [\frac{\partial f(\bar{i}, \bar{e}, t)}{\partial t} + \triangledown \cdot (v f(\bar{i}, \bar{e}, t)) - \sigma(\bar{i}, \bar{e}, t)] dV = 0 \quad . \tag{2.7}$$

Since the defined region V is arbitrary, the integrand must vanish from everywhere in the
particle space. So, the equation (2.7) leads to

$$\frac{\partial f(\bar{i}, \bar{e}, t)}{\partial t} + \triangledown \cdot (v f(\bar{i}, \bar{e}, t)) - \sigma(\bar{i}, \bar{e}, t) = 0 \quad . \tag{2.8}$$

The above equation is the general population balance equation and the first term in the
equation represents the change in the number density function in the particle state space
with respect to time. The second term represents the convective flux in the direction of
external and internal coordinates. Finally, the third term in the equation represents the
sink and the source terms in the particle state space.

For an ideally-well mixed system of constant volume V in which the particles have no spatial dependence, equation (2.8) is integrated over volume V to give the following

$$\frac{\partial(V f(\bar{i}, t))}{\partial t} + V \triangledown \cdot (v_i f(\bar{i}, t)) - V \sigma(\bar{i}, t) + \sum_k Q_k f_k(\bar{i}, t) = 0 \quad . \qquad (2.9)$$

The index k in equation (2.9) represents input and output streams to the volume V and Q_k represents the volume flow rate of these streams. Q_k is taken as positive for flow out of the volume V and as negative for flow into the volume V. The above equation is diversely used in many applications pertaining to dispersed phase processes in continuous reactors. However, it has to be supplemented with an initial condition and a boundary condition. A draft tube baffle (DTB) continuous crystallizer will be considered in this work and therefore the above equation will serve as a basis for deriving a model for the dispersed phase.

2.2   Model Development

A crystallizer in continuous mode of operation with fines dissolution and classified product removal is depicted in Fig. 2.1. It shows a DTB continuous crystallizer equipped with a marine type impeller which is placed at the bottom section inside the draft tube. Inside the crystallizer, the flow is directed by the impeller revolutions from bottom of the draft tube to the top section of the crystallizer. The draft tube is provided with interior baffles. The crystal slurry is circulated downwards along the outside of the draft tube. In the outer shell of the crystallizer, there is a settling zone. In the settling zone an upward flow causes fines classification. It is achieved by liquid removal from this zone, which is set to carry with it particles of the desired size, against gravitational setting, while allowing particles of larger sizes to remain in the crystallization zone [13]. The disposition of the overflow leaving the DTB depends upon the operating conditions. The fine crystals are removed and are dissolved by creating under saturation conditions through an external heat exchanger. The solution due to fines dissolution is recycled to the bottom section of the crystallizer along the feed input, thereby increasing the supersaturation. Changes in the fines removal rate influence the cut size of the fines classification system [36, 6], as a direct consequence of an increased vertical velocity in the annular zone. The flow rate also determines the residence time in the heat exchanger and the temperature rise of the fines flow. The degree of dissolution is determined by a combination of these effects. This
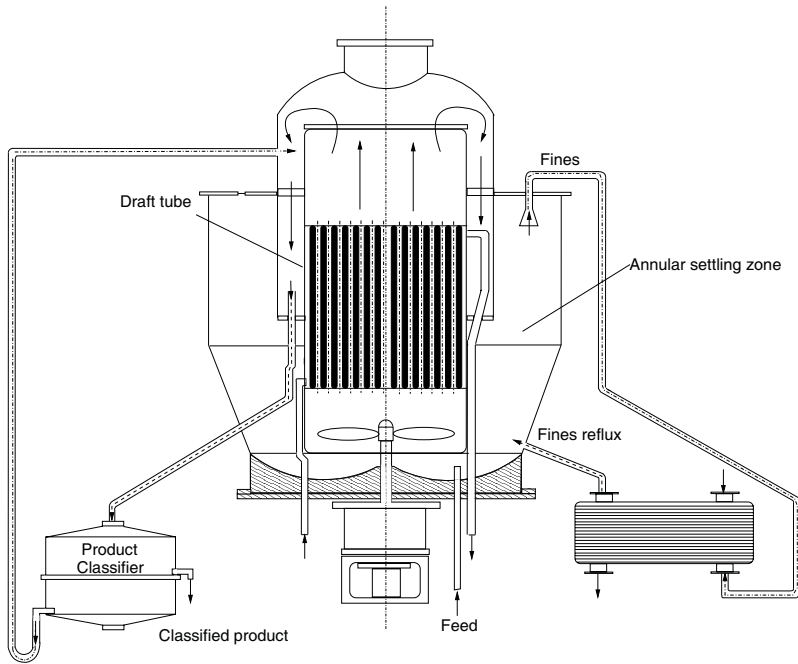
Figure 2.1: Continuous Crystallizer with fines dissolution and classified product removal according to Gerla [20].

type of operation mode is done to achieve a coarser crystalline product (large crystals) and narrow CSD.

In order to produce crystals of controlled size with a specific crystal length from the crystallizer, a product classifier is used. This classifier can be a vibrating screen, a classifier, a wet screen, a fluidized bed or a separating centrifuge. The reflux stream from the classifier consists of small crystals and is returned to the crystallizer. Usually, in industry, the product stream consisting of larger crystals is removed as final product or further fed to another separation unit.

The crystallization process comprises two phases. One is the solid phase consisting of crystals which are dispersed in the continuous liquid phase. The solid phase is called dispersed phase. Modeling of the dispersed phase is done using population balance equa-

tion. The modeling of the continuous phase is based on common mass balance equations. In the following sections, an elaborate discussion is given on the modeling along with model assumptions and the empirical relations used for the kinetics of the crystallization process.

2.2.1 Modeling the Dispersed Phase

In the dispersed phase the crystals are assumed to maintain their shape during crystal growth and attrition. They are characterized by a linear dimension L, which represents the crystal length. In order to use the population balance modeling approach, as discussed in the earlier section, a number density function has to be introduced, which represents the number of particles per particle properties of interest. In this work, the particle properties are restricted to only crystal length. The distribution of particles with respect to crystal length L is given by the number density function

$$f = f(L, t) \quad . \tag{2.10}$$

continuous liquid phase (L)　　　　　dispersed solid phase (S)

$\dot{n}_{nuc}$　　$\dot{f}_{nuc}$

$\dot{n}_{gr}$　　$\frac{\partial (Gf)}{\partial L}$

$\dot{f}_{attr}^{+} - \dot{f}_{attr}^{-}$

$\dot{n}_{diss}$　　$\dot{f}_{diss}$

Phase Boundary
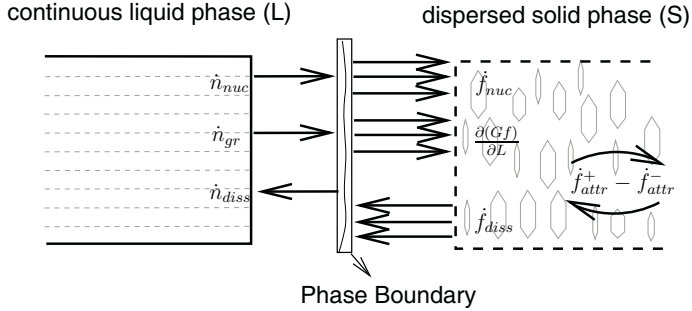
Figure 2.2: Interaction between the continuous liquid phase and the dispersed liquid phase in a crystallizer [57].

The continuous phase comprises of solute (dissolved crystals) and a solvent. During the crystallization, it is mainly the solute and some amount of the solvent will be transferred from the continuous liquid phase to the dispersed solid phase. Interaction between these two phases is depicted in Fig. 2.2. In this figure, there exists a phase boundary between the continuous phase and the dispersed phase [57]. Mass transfer takes place between the

continuous liquid phase and the dispersed solid phase across the phase boundary due to nucleation, growth and dissolution. $\dot{n}_{nuc}$, $\dot{n}_{gr}$ and $\dot{n}_{diss}$ represent the total molar fluxes due to nucleation, growth and dissolution processes. However, in reality there is no clear cut phase boundary between these two phases. Each individual crystal contributes to the overall phase boundary and hence, to the overall fluxes due to the transfer processes. The transfer processes are indicated by arrows in Fig. 2.2. The intra particle phenomena that occur inside the dispersed phase are given by fluxes $\dot{f}_{nuc}$, $\dot{f}_{attr}^{\mp}$, $\dot{f}_{diss}$ and $\partial(Gf)\partial L$. It should be noted that these phenomena don't affect the surroundings of the dispersed phase. In these phenomena, agglomeration of crystals is neglected and hence it is not depicted in the figure. More details pertaining to these phenomena are explained in detail in the subsequent sections.

The continuous crystallization process is modeled under the following assumptions:

- ideal mixing so that no spatial variations have to be considered

- isothermal operation

- constant overall volume (liquid+solid)

$$V = V_S + V_L = \text{const.} \tag{2.11}$$

- the withdrawn slurry is representative for the content of the crystallizer

- the volume change due to crystallization is negligible

- ideal classification of fines and product removal

- there is no time delay for fines removal and product classification.

In equation (2.11) V is the overall volume of the crystallizer and V_S and V_L represent the volume of the solid and the liquid phase.

The population balance equation for the dispersed solid phase is then obtained as :

$$\frac{\partial f(L,t)}{\partial t} = -\frac{\partial(Gf(L,t))}{\partial L} + \frac{q}{V}f_{feed} + \dot{f}_{nuc} + \dot{f}_{attr}^{\mp} - \dot{f}_{diss} - \frac{q_f}{V}f_f + \frac{q_{class,in}}{V}f_{class,in} - \frac{q_{prod}}{V}f \tag{2.12}$$

In the above equation, $f(L,t)$ represents the volume based number density function. V represents the volume of the crystallizer and G the growth rate of crystals which is dependent on concentration and length. An inflow of crystals due to feed and the classifier is
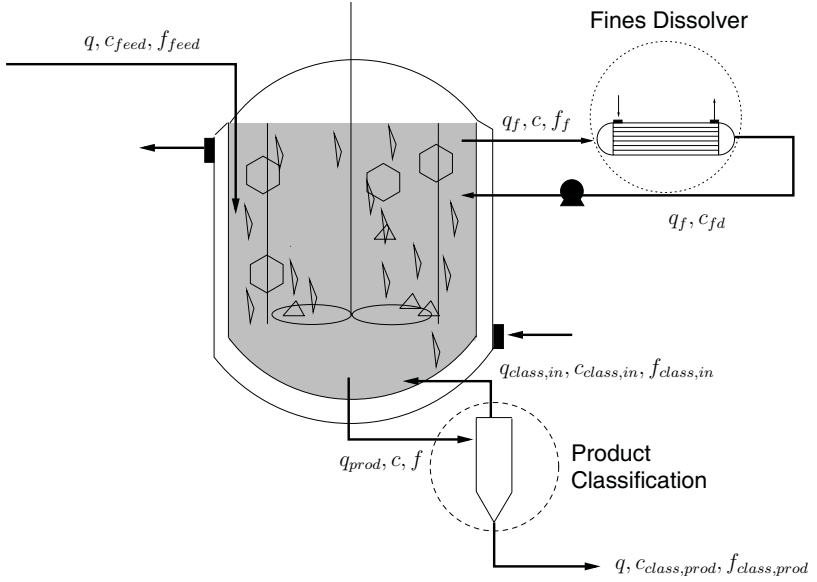
Figure 2.3: Structural decomposition of a DTB continuous crystallizer with interchanging streams.

given by $f_{feed}, f_{class,in}$. The outflows of crystals due to fines dissolution and to the product classifier is given by f, f_f. Particle phenomena, i.e. nucleation, attrition and dissolution are given by $\dot{f}_{nuc}$, $\dot{f}_{attr}^{\mp}$ and $\dot{f}_{diss}$. The initial and boundary conditions for this population balance equation are given by

$$f(L, t = 0) = f_0(L) \qquad \text{and} \qquad f(L = 0, t) = f_b(t) \quad . \qquad (2.13)$$

The volume of each individual crystal V_P is given by

$$V_P = k_v L^3 \quad , \qquad (2.14)$$

where k_v is an appropriate geometric shape factor and L is the characteristic length of the crystal. Assuming that the crystals maintain their shape during growth or breakage, the total volume of the solid phase is calculated by integrating from the lower boundary of crystals with minimum length to the upper boundary of crystals with maximum length. It

16

is given by

$$V_S(t) = k_v \int_{L_0}^{L_\infty} L^3 f(L,t) dL \quad . \tag{2.15}$$

The fines dissolution rate $f_f \frac{q_f}{V}$ in equation (2.12) is calculated in the following way. Assuming the classification of fines is done ideally, the number density function is given by

$$f_f = (1 - h(L - L_f))f \quad , \tag{2.16}$$

where $h(L - L_f)$ is the Heavyside unit function and L_f is the fines cut size. The Heavyside function is defined as

$$h(L - L_f) = \begin{cases} 0 & \text{if } L \leq L_f \\ 1 & \text{if } Ł > L_f \end{cases} \quad .$$

If $R_1 = q_f/q$ is the reflux ratio of volumetric streams between fines flow rate and product flow rate, then

$$f_f \frac{q_f}{V} = R_1 \frac{q}{V} (1 - h(L - L_f))f \quad . \tag{2.17}$$

For the definition of the flow rates q_f, q_q and q see Fig. 2.3. It should be noted that these definitions are slightly different from those introduced by Randolph & Larson [73] for their so called R, z crystallizer model. Replacing $R_1(1 - h(L - L_f))$ by classification function $h_f(L)$, the equation (2.17) reduces to

$$f_f \frac{q_f}{V} = \frac{q}{V} h_f(L) f \quad . \tag{2.18}$$

Similarly, the number density function $f_{class,in}$ in equation (2.12) for classified product is given the following way. Assuming the classification of product is done ideally, the number density function is given by

$$f_{class,in} = (1 - h(L - L_p))f \quad , \tag{2.19}$$

where L_P is the classified product cut size.

If $R_2 = q_{class,in}/q$ is the reflux ratio of volumetric streams between the flow rate of crystals that are returned to the crystallizer after product classification and product flow rate, then

$$f_{class,in} \frac{q_{class,in}}{V} = R_2 \frac{q}{V} (1 - h(L - L_p))f \quad . \tag{2.20}$$

The term $\frac{q_{prod}}{V} f$ in equation (2.12) can be simplified in terms of reflux ratio R_2 and is given by

$$\frac{q_{prod}}{V} f = (R_2 + 1) \frac{q}{V} f \quad . \tag{2.21}$$
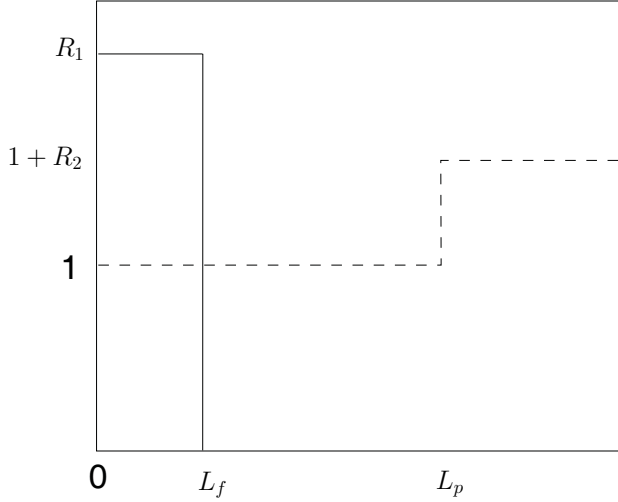
Figure 2.4: Classification functions $h_f(L)$ (solid line) and $h_p(L)$.
(dashed line)

Substituting equations (2.16), (2.17), (2.20) and (2.21) in equation (2.12), the equation reduces to

$$\frac{\partial f(L,t)}{\partial t} = -\frac{\partial(Gf(L,t))}{\partial L} + \frac{q}{V}f_{feed} + \dot{f}_{nuc} + \dot{f}_{attr}^{\mp} - \dot{f}_{diss} - \frac{q}{V}(h_f(L) + h_p(L))f \quad . \quad (2.22)$$

The classification function specifying product classification is given by

$$h_p(L) = 1 + R_2 h(L - L_p) \quad . \quad (2.23)$$

The plot of $h_f(L)$, $h_p(L)$ is shown in Fig. 2.4.

This concludes the mathematical modeling of the dispersed phase for the DTB continuous crystallizer. Based upon this model, different models are deduced in the following sections with corresponding assumptions. The mass balance of the continuous phase with respect to the different models is also discussed.

2.3 Models

2.3.1 Model 1

Model1 is based on the following assumptions:

- ideal mixing

- isothermal operation

- constant overall volume (liquid+solid)

- nucleation of crystals of negligible size

- size independent growth rate

- no particle breakage, attrition, agglomeration and dissolution

- the feed stream contains no particles i.e. $f_{feed}(L) = 0$

Modeling the Dispersed Phase for Model 1

Using the above assumptions, equation (2.22) reduces to

$$\frac{\partial f(L,t)}{\partial t} = -\frac{\partial(Gf(L,t))}{\partial L} - \frac{q}{V}(h_f(L) + h_p(L))f \quad , \tag{2.24}$$

with the following initial and boundary conditions

$$f(L, t = 0) = f_0(L) \qquad \text{and} \qquad f(0,t) = \frac{B(c,t)}{G(c,t)} \quad , \tag{2.25}$$

with the particle size distribution $f(L,t)$ and $h_f(L)$ and $h_p(L)$ are the Heavyside functions.

The dependence of the nucleation and growth rates on the solute concentration *c(t)* are expressed by the following empirical power laws:

$$G(c,t) = k_g(c(t) - c_{sat}(T))^g \quad , \tag{2.26}$$

$$B(c,t) = k_b(c(t) - c_{sat}(T))^b \quad , \tag{2.27}$$

where k_g and k_b are the coefficients for the growth and nucleation rate expressions. g and b are the exponents for the growth and nucleation rates, and $c_{sat}(T)$ is the saturation concentration of the solute at the given temperature T.

Modeling the Continuous Phase for Model 1

The mass balance of the solute in the liquid phase is given by the ordinary differential equation

$$\frac{d(V \epsilon c M_A)}{dt} = qc_{feed}M_A - qc\epsilon M_A - 3Vk_v\rho_S G \int_0^\infty fL^2 dL$$
$$+ qk_v\rho_S \int_0^\infty h_f(L)fL^3 dL \quad . \tag{2.28}$$

In this equation, V is the volume of the crystallizer, M_A is the molar mass of the solute, c is the concentration of the solute, ρ_S is the density of the crystals and ϵ is the void fraction. The later is the ratio of the liquid phase volume to the total volume of the crystallizer and is given by

$$\epsilon = 1 - k_v \int_0^\infty fL^3 dL \quad . \tag{2.29}$$

The quantity k_v is the volume shape factor of the crystals.

The left hand side of equation (2.28) is the total change in mass of the solute in the liquid phase. This consists of the solute entering and leaving the crystallizer with the liquid, the mass of the solute which is consumed by crystal growth and the mass of solute that is added again from the fines dissolution.

Differentiating equation (2.29) with respect to time t yields

$$\frac{d\epsilon}{dt} = -k_v \int_0^\infty \frac{\partial f}{\partial t}L^3 dL \quad . \tag{2.30}$$

After substituting the PBE (2.24) and partial integration, this relationship for the temporal change of the void fraction is given by

$$\frac{d\epsilon}{dt} = -3k_v G \int_0^\infty fL^2 dL + \frac{q}{V}k_v \int_0^\infty (h_f(L) + h_p(L))fL^3 dL \quad . \tag{2.31}$$

By solving equation (2.31) for $3k_v G \int_0^\infty fL^2 dL$ and substituting it into equation (2.28), the mass balance of the solute in the liquid is finally obtained as

$$M_A \frac{dc}{dt} = \frac{q(\rho_S - M_A c)}{V} + \frac{\rho_S - M_A c}{\epsilon}\frac{d\epsilon}{dt} + \frac{qM_A c_{feed}}{V\epsilon} - \frac{q\rho_S}{V\epsilon}(1 + k_v n_{LS}) \tag{2.32}$$

with

$$n_{LS} = \int_0^\infty (h_p(L) - 1)fL^3 dL \tag{2.33}$$

the mass that is transfered from the liquid to the solid phase. The initial condition of the ODE is given by

$$c(t = 0) = c_0 \quad . \tag{2.34}$$

2.3.2 Model 2

Model 2 is taken directly from the contributions of Mitrović [57] and Gerstlauer et al. [22]. A short description of this model is discussed in this section. For a detailed derivation of the mathematical and technical aspects, the reader is referred to the work by Mitrović [57] and Gerstlauer et al. [22]. Compared to model 1, additional population phenomena are considered like the birth of nuclei (primary nucleation) whose sizes are different from zero in model 2. The nucleation rate is considered as a boundary condition for model 1. In model 2 the nucleation is considered as a source term. Furthermore, the size dependent growth rate and attrition (secondary nucleation) caused by crystal - stirrer collisions are considered in model 2. A short overview regarding the population phenomena is given in the following paragraphs. For more details, the reader is referred to section 2.4.

The classical thermodynamic theory [87] suggests that molecules form stable and unstable unions and clusters. Depending on the size and the energy of these molecular clusters, unstable clusters disintegrate in further processes, while the stable ones grow into potential nuclei. Primary nucleation occurs spontaneously within a pure supersaturated liquid (homogeneous nucleation) or may be induced by foreign particles (heterogeneous nucleation) such as dust or impurities at reduced supersaturation in comparison to homogeneous nucleation.

In industrial crystallizers, homogeneous nucleation is rarely encountered. The solution inside a crystallizer is usually contaminated with foreign particles, i.e. heterogeneous nucleation is prevalent. A common assumption is that the same kinetic equations are used for both types of nucleation. One important property to know in nucleation is the size of the newly formed nuclei, the so called critical crystal length. The nucleation rate used in this model [57, 22] was originally proposed by Mersmann et al. [55]. It is mainly dependent on the supersaturation and the temperature inside a crystallizer. It also depends on natural constants such as Avagadro's number and Boltzmann's constant. Furthermore, it is also influenced by the properties of a specific chemical system like the diffusion coefficient (which is also dependent on the temperature), the saturation concentration of the solute, the heterogeneous nucleation factor, the molecule diameter of the solute and the surface tension.

The growth of crystals is a quite complex chemical and physical process. Depending on the chemical system and the actual conditions inside a crystallizer, different growth mechanisms are prevalent. For model 2, a growth rate expression accounting for diffusion and integration limited growth derived by Mersmann et al. [55] is used. This growth rate

is a function of crystal length L and depends on a number of additional factors such as mass transfer coefficient, integration coefficient, supersaturation and crystal strain energy. According to the work by Gahn [14], a modified supersaturation definition accounting for the individual strain energy of crystals is used to describe the growth rate of crystals. As a result, the driving force may become negative at high strain energy values. For negative growth rates (dissolution of crystals) only the mass transfer limited part is considered. Between the positive and negative growth regimes of the population, a specific crystal length with zero growth rate is identified. The crystals of this specific length do not grow at all. For more details pertaining to this phenomenon the reader is referred to work by Mersmann et al. [55] and Gahn [14], Gahn & Mersmann [17, 18].

The next phenomenon to analyze is the breakage of particles. Because we are considering a draft tube baffle (DTB) crystallizer, the dominating process is attrition of crystals due to collisions with the stirrer. In crystallization literature, the breakage or attrition of crystals is also referred to as secondary nucleation [51]. The collision of crystals with the stirrer leads to generation of an abraded original crystal with a length somewhat smaller than the removed crystals and a number of small attrition fragments resulting from crystal stirrer collision. Therefore, source and sink terms due to attrition are considered in model 2. For further details concerning the equations of this attrition phenomenon, the reader is referred to work by Gahn [14] and Gahn & Mersmann [17, 18].

So, the main difference between model 1 and 2 is that model 2 has a detailed kinetics. The summary of the model equations used for model 2 is given in the following.

Modeling the Dispersed Phase for Model 2

Model 2 is modeled under the following assumptions:

- ideal mixing

- isothermal operation

- constant overall volume (liquid+solid)

- the feed stream contains no particles, i.e. $F_{in}(L) = 0$

- dissolution of crystals is negligible.

Based on the assumptions mentioned above, the PBE is given by

$$\frac{\partial F(L,t)}{\partial t} = -\frac{\partial (G_L F(L,t))}{\partial L} + \dot{F}_{nuc} + \dot{F}_{attr}^{\mp} - \frac{q}{V}(h_f(L) + h_p(L))F \quad , \qquad (2.35)$$

with the following initial and boundary conditions

$$F(L, t = 0) = F_0(L) \qquad \text{and} \qquad F(0, t) = 0 \quad . \qquad (2.36)$$

$\dot{F}_{nuc}$ represents the particle number flux due to nucleation and $\dot{F}_{attr}^{\mp}$ represents the source and sink due to attrition. Determination of these fluxes and the size dependent growth rate are given in Section 2.4. The reader should not be confused with the volume based number density function $f(L,t)$ used for model 1, with number density function $F(L,t)$ used for model 2. In fact they are interrelated by $F = V_r \cdot f$, where V_r represents the spatial volume in which the particle population lives. As already stated, model 2 is directly taken from [57, 22] and it is used as it is.

Modeling the Continuous Phase for Model 2

The liquid phase in the crystallizer comprises of solute (component A) and solvent (component B). The fundamental balance equations of the liquid phase are derived using an overall mole balance and the mole balance of solute A. The total mole balance is given by

$$\frac{dn_L}{dt} = \dot{n}_{L,feed} + \dot{n}_{L,f,in} + \dot{n}_{L,class,in} - \dot{n}_{L,prod} - \dot{n}_{L,f,out} - (\dot{n}_{gr} + \dot{n}_{nuc}) \quad (2.37)$$

The mole balance of the solute A is given by

$$\frac{dn_{L,A}}{dt} = x_{L,A,feed}\dot{n}_{L,feed} + x_{L,A,f,in}\dot{n}_{L,f,in} + x_{L,A,class,in}\dot{n}_{L,class,in} - x_{L,A}\dot{n}_{L,prod}$$
$$-x_{L,A}\dot{n}_{L,f,out} - (\dot{n}_{gr} + \dot{n}_{nuc}) \quad . \qquad (2.38)$$

The appropriate initial conditions for both the ODEs are given by

$$n_L(t = 0) = n_{L,0} \qquad n_{L,A}(t = 0) = n_{L,A,0} \quad . \qquad (2.39)$$

In the above equations, the left hand side represents the total change in number of moles with respect to the whole system and component A, while the terms $\dot{n}_{L,i}$ and $x_{L,A,i}$ on the right hand side represent the mole flux and mole fraction of the respective streams that are entering and leaving the crystallizer. The terms $\dot{n}_{gr}$ and $\dot{n}_{nuc}$ represent the mass fluxes

that are transfered between the continuous and the dispersed phase due to nucleation and growth. These are given by

$$\dot{n}_{nuc} = c_S k_v \int_{L_0}^{L_\infty} L^3 \dot{F}_{nuc}(L) dL \qquad (2.40)$$

and

$$\dot{n}_{gr} = 3c_S k_v \int_{L_0}^{L_\infty} L^2 G_L(L, \Delta c) F(L,t) dL \quad , \qquad (2.41)$$

where c_s is the molar density of the crystals. Due to the volume constraint $V = $ const., the two ODEs (2.37), (2.38) can be replaced by a single equation for the mole fraction $x_{L,A}$ describing the composition of the liquid phase

$$
\begin{aligned}
n_L \frac{dx_{L,A}}{dt} = \; & (x_{L,A,feed} - x_{L,A})\dot{n}_{L,feed} + (x_{L,A,f,in} - x_{L,A})\dot{n}_{L,f,in} \\
& + (x_{L,A,class,in} - x_{L,A})\dot{n}_{L,class,in} - (1 - x_{L,A})(\dot{n}_{gr} + \dot{n}_{nuc}) \quad (2.42)
\end{aligned}
$$

with initial condition

$$x_{L,A}(t = 0) = x_{L,A,0} \quad . \qquad (2.43)$$

The total number of moles in the liquid phase is calculated by assuming an ideal mixture. It is given by

$$n_L = \frac{V_L \rho_A \rho_B}{x_{L,A} M_A \rho_B + (1 - x_{L,A}) M_B \rho_A} \quad . \qquad (2.44)$$

In this equation ρ_A and ρ_B represent the density of solute and solvent while the volume of the liquid phase V_L is given by

$$V_L = V - V_S = V - k_v \int_{L_0}^{L_\infty} F(L,t) L^3 dL \quad . \qquad (2.45)$$

The molar concentration of the solute in the liquid phase which is used for calculating the growth rate is given by

$$c = \frac{n_L}{V_L} x_{L,A} \quad . \qquad (2.46)$$

2.3.3 Model 3

In the context of modeling a specific DTB crystallizer, it was reported that besides fines dissolution, larger crystals are dissolved due to entry of an undersaturated fines reflux stream [20, 7]. For example, in the case of crystallization of Ammonium sulphate in the DTB crystallizer at the TU Delft, there is a high heat input in the heat exchanger to
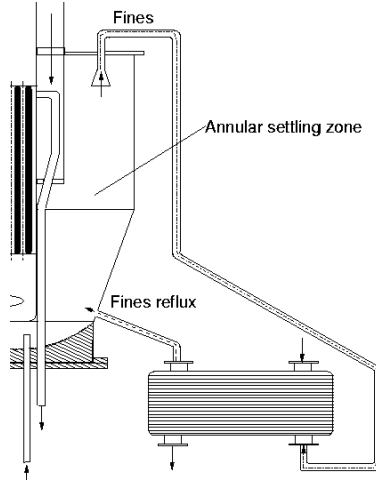
Figure 2.5: Fines dissolution pipe system of the considered DTB crystallizer at the TU Delft [20].

the reflux stream of fines leading to a noticeably increased temperature of about $60\,°C$ to $69\,°C$, while the crystallizer is operated at $50\,°C$. This reflux stream enters the region where the annular zone is connected to the forced circulation of the suspension around the draft tube as depicted in Fig. 2.5. In this region, there are large particles that have settled down and are scarcely moving. As a result, some amount of large crystals gets dissolved due to the considerable temperature difference between the reflux stream and the crystallizer. Therefore, this effect will be considered and model is described in the following.

Model 3 is similar to model 1 except for the fines classification function h_f which is replaced by non-ideal fines classification h_{fd} (see Fig. 2.6), which is explained in the following. The non-ideal fines classification was proposed in the work by Mitrović [57]. It accounts for the dissolution of large crystals in the settling zone of the crystallizer due to an increased temperature of the recycle from the fines dissolution. Therefore, a dissolution factor [86] is added to the ideal fines classification function, which is given by

$$h_{fd}(L) = R_1((1 - h(L - L_f) + k_{fd}h(L - L_{fd})) \quad , \qquad (2.47)$$

where L_{fd} is the cut size of the large crystals that are being dissolved at the rate of k_{fd}
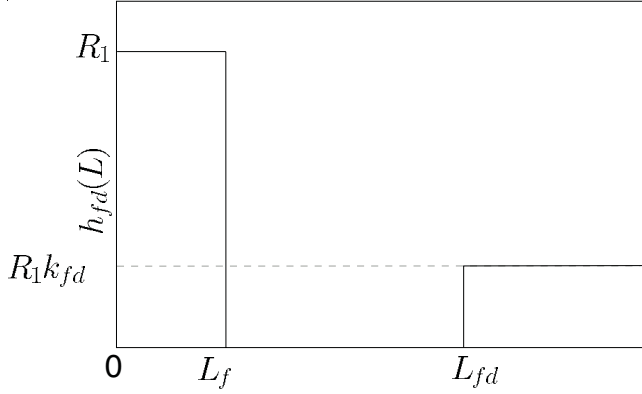
Figure 2.6: Piecewise constant classification $h_{fd}(L)$.

times the fines dissolution rate R_1.

This concludes the discussion of the various models that will be used for the stability analysis of continuous crystallization processes. The population balance models that are mentioned above are partial integro differential equations (PIDE). The numerical solution of these equations is carried out by application of a method of lines (MOL) with finite volume approach. Using a MOL the population balance is discretized along the property coordinate, i.e. the crystal length L is approximated with a finite number of N discretization points, thereby converting the PIDE into a set of ordinary differential equations (ODEs). More details regarding the discretization scheme can be found in Appendix A.1. The converted ODEs are integrated over time to determine the dynamic behavior of the crystallization process.

The next section gives an overview of various population phenomena like size dependent growth rate, nucleation and attrition that are incorporated in the different models.

2.4 Population Phenomena

The kinetics involved in crystallization from suspension include nucleation, growth and breakage or attrition of crystals. Attrition or breakage of crystals leads to secondary nucleation. It is the relation of the degree of nucleation to crystal growth that controls the product crystal size and CSD. Therefore this is a crucial aspect of industrial crystallization processes. Thus, it is necessary to have relevant information about the kinetics of the population phenomena to incorporate them into the mathematical model for better qualitative results. In the subsequent sections these kinetics are briefly discussed.

2.4.1 Primary Nucleation

Birth of new crystals or nucleation from a solution is only possible if a solution is supersaturated. The mechanisms by which the nucleation occurs are twofold: primary and secondary nucleation. Various mechanisms are shown in Fig. 2.7. Primary nucleation occurs in the absence of crystalline surfaces. It is again subdivided into homogeneous, heterogeneous and surface nucleation. On the contrary, secondary nucleation occurs only in the presence of crystals and their interaction with the crystallizer walls, crystal-impellers, crystal-crystal collisions etc. In other terms it is also called attrition or breakage. A mechanism pertaining to attrition is given in Section 2.4.2.
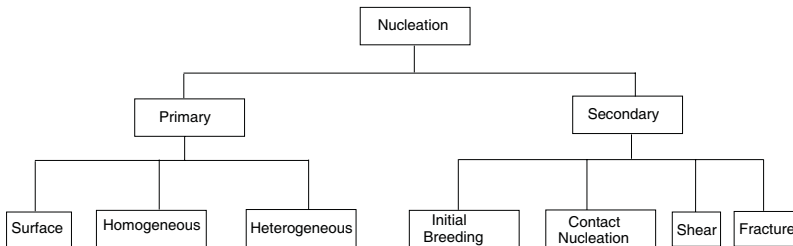
Figure 2.7: Mechanisms of crystal nucleation [73].

At a given temperature the mean concentration of a supersaturated solution is constant. However, the fluctuations in concentration locally will give rise to the formation of a number of clusters. According to the classical nucleation theory proposed by Volmer

[87] and Nielsen [64], these clusters are formed by an attachment and a detachment of molecules as shown below.

$$A + A \rightleftharpoons A_2$$
$$A_2 + A \rightleftharpoons A_3$$
$$A_3 + A \rightleftharpoons A_4$$
$$A_2 + A_2 \rightleftharpoons A_4$$
$$\cdots \quad \cdots \quad \cdots$$
$$\cdots \quad \cdots \quad \cdots$$
$$A_{c-m} + A_m \rightleftharpoons A_m \tag{2.48}$$
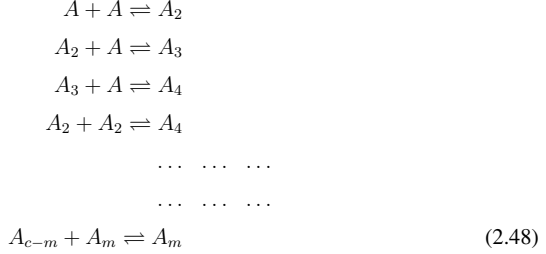
In an undersaturated solution or a just saturated solution the system of cluster formation and cluster decay is in equilibrium. As a result, the solution is stable against new phase formation. However, in a supersaturated solution the formation of clusters continues until it reaches a critical size. These clusters are either stable or unstable depending upon their Gibbs free energy. For the formation of new particles viz., nuclei, these clusters need to cross the critical Gibbs free energy barrier which is dependent on supersaturation.

According to Dirksen & Ring [11], the critical length L_{crit}, which accounts for a minimal size of the stable cluster, can be estimated by a modified Gibbs-Thomson equation. The critical crystal length is given by

$$L_{crit}(S_{rat}) = \frac{2\gamma_{LS}}{RTln(S_{rat})} \frac{M_S}{\rho_S} \quad . \tag{2.49}$$

It mainly depends on the surface tension between the liquid and solid phase γ_{LS}, the absolute temperature of the crystallizer T and the supersaturation S_{rat}. The other parameters in this equation are, the universal gas constant R and the molar mass and density of the crystal M_S and ρ_S. It should be noted that L_{crit} is not constant, and it changes with supersaturation. That means, a higher supersaturation leads to lower critical length and lower supersaturation to a higher critical length.

Spontaneous or homogeneous nucleation occurs in a supersaturated solution only when the solution is free of impurities and the presence of other physical features such as the crystallizer walls, stirrers and baffles. That is, homogeneous nucleation is difficult to observe in practice and also requires a high supersaturation. Contrary to this, heterogeneous nucleation occurs in the presence of foreign or dissolved impurities and requires a relatively low supersaturation. In common practice, the same type of kinetic equations are used for both nucleations.

In this work two models are considered for determining the nucleation rate. One is a power law model, which is just a function of the concentration difference and where the size of the nuclei is negligible, i.e., $L_{crit} = 0$. The other is a detailed model, where the size of the nuclei is considered and is also dependent on many other factors. These models are explained in the following.

Power law model

A general theory for the prediction of nucleation rates does not exist. Most of the correlations are based on a power law model which is fitted to experimental results. The power law is given by

$$B = k_b m_t (c - c_{sat})^b \quad . \tag{2.50}$$

From equation (2.50), it is evident that the nucleation rate is dependent on the degree of concentration difference. The constants k_b and b are determined from experiments and vary with suspension density, agitator stirring rate, crystal-agitator collisions etc. c_{sat} is the saturation concentration of the solute at the operating temperature, c is the concentration of solute and m_t is the suspension density based on third moment defined by

$$m_t = k_v \rho_S \int_{L_0}^{L_\infty} f(L,t) L^3 dL \quad . \tag{2.51}$$

A pilot or bench scale testing to obtain kinetic parameters is usually unavoidable. Randolph & Larson [73] and Gahn & Mersmann [16] suggested the use of a CMSMPR crystallizer for laboratory determination of growth and nucleation rates. The empirical model given above is used for model 1 to describe both primary nucleation and attrition in crystallization processes.

Detailed model

According to Mersmann et al. [55, 53] and with the extension of the classical nucleation theory by Kind & Mersmann [32], the rate of primary nucleation B_{prim} per unit volume of continuous phase per second is given by

$$B_{prim} = \frac{3}{2} D_{AB} \left(N_A c_{sat} S_{rat} \right)^{\frac{7}{3}} \sqrt{C_{het} \frac{\gamma_{SL}}{k_B T}} V_m \exp \left[- C_{het} \frac{16\pi}{3} \left(\frac{V_m}{\ln S_{rat}} \right)^2 \left(\frac{\gamma_{LS}}{k_B T} \right)^3 \right] \quad . \tag{2.52}$$

The given equation is a function of relative supersaturation S_{rat} and temperature T inside the crystallizer. Besides this, B_{prim} depends on the molecule volume V_m, the binary diffusion coefficient D_{AB}, the solubility c_{sat} and the surface tension γ_{LS} which change with the chosen chemical system. γ_{LS} and D_{AB} are directly related to the temperature T, the solubility c_{sat} and the molar concentration of crystallizing substance ρ_S/M_S [55, 50, 21]. The nucleation rate also depends on physical constants like the Avogadro number N_A and the Boltzmann constant k_B. The parameter C_{het} determines whether nuclei are generated by homogeneous ($C_{het} = 1$) or heterogeneous ($0 < C_{het} < 1$) primary nucleation.

The surface tension γ_{LS} used in equation (2.52) is given by Mersmann [50] as

$$\gamma_{LS} = 0.414 k_B T \left(\frac{\rho_S N_A}{M_S} \right)^{\frac{3}{2}} ln\left(\frac{\rho_S}{M_S} \frac{1}{c_{sat}} \right) \quad . \tag{2.53}$$

In addition to homogeneous or heterogeneous nucleation, a new source of nuclei is reported in the literature [53, 30, 54]. Compared to primary nucleation, these nuclei are formed at low supersaturation upon the crystals present in the solution or in the immediate vicinity of such crystals. This nucleation is called catalytic nucleation or surface nucleation. Up to now, this mechanism is poorly understood. However, the origin of these nuclei is not due to an attrition or breakage process [53]. In fact, surface nuclei are formed even in absolute rest wherein only motionless crystals are present.

The rate of surface nucleation, B_S, in nuclei per unit volume of continuous phase depends on the diffusivity, D_{AB} and relative supersaturation S_{rat}. It is given by [53, 30, 54]

$$B_S = E \frac{A_D}{V_L} \frac{D_{AB}}{d_m^4} \exp\left(- \frac{\pi}{9 ln\, S_{rat}} \left[ln \frac{\rho_S}{M_S c_{sat}} \right]^2 \right) \quad . \tag{2.54}$$

In this equation, A_D represents the surface area of all the particles in the dispersed phase and E represents the efficiency factor. This efficiency factor represents a portion of surface nuclei that is removed to become volume nuclei. According to Mersmann [53] this efficiency factor E has only a weak influence on the overall nucleation rate and is therefore set to one in this work. For a more comprehensive review of the different nucleation mechanisms, the reader is referred to articles by Mersmann [53], Kim & Mersmann [30], Mersmann & Bartosch [54].

The total nucleation rate used for model 2 is obtained by considering all the nucleation processes. It is calculated as

$$B_{nuc} = B_S + B_{prim} \quad . \tag{2.55}$$

A mono sized nucleation at the critical crystal length L_{crit} is considered for model 2. Therefore, it is formulated by using a Dirac delta function. The mono sized distribution $\dot{F}_{nuc}$ is given by

$$\dot{F}_{nuc} = \delta(L - L_{crit})B_{nuc}V_L \quad . \tag{2.56}$$

In this equation V_L represents the volume of the continuous solvent phase.

2.4.2 Attrition

In an industrial crystallizer, contact between crystals and crystal-crystallizer parts increase the rate of production of potential nuclei [19]. Whether attrition or breakage prevails, is determined by the operating conditions of the crystallizer and the substance to be crystallized [15, 35]. For example, when brittle substances are crystallized at a relatively low supersaturation and a high specific power input, attrition is the dominant mechanism. A physical model with a mechanical and a kinetic term was developed for the calculation of attrition rates [89, 19, 16, 14, 15, 55]. The mechanical term describes the effect of the attrition rate and the size distribution of attrition fragments. The effective nucleation rate can be estimated by knowing the size distribution of attrition fragments and the size of effective nuclei.

The dominant crystal size reduction phenomenon in a DTB crystallizer is attrition of the crystals with the stirrer. This is due to uniform flow pattern created in the DTB crystallizer. As a result the collision between crystals is less, since all crystals are heading in the same direction. The collision of crystals with the stirrer leads to the generation of an abraded original crystal of a length L_R which is somewhat smaller than the original crystal length L_R, and a number of small attrition fragments within a specific length range $[L_{frag,min}, L_{frag,max}]$. A schematic of an attrition event within the particle space is shown in Fig. 2.8.

According to this figure, the crystal- stirrer collisions lead to the following particle number fluxes in the population balance equation:

- a particle number flux $\dot{F}_{attr}^{-}$ due to the removal of original crystals that collide with the stirrer.

- a particle number flux $\dot{F}_{attr,2}^{+}$ due to the generation of abraded original crystals with a length somewhat smaller than the original crystal.
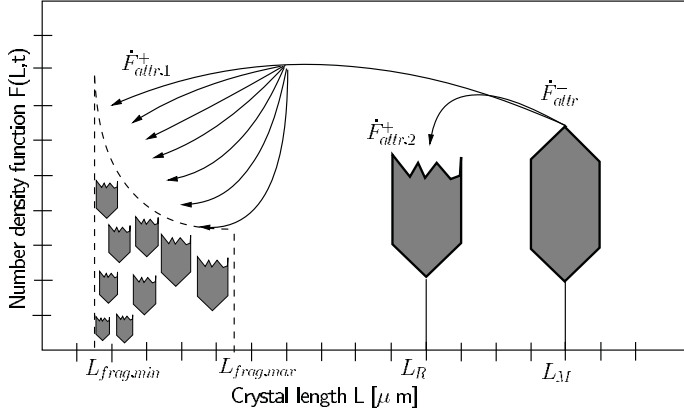
Figure 2.8: Schematic of an attrition event according to Gerstlauer et al. [22].

- a particle number flux $\dot{F}^+_{attr,1}$ due to generation and distribution of attrition fragments resulting from crystal-crystal stirrer collision

In other words, these are the sink and source terms in the population balance equation. The overall particle number flux due to attrition $\dot{F}^\pm_{attr}$ is given by

$$\dot{F}^\mp_{attr}(L) = -\dot{F}^-_{attr}(L) + \dot{F}^+_{attr,2}(L) + \dot{F}^+_{attr,1}(L) \quad . \tag{2.57}$$

The kinetic expressions of different particle number fluxes due to attrition were proposed by Gahn & Mersmann [17] and are discussed in the following.

The particle number flux $\dot{F}^-_{attr}$ due to attrition is dependent on the attrition rate $\beta_{attr}(L)$ and the number density function $F(L)$. It is given by

$$\dot{F}^-_{attr}(L) = \beta_{attr}(L)F(L) \quad . \tag{2.58}$$

The attrition rate is dependent on the volumetric flow rate of the stirrer and the volume of the crystallizer. Moreover, it is dependent on the probability and the velocity that an individual crystal strikes the stirrer blade. For a given system, the velocity and probability of contacts between a crystal and the stirrer depend on the size and shape of the particles and on the flow pattern around the stirrer blade.

The particle number flux $\dot{F}^+_{attr,2}$ generated due to abrasion of the original crystals with a length L somewhat smaller than the original crystal length L' is obtained by integrating over all particles having a length larger than L. It is given by

$$\dot{F}^+_{attr,2} = \int_0^{d_{st}/2} \int_L^{L_{max}} \delta(L_R(L',r) - L)\dot{F}^-_{attr}(L',r)dL'dr \quad . \tag{2.59}$$

$\dot{F}^-_{attr}(L',r)$ represents the sink term due to crystal-stirrer collisions. The Dirac-delta function $\delta(L_R(L',r) - L)$ picks out one crystal whose attrition results in an abraded original crystal with length L_R. This length can be obtained by a simple volume balance

$$k_v L_R^3(L',r) + V_{P,attr}(L',r) = k_v L'^3 \quad . \tag{2.60}$$

The term $V_{P,attr}$ in the above equation is the volume removed from an individual crystal during one attrition event. It depends on the attrition resistance of the crystal [16] which in turn is related to the mechanical properties of the crystal.

The particle number flux $\dot{F}^+_{attr,1}$ describing the generation of small attrition fragments is given by

$$\dot{F}^+_{attr,1} = \int_0^{d_{st}/2} \int_L^{L_{max}} [h(L-L_{min})-h(L-L_{max}(L',r))]N_{frag}((L',r)f_{frag}(L',r)\dot{F}^-_{attr}(L',r)dL'dr \quad . \tag{2.61}$$

In the above equation $N_{frag}(L',r)$ represents the number of attrition fragments produced during one attrition event. f_{frag} represents the size distribution of the attrition fragments which is dependent on the size of the original crystal L', the length of the resulting fragment L and the stirrer radius r. Furthermore, the length of these attrition fragments is dependent on the mechanical properties of the crystal [16].

This concludes the summary of equations pertaining to the attrition processes. For more comprehensive information regarding the attrition process the reader is referred to [14, 69, 77]. The above equations will be used to calculate the particle number flux for sink and source terms due to attrition in model 2.

2.4.3 Crystal Growth

The final CSD and the production of crystals with sufficient purity are significantly influenced by the rate of crystal growth along with the nucleation. The main objective of a laboratory or an industrial crystallizer [52] is to obtain a crystalline product with a large median crystal size L_{50} in order to facilitate solid - liquid separation and drying. The growth rate of a single crystal depends on the supersaturation, the crystal surface, the degree of deformation of lattice, the kind of solvent and the presence of impurities.

Due to the non-idealities of crystal growth, different expressions were suggested in the literature. For a more comprehensive review, the reader is referred to the article by Dirksen & Ring [11]. In general, crystal growth is a two step process [27]. One is the diffusion of the solute from the bulk solution to the crystal/solution interface. Another is the integration of the solute into the crystal lattice.

Two types of growth rate expressions are used in this work. For models 1 and 3, a simple power law model is used. The growth rate from the power model is size independent and it takes into account both the diffusion and integration controlled mechanisms. This model is a function of the overall concentration driving force and is given by

$$G = k_g(c - c_{sat})^g \quad , \tag{2.62}$$

where c is the concentration of the solute in the solution, and c_{sat} is the saturation concentration of the solution at a particular temperature. g and k_g are the order and coefficient of the growth rate expression. The power g in the growth equation is normally a number between 1 and 2. The constant k_g is a function of temperature.

A growth rate expression proposed by Mersmann et al. [55] which is size-dependent, is used for model 2. By assuming the integration step as a second order reaction with respect to supersaturation, the following is the growth rate expression

$$\frac{G_L(L)}{2k_d(L)} = \frac{\Delta c}{c_S} + \frac{k_d(L)}{2k_r c_S} - \sqrt{\left(\frac{k_d(L)}{2k_r c_S}\right)^2 + \frac{k_d(L)}{2k_r c_S}\frac{\Delta c}{c_S}} \quad . \tag{2.63}$$

$$\Delta c(L) = c - c_{sat,real}(L) \quad , \tag{2.64}$$

where k_d is the mass transfer coefficient, k_r is the integration rate constant, c_S is the molar concentration of the crystallizing substance and Δc the supersaturation. The first term in the right hand side of the above equation represents the integration limited growth and the remaining terms account for the diffusion limited growth.

The mass transfer coefficient k_d is estimated by using a Sherwood relation which has been developed by Mersmann et al. [55], while D_{AB} is estimated by using the Stokes-Einstein equation [18]. During attrition a certain amount of internal strain will be present in the attrition fragments. The presence of strain in the fragments leads to an increased solubility $c_{sat,real}$ in comparison to the solubility c_{sat} of ideal stress free crystals:

$$c_{sat,real}(L) = c_{sat} \exp\left(\frac{\Gamma_s}{RTL}\right) \quad . \tag{2.65}$$

Note that k_r, the integration rate constant and Γ_s, the individual strain energy, are constant for a particular chemical system. But they have to be determined from experimental data [62, 18, 90, 45, 7]. The integration rate constant k_r describes the solute integration into the lattice. It does not depend on fragment size (similar structure surfaces). It is constant for a given substance, purity of the solution, and temperature.

At higher strain energy values, $\Delta c(L)$ may become negative. In that case, the equation (2.64) reduces to

$$\frac{G_L(L)}{2k_d(L)} = \frac{\Delta c}{c_S} \quad , \tag{2.66}$$

as the dissolution rate must be mass transfer limited only.

Between the positive and the negative growth rate of crystals, there exist crystals with a specific length that has a zero growth rate. This specific length can be obtained by setting equation (2.65) to zero. This leads to an expression for the length of crystals having zero growth rate

$$L_0 = \frac{\Gamma_s}{RT}\left(ln\frac{c}{c_{sat,real}(L)}\right)^{-1} \quad . \tag{2.67}$$

From the above equation it is evident that the L_0 is constant at a particular temperature T and concentration c.

It must be noted that the nuclei that are formed due to primary nucleation do not have strain energy and have a perfect lattice structure. On the other hand, as described earlier, the secondary nuclei or attrition fragments that are formed due to attrition have strain energy and structural defects. In that case, two growth rates have to be used. One is for crystals having no structural defects and lattice strain energy, and the other is for crystals having both. Usually, continuous crystallizers are operated in such a way that primary nucleation only occurs during start-up. The major source of nuclei is due to attrition. Therefore, the crystals are assumed to have lattice strain energy and only one growth rate

is used for model 2. This concludes the section pertaining to the kinetics of crystallization processes.

2.5   Summary

Three different population models that will be used in this work were presented. (i) A model with simple kinetics and ideal fines classification (model 1), (ii) a model with complex kinetics involving breakage due to attrition and ideal fines classification (model 2), and (iii) a model with simple kinetics and non-ideal fines classification (model 3). The models were based on the material balance for a continuous phase and a population balance for the dispersed phase. An overview of mechanisms and empirical equations pertaining to the kinetics of crystallization processes was given. These empirical equations will be incorporated in the respective mathematical models mentioned above and models are numerically simulated to study the dynamic behavior of crystallization processes.

Chapter 3

Experiments

This chapter describes the experimental equipment and procedure that will be used to determine the growth rate parameters for model 2 of the KCl - H_20 system. The operation of the crystallizer and the hardware used will be discussed below. The instruments that are used to measure the CSD and concentrations are also described briefly.

3.1   Operation of the Pilot Plant

The pilot plant crystallizer used in this experimental study has an estimated volume of 20 litres and is made of glass. Fig. 3.1 shows a schematic of the crystallization vessel. The dimensions of the crystallizer are given in Fig. 3.1. It is double walled and round bottomed with a stainless steel head plate with several sample ports. The vessel has six baffles and a draft tube. A marine type propeller (stirrer) is situated inside the draft tube to stir the slurry. The stirrer motor has a speed range for 0 to 1000 rpm. The crystallizer is operated in quasi continuous mode. The bottom of the crystallizer is equipped with a membrane valve and it opens every few seconds. The opening time of the valve is adjusted in a such a way that the volume of the slurry inside the crystallizer is kept constant. The product slurry is discharged from the crystallizer into a buffer tank through a plastic pipe. A temperature sensor is installed inside the crystallization vessel and the operating temperature of the crystallizer is controlled with a programmable thermostat.

310 mm

470 mm

190 mm

90 mm

30 mm
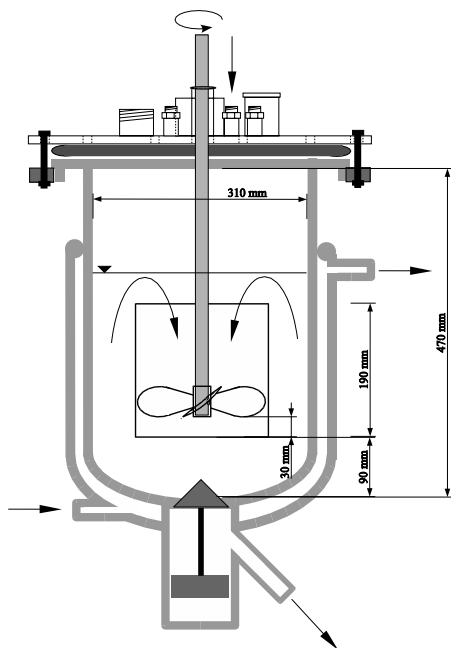
Top view of the draft tube with baffles

190 mm

Figure 3.1: Crystallization vessel.

38

Tube

Double wall tube (heating or cooling by thermostat)

Pneumatic valve with water cleaning and air drying

Hand valve

HX	Thermostat
B	Vessel
C	Reactor
P	Pump
M	Motor
TI	Temperature Indicator
TIC	Temperature Indicator Control
RI	Resistance Indicator
SI	Speed Indicator

M2

C

HX 2

B 2

HX 3

HX 5

HX 4

MI

HX 1

B 1

P 1
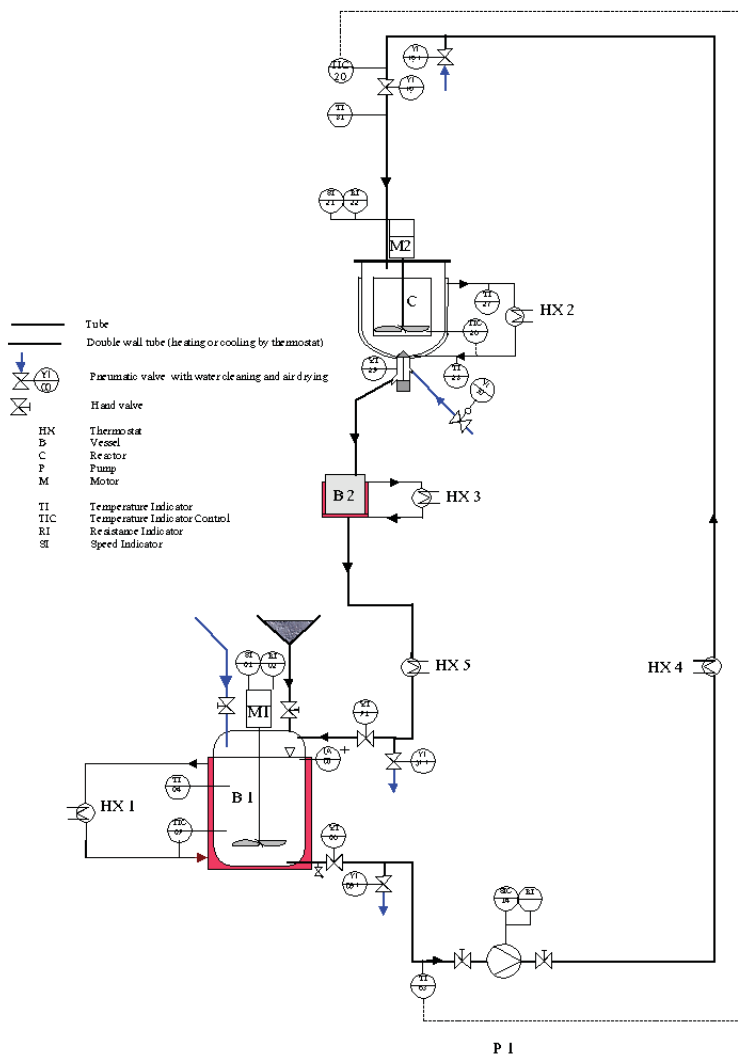
Figure 3.2: Flow sheet of the pilot plant crystallizer.

39

A schematic of the whole crystallization plant is given in Fig. 3.2. All pipes that are connected between the vessels are well insulated to prevent any loss of heat. As a result, blockage of the system can be avoided. The whole process is operated in closed loop in order to obtain a relatively small equipment volume as well as low consumption of crystalline material.

The feed tank B1 is made of PVDF (Poly Vinylidene Flouride), as the KCl solution is highly corrosive. It is double walled and is equipped with a stirrer. The temperature inside the feed tank is controlled by a thermostat. An initial feed is prepared from tap water and technical grade KCl. Feed is supplied to the crystallizer from the feed tank by an electrically driven tube pump. The temperature inside the feed tank is always raised by 5K above the satu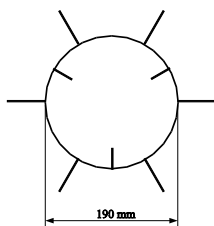ration temperature in order to ensure a crystal free feed. The temperature of the feed will be eventually brought down close to the saturation temperature by the heat exchanger HX4 before entering the crystallizer.

For a low consumption of crystalline material, the product slurry drawn from the buffer tank is recycled. The recycling process takes place in the following way. The slurry flows from the crystallizer into the buffer tank B2. The buffer tank is heated to a higher temperature above the operating temperature of the crystallizer by the heat exchanger HX3. Thus, the buffer tank acts as a transient dissolver. The slurry from the buffer tank passes through the double walled pipe, which is heated by heat exchanger HX5. The temperature is about 20K above the operating temperature of the crystallizer. This pipe is in turn connected to the feed tank. The crystallization vessel C is kept at a considerable height above the feed tank. Due to the gravitational force, the slurry flows down through the insulated pipe. The additional crystals that are present in the slurry coming from the buffer tank get dissolved due to the high temperature and the long length of the pipe. A crystal free solution enters the feed tank.

A rinse water system is present, with inputs at different locations in the process. Rinse water is used to remove scaling, which causes blockage of tubes and also to clean the system after experiments. In addition, the system is also equipped in such a way that air can be pumped into the pipes after rinsing with the water. This helps in drying the pipe as well as in removal of small crystals, if necessary, by force.

3.2 Measuring Devices

Monitoring and control of crystallization processes is based on information concerning concentration and CSD. The CSD describes the state of the solid phase and its final value affects significantly the downstream processing. Concentration and temperature are required to specify the crystallization driving force. The most challenging problem in the crystallization process is to find suitable measuring devices for inline and offline measurement. Because of growing demand for higher product quality and process control, has to lead to the development of a number of sensors [23] to monitor the process variables which in turn is the key for process information. Concentration can be estimated by different methods [27], and all of them are based on the measurement of some property associated with solution concentration and on information on phase equilibrium. Monitoring of the CSD is based on different light scattering techniques.

In the subsequent paragraphs, an overview of the equipment used for measuring the concentration and the CSD will be discussed briefly along with their advantages and disadvantages. However, emphasis is on the Laser diffraction spectrometer and the Densitometer.

3.2.1 Measurement of Crystal Size

Focused Beam Reflectance Method (FBRM): The FBRM is based on a principle which is explained in the following way. A high velocity rotating infra red laser beam propagates through the sapphire window on the cylindrical probe tip into the suspension. As soon as the beam hits the particle, it is reflected and back propagated through the probe window. These optical pulses are collected by the probe optics and passed via fibre-optic cable to the detector. They are converted by the detector into electronic signals, which are analyzed for their duration in the time domain. The corresponding chord length s is calculated by multiplying the time Δt for the beam to cross the particle with the velocity of the beam v_b. The chord length counts are summed up in a finite number of chord length interval thus yielding the chord length distribution (CLD) [76, 80, 2].

The number of particle counts measured by FBRM largely depends [58] on the operating conditions and more particularly on the hydrodynamic conditions, solvent, temperature, focal point position, particle shape, size distribution relative indexes of refraction, size exclusion at the tip, particle surface roughness and spectral reflection characteristics of the particle and solvent.

Therefore, it will be difficult to reconstruct the CSD from CLD by excluding all the effects. Moreover, the instrument was tested in the pilot plant crystallizer and it failed due to the following reasons. The reason for the failure is that the FBRM failed to differentiate between the crystals and the air bubbles that are formed at high stirring rates in the crystallizer. In addition to this, the instrument failed to measure the particles which are beyond 1000 μm. The particles size (as shown in section 3.5) that are measured experimentally, under the microscope, are larger than 1000 μm. Owing to the limitations mentioned above this instrument was not used.

Laser Diffraction Particle Size Analysis: The Laser Diffraction Particle Size Analysis 1180 is patented by CILAS (Madison, WI, USA). It is used to measure the size of particles (powders, suspension and emulsions) for both offline and online measurements and is based on a principle using diffraction and diffusion phenomena of a laser beam. A diffraction pattern, called Airy pattern is obtained when a particle is lightened by a laser source [10]. The light intensity I depend on the diffraction pattern and is a function of the diffraction angle α. The pattern is composed of concentric rings and the distance between them depends on the particle size.
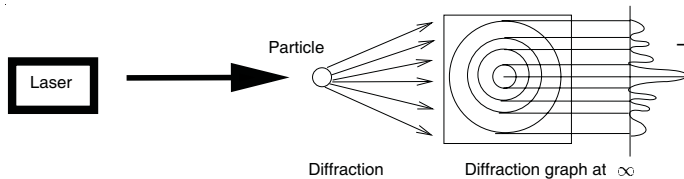
Figure 3.3: Principle of CILAS [10].

The diffraction pattern is observed at a defined distance when a convergent lens is placed between the laser beam and the detector. The detector is placed at the focal length. The diffraction patterns of particles having the same size converge at the same point wherever their location is with respect to the lens.

A charge couple device (CCD) camera equipped with a digital processing unit (DSP) is fixed to the instrument. This CCD camera acquires a projected particle image. With corresponding software a numerical diffraction pattern is obtained from the projected

image and thereby the corresponding CSD is obtained. For more details the reader is referred to [10].

For measuring the CSD, the following working conditions have to be optimized: (i) choice of carrier liquid (ii) choice of dispersing agent (iii) choice of power and duration of ultrasonics (iv) choice of level concentration. After satisfying the above conditions, the sample to be measured is dried and dispersed in a carrier liquid in a tank. The pump circulates the carrier liquid with dispersed powder and reaches the CCD cell where the diffraction patterns are acquired by the CCD sensors. This information is passed on to the computer where the corresponding CSD distribution of the sample is obtained.

Sieve Analysis: This is one of the simplest and oldest offline measurement method. For determining the CSD, the sample is sieved with different mesh sieve openings. However, the principle drawbacks of this measurement method are (i) it cannot be used for control purposes (ii) sieving is tedious and time consuming in particle sample preparation and sample drying (iii) the sampling procedure can lead to crystal damage (iv) agglomeration may take place during the drying process.

Imaging: This is another offline method used in analyzing the CSD. A normal CCD camera with a microscopic lens can be used for this purpose. A stroboscopic light source is used to illuminate the particles. The picture can be seen directly on the computer monitor which processes the data. Apart from the particle shape, the CSD can also be calculated. The drawback of this method is that the number of particles in a single picture is limited. Therefore the CSD is not very accurate.

3.2.2 Concentration Measurements

Densitometer: This instrument can be used for both online and offline measurements and is one of the most reliable. It consists of a measurement cell comprising a borosilicate glass U tube inside a thermostated jacket. The cell typically holds about 0.7ml of sample. The instrument works on the principle of natural frequency of a cell filled with a sample solution. The cell is stimulated to undamped vibrations and the natural frequency of the cell is transferred to a receiver electronically to calculate the density of the solution. A series of calibration runs has to be performed to obtain densities of solutions of known concentration and temperature. The concentration of the solution can be determined from
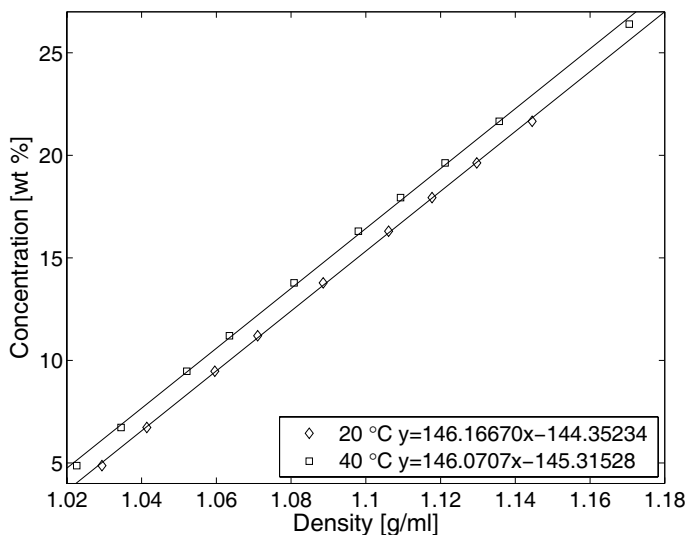
Figure 3.4: Calibration curve of the densitometer for the KCl - H_2O system.

the corresponding calibration curve. The accuracy of this instrument is in the range of $10^{-1} kg/m^3$ to $10^{-3} kg/m^3$. Data from the calibration runs show that the relationship between concentration (weight %) and temperature is linear. Linear regression is then used to obtain a relationship between the concentration and the density at different temperatures. In the case of measuring the concentration of KCl, the calibration curve is given in Fig. 3.4.

Refractometer: This instrument can also be used for both on-line and off-line measurements and is as reliable as the densitometer. It works on the principle of total reflection. The refractive index of the solution depends on temperature and the density of the solution. Light is transmitted though a prism (present in the instrument) in contact with the crystallization slurry. A portion of the light reaching the prism/solution interface is deflected into the solution. The intensity of the incident light that remains in the prism is dependent on the difference between the refractive indexes of the glass and the solution. Both turbid and dark samples can be measured with this instrument. However, the measurement is sensitive to ambient light and to the presence of air bubbles that may
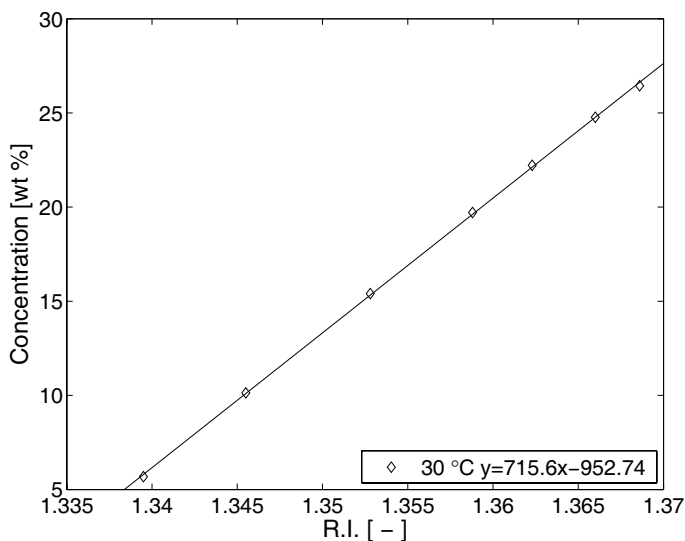
Figure 3.5: Calibration curve of the refractometer for the KCl - H_2O system.

adhere to the surface of the prism. The concentration of the solution can be determined from the corresponding calibration curve. The calibration curve for measuring the KCl concentration is shown in Fig. 3.5.

Liquisonic: This is one of the most modern equipment that is available in the market for determining inline measurements of concentration as well as for determining the metastable zone width of the process. It works on the principle where a transmitter transmits a pulse which is ultrasonic and time is measured by the receiver. The sonic velocity is determined as the distance between the transmitter and the receiver is fixed. This sonic velocity changes with the density of the solution and temperature. However, the major drawback in utilizing the instrument is that it can't give accurate results when the solution is suspended with a high density of particles or small air bubbles, which has been tested in the pilot plant crystallizer. For an effective use of the instrument, it has to be placed in the quit zone of the crystallizer where the effects mentioned above will be minimum, or else the solution must be particle free.

This completes the section describing some of the various measuring devices that are commonly used in measuring the process variables for understanding crystallization processes. The instruments that are utilized in the experiments for measuring concentration and CSD are the densitometer and CILAS. In the next section a short description of determining the metastable zone width for the KCl - H_2O system is given.

3.3   Estimation of the Metastable Zone Width

In industrial crystallization processes [83], the CSD, the mean crystal size as well as external habit and the internal structure of the crystals are very important for further downstream processing. With respect to product characteristics, nucleation has a stronger influence than crystal growth. In turn, this nucleation is related to the meta stable zone width of the system. For the design of products by crystallization processes, it is essential to measure the metastable zone width. Only optimum nucleation and optimum growth rate can lead to product quality. This is explained in the following way.

For example, if there is high supersaturation, that means the crystallizer is operated outside the metastable zone width. A large number of nuclei are formed due to primary nucleation. This will lead to a low product quality due to liquid inclusions and dendritic growth. Contrary, if the crystallizer is operated in such a way that the supersaturation is near to the saturation limit, this will lead to a slow growth rate, which requires long retention times and high purity. However, this is not desirable due to economic reasons. In industrial crystallization processes a compromise between product quality and economic efficiency has to be found. As a rule of thumb, the crystallizer has to be operated in the middle of the meta stable zone width.

The metastable zone width in the primary nucleation is important if the crystallizers are operated at high supersaturation [30] and unseeded. As most of the industrial crystallizers are seeded and are operated mostly within the metastable zone width of the secondary nucleation. The metastable zone width of the secondary nucleation is measured using a poly thermal method. The metastable zone width varies with many other factors like presence of impurities, mechanical agitation of solution, viscosity etc.

The poly thermal method [66] is based upon measuring the metastable zone width at different cooling rates. For estimating the metastable zone width at a particular temperature, a saturated solution is prepared in a closed double walled flask. The flask is equipped

with a magnetic stirrer and is connected to a thermostat for controlling the temperature in the flask. In addition to this, the flask is equipped with a turbidity meter to measure the turbidity of the solution and also with a temperature sensor. Both the instruments are connected to the computer. Initially, the saturated solution is heated above saturation temperature by a few degrees centigrade. If there are any crystals, they will be dissolved. Now the solution is cooled to the saturation temperature and a few crystals (2 to 3) are added to the solution. The solution is further cooled at a particular cooling rate. As long as the solution is crystal free, the turbidity of the solution remains constant. However, as the dependence of the nucleation rate on the supersaturation is very marked near the limit of the metastable zone, the turbidity of the solution changes. The temperature at which the turbidity of the solution changes is the metastable temperature. In the case of the KCl - H_2O system, the change of turbidity with temperature at a particular cooling rate is shown in Fig. 3.6. The first change in turbidity at 20 $^\circ C$ depicted in Fig. 3.6 is the result of addition of few crystals (2 to 3). The second change is due to formation of crystals. After cooling the solution to a particular temperature at which a sufficient number of crystals are formed, the temperature of the solution is slowly raised to a few degrees
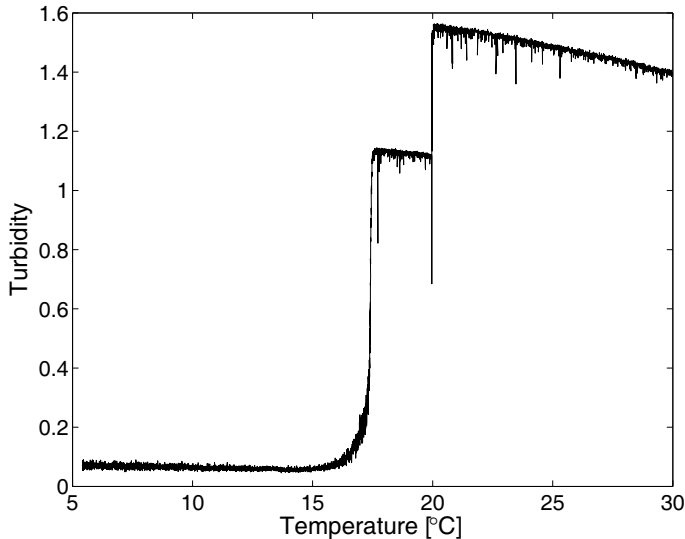
Figure 3.6: Turbidity vs. Temperature at a 5 Kph cooling rate for the KCl - H_2O system.
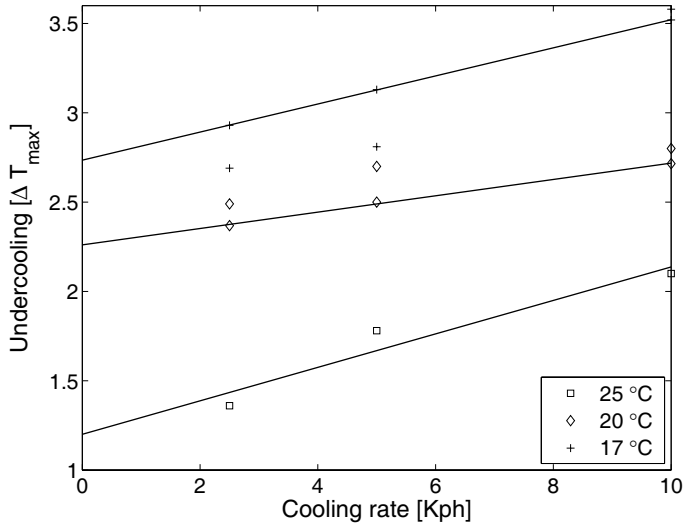
Figure 3.7: Metastable zone width of KCl - H_2O system.

centigrade above the saturation temperature. The temperature is held constant for some time so that all the crystals will be dissolved and the procedure is repeated at different cooling rates.

Fig. 3.7 shows data of the metastable zone width as a function of different cooling rates and temperature, for the KCl - H_2O system. At a particular temperature the saturated solution is cooled at different cooling rates i.e. at 2.5, 5 and 10 Kph. The temperature is then recorded at which turbidity changes. The metastable zone width is then determined at 0 Kph. This can be obtained by extrapolating the data at different cooling rates. The solid line depicted in Fig. 3.7 represents the extrapolation curve. The solubility diagram along with metastable zone width for the KCl - H_2O system is shown in the Fig. 3.8. Fig. 3.8 shows that as the temperature decreases the metastable zone width increases. This is consistent with observations published in literature. The experiment is repeated twice so that it is reproducible. The ∘ in the Fig. 3.8 represents the operating point of the continuous crystallizer for the experiments. This concludes the section pertaining to an estimation of the metastable zone width. This information is essential for the operation of a continuous crystallizer. The next section discusses the operation of a continuous
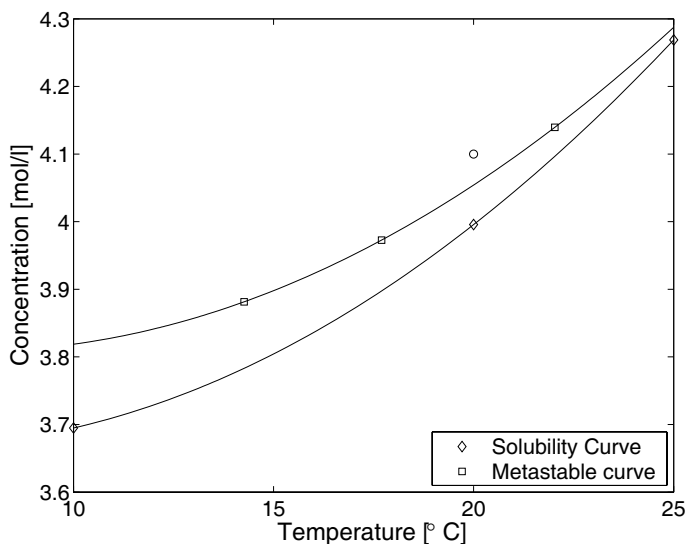
Figure 3.8: Metastable zone width for heterogeneous nucleation as a function of temperature for KCl - H_2O system.

crystallizer.

3.4 Crystallizer Operation

The typical operation of a crystallizer is outlined below. The whole procedure is based on the sequence function chart depicted in Fig. 3.9. This is composed of "step" and "transition". A "step" is denoted by a box that indicates the state of the process. A "transition" is indicated by a bold line which shows the condition to make a move to the next "step". Actual operations are indicated by items at the side of "step", "S" means actual operation and "R" means reset.

First, the feed line is activated after start-up and the solution of a desired concentration is charged into the crystallizer. The temperature of the feed solution must be $5K$ above the saturation temperature. Otherwise, the feed solution gets cooled in the process of charging
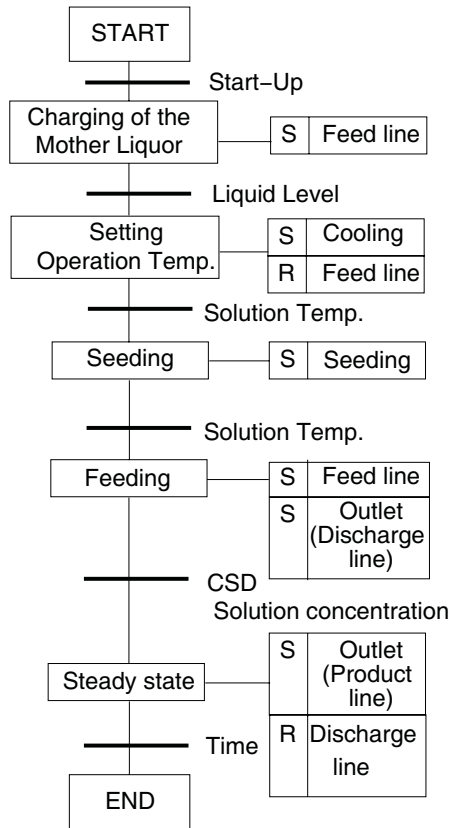
Figure 3.9: Operation procedure described by a sequential function chart [81].

the crystallizer. As a result the pipe of the feed line gets blocked due to formation of crystals. The feeding is stopped when the desired hold up in the crystallizer is reached. This whole feed line is purged, initially with water and then with air. The stirrer is started and the solution inside the crystallizer is cooled to the desired operation temperature at 20 °C.

Seed crystals are then added to the solution when a stable desired operation temperature is reached. After that, the feed line is activated. The discharge of the product is started

immediately after the feed solution starts entering the crystallizer. The moment when feeding is restarted is defined as time 0. The concentration of the solution inside the crystallizer is measured by taking a sample that is crystal free, with a syringe having a filter, at every 30 min. The sample is then kept in a water bath. The water bath temperature is set to $40\,^\circ$C. The sample is then analyzed offline by using a densitometer at $40\,^\circ$C. In addition to the densitometer, a refractometer is also used to analyze the concentration of the solution to cross check the measured concentration with the densitometer. For determining the CSD, a sample of slurry that is discharged from the crystallizer is taken after every 1hr on to a filter. After filtering, the product crystals are washed with ethanol so that there will be no mother liquor adhering to the crystals. The crystals are dried and analyzed offline with CILAS for determining the CSD. The crystallizer is then operated until the steady state is reached.

3.5 Experimental Results

As mentioned earlier, the parameters k_r and Γ_S for the growth rate of KCl crystals are unknown. For determination of these parameters, experiments are performed at different operating conditions of the crystallizer which are given in Table 3.1 (power input, residence time and temperature).

Description	Symbol	Value	Unit
Type of Crystallizer	DTB	-	-
Total slurry volume	V	22.4E-03	m^3
Concentration of solute in feed	c_{feed}	4.1	$\frac{mol}{l}$
Initial concentration of solute in the crystallizer	c_{sat}	3.99	$\frac{mol}{l}$
Temperature inside the crystallizer	T	293.15	K
Pumping capacity	N_{pump}	0.3	-
Impeller type	Propeller	-	-
Number of blades	a_{st}	3	-
Angle of blades	β_{st}	30	$^\circ$
Edge of the impeller	b_{edge}	0.002	m
Breadth of the impeller	b_{blade}	0.028	m
Impeller diameter	d_{st}	0.180	m
Draft tube diameter	d_{dt}	0.190	m
Impeller rotation speed	ω_{st}	400, 600, 800	$\frac{1}{min}$
Mean specific power input	ϵ	1.1, 1.8, 2.5	$\frac{W}{kg}$
Residence time	τ	26.7, 32.5	min

Table 3.1: Operating conditions and parameters of the KCl - $H_2 0$ system

Fig. 3.10 shows the typical progress of the median particle size L_{50} with respect to residence time. The mass median crystal size L_{50} is defined as the characteristic length up to which half of the overall crystal mass is reached. It is given by

$$k_v \rho_A \int_{L_0}^{L_{50}} L^3 F(L,t)dL = \frac{k_v \rho_A \int_{L_0}^{L_\infty} L^3 F(L,t)}{2} = \frac{m_S}{2} \qquad (3.1)$$

Initially, due to low supersaturation c/c_{sat}, the median particle size is small. The particle size increases with increase in supersaturation with a high driving force. After 5 residence times, the particle size decreases due to the formation of small crystals. The formation

52
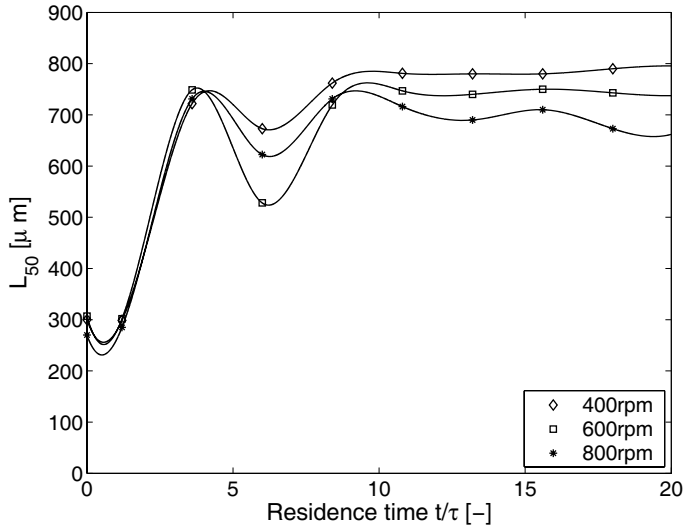
Figure 3.10: L_{50} Median crystal length vs. Time at different stirring speeds.

of small crystals is due to the attrition of large crystals with the stirrer of the crystallizer. In other words, it can be termed as high secondary nucleation rate. Due to the presence of a large number of attrition fragments, the total surface area of the crystals increases resulting in a decrease in supersaturation. The variation of supersaturation with respect to residence time is also shown in Fig. 3.11. After 8 -10 residence times, the mean particle size and supersaturation is almost steady. Experiments are performed at different stirrer speeds i.e. with 400 rpm, 600 rpm and 800 rpm. From Fig. 3.10, it is seen that as the stirrer speed is increased the mean particle size decreases. However, the decrease in mean particle size is not significant. In case of a stirrer speed of 400 rpm, the mean particle size at steady state is $800\mu m$. For stirrer speed of 600 rpm the mean particle size is $750\mu m$. From the above result it can be concluded that the KCl crystal is attrition resistant. This conclusion is consistent with the observations of Mersmann [51]. The observations are given in Table 3.3.

In case of a stirrer speed of 800 rpm, the mean particle size decreases further to a value of $670\mu m$. This can be explained in the following way. Due to the very high stirrer speed, the operation temperature in the crystallizer is increased by $1.5°C$ due to an additional amount
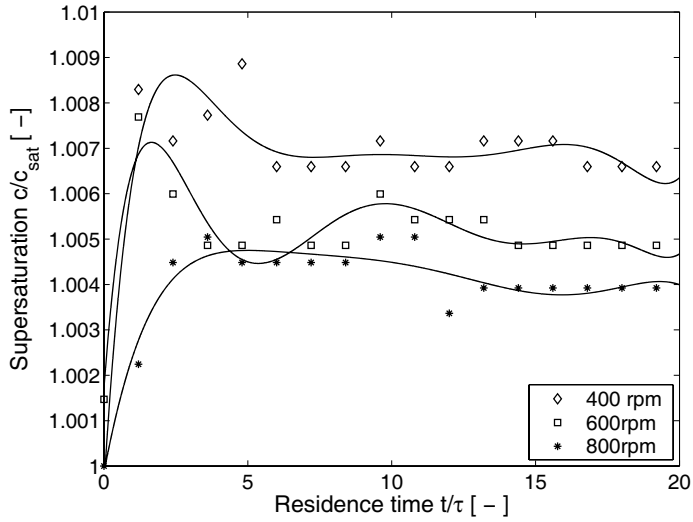
Figure 3.11: Supersaturation vs. Time at different stirring speeds

of energy added by agitation. This happened in spite of having a temperature controller inside the crystallizer. Subsequently, the driving force also decreases. This conclusion is further strengthened by observation of a decrease of supersaturation compared with other stirring speeds. Photographs of attrition resistant KCl crystals taken from microscope at different stirring speeds at steady state are shown in Fig. s 3.12, 3.13, 3.14. In the Fig. s 3.12, 3.13, 3.14, it shows that the corners of potassium chloride are not rounded. The above experimental results will then be used for the estimation of growth rate parameters.
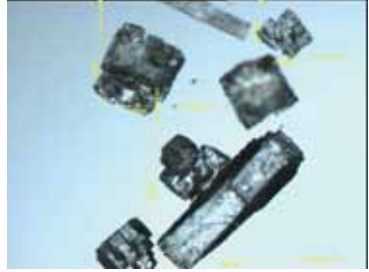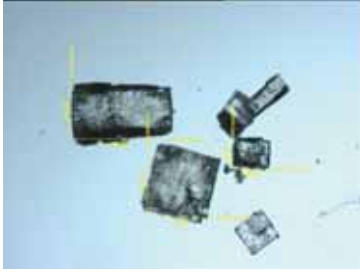
Figure 3.12: Photographs of KCl crystals with stirring speed of 400 rpm.
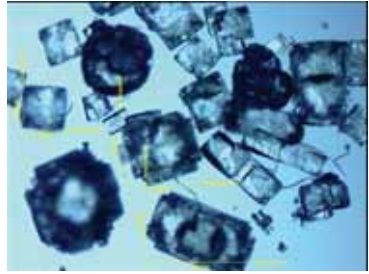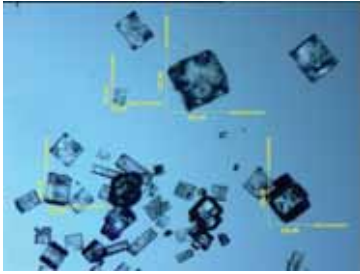
Figure 3.13: Photographs of KCl crystals with stirring speed of 600 rpm.
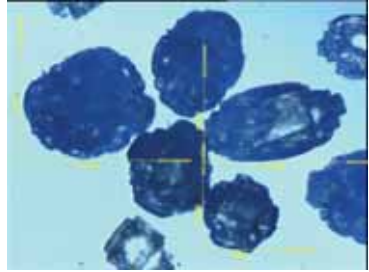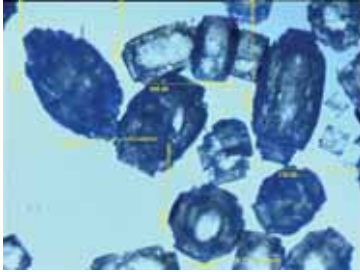
Figure 3.14: Photographs of KCl crystals with stirring speed of 800 rpm.

3.6 Estimation of Parameters

Estimation of the growth parameters k_r and Γ_S is a fitting process. They are estimated from the steady state values obtained from the experimental runs. For example, one can choose the median crystal size L_{50} as a measure of the number density function and super-
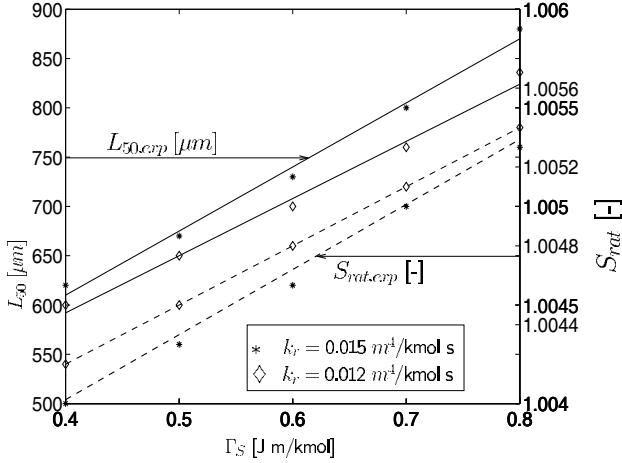
Figure 3.15: Determination of the growth parameters of KCl crystals in aqueous solution at $20°C$ from CMSMPR experiment $\bar{\epsilon}$ = 2.5 W/kg, τ = 26.7 min, m_t =15 kg/m^3.

saturation c/c_{sat} as a measure of concentration. Results from one experimental run will be used to estimate the parameters. For this, we consider the results of the experimental run with a stirring speed of 600 rpm and residence time $\tau = 26.7$ min.

Numerical simulation for the model 2 is performed under these set of operating conditions and with the some set of initial parameters for k_r and Γ_S. The steady state value that is obtained from the numerical simulation is compared with the experimental value. Fig. 3.15 is a plot between the median crystal size L_{50} (from numerical simulation) and Γ_S, with the supersaturation value (from the numerical simulation) on the secondary axis. Fig. 3.15 shows that the median crystal size increases with an increase in k_r, the growth rate of crystals. At the same time supersaturation decreases. However, with the increase in surface related strain energy Γ_S both supersaturation and median crystal size also increase. High values of Γ_S lead to dissolution of fragments and smaller values of total crystal surface for growth. From the experimental results only one combination of parameters will fit both supersaturation and median crystal size. From Fig. 3.15 the values are, $k_r = 0.015\,[m^4/kmols]$ and $\Gamma_S = 0.62\,[Jm/kmol]$.

3.7 Model Validation

With the above set of estimated parameters, a numerical simulation is performed under different sets of operating conditions given in Table 3.2. In order to check the consistency of the estimated values, the calculated data that is obtained from the numerical simulations is compared with the experimental data . The values are given in Table 3.2 and it shows a deviation of median crystal size from the experimental results which is less than 3% at higher stirrer speeds and around 10% at lower stirrer speeds. In case of supersaturation the deviation is less than 1%.

Operating conditions				Median size		Supersaturation	
Impeller speed	τ	c_{feed}	Temp	Exp	Theo	Exp	Theo
[1/min]	[min]	[mol/l]	[C]	μm	μm	[-]	[-]
400	26.7	4.1	20	820	920	1.006	1.0052
800	26.7	4.1	21.5	670	650	1.004	1.0042
600	32.5	4.1	20.0	780	800	1.0042	1.0042

Table 3.2: Calculated and experimental values of the median size and supersaturation obtained in a 20 litre DTB crystallizer for different operating conditions

The parameters that are obtained from the above experimental results will now be used for predicting the mean crystal size (which is the characteristic size used in the investigation of Beer & Mersmann [3]) for different crystallizer size and operating conditions. The experimental data are taken from Beer & Mersmann [3]. The DTB crystallizer (6 litre) was operated at a slightly higher temperature ($23°$C instead of $20°$C) than the considered pilot plant scale crystallizer (20 l). The mean size of the particles is given by

$$\bar{L} = \frac{\int_{L_0}^{L_\infty} FLdL}{\int_{L_0}^{L_\infty} FdL} \tag{3.2}$$

Table 3.3 shows that for all the experiments the calculated mean size is higher than the experimental value by approximately 10%. With respect to crystallization processes these deviations are considered to be very small.

From the above results, it can be concluded that model 2 of the continuous crystallizer (CMSMPR) is able to predict the steady state values for different operating conditions. Therefore, the given model 2 and the estimated parameters for KCl crystals will be used

Operating conditions				Mean size	
Impeller speed	τ	c_{feed}	Temp	Exp	Theo
[1/min]	[min]	[mol/l]	[C]	μm	μm
460	5	4.2743	23	340	410
600	5	4.2743	23	280	320
800	5	4.2743	23	210	250

Table 3.3: Calculated and experimental values of the median size and supersaturation obtained in a 6 litre DTB crystallizer for different operating conditions

in analyzing the nonlinear behavior of continuous crystallization processes which will be discussed in the next chapter.

3.8 Summary and Discussion

In this chapter, the experimental results for the KCl - $H_2 0$ system were presented. The two unknown parameters k_r and Γ_s of KCl crystals in aqueous solution were determined with one set of experimental results. These parameters will be used in determining the growth rate of crystals in model 2 of the KCl - $H_2 0$ system. Different operating parameters were changed to check the consistency of predicted result and experimental result. It was shown that the variation between the experimental and theoretical values is less than 10% in case of median crystal size and 3% in case of supersaturation.

In the next chapter, the nonlinear behavior of continuous crystallization processes for different operational modes will be addressed. For analyzing the nonlinear behavior of continuous crystallization processes two chemical systems will be considered. One is the crystallization of KCl and the other is $(NH_4)_2 SO_4$ from aqueous solution. By means of numerical bifurcation analysis, the instability regions are predicted for model 1 in the space of adjustable operating parameters like fines dissolution rate, classified product removal rate, residence time etc. For a finite number of operating points, dynamic simulations are carried out with model 2. The predictions by model 2 are compared to the predictions by model 1 in terms of stability, evolution of mass density function (MDF) and the mass median crystal size L_{50}. Finally, the influence of non-ideal fines classification as proposed by Mitrović [57] is studied.

Chapter 4

Stability Analysis

The main aim of this work is the theoretical prediction and analysis of the non-linear behavior of crystallization processes. In this chapter, the results of the numerical bifurcation analysis of continuous crystallization processes are presented. The influence of the most important parameters on crystallizer stability is studied. These are the operational parameters R_1, the recycle ratio of the fines dissolver, R_2, the recycle ratio of the product classification, and the residence time τ (see Fig. 2.3 and Equation 2.17 and 2.20 where R_1 and R_2 are introduced).

As a first step towards the theoretical analysis a fairly simple population balance model (model 1) including fines dissolution and classified product removal is considered. By means of numerical bifurcation and stability analysis, regions in the parameter space of the operating conditions and the physical properties with periodic behavior are predicted. Due to the simplicity of the underlying model the results are only of qualitative nature. Further the work is extended by prediction of the nonlinear behavior of the more detailed model (model 2).

For the subsequent numerical bifurcation analysis the simulation environment DIVA is used (see e.g. Mangold et al. [47] and references therein). DIVA provides continuation methods for the direct calculation of parameter dependent steady state and periodic solution branches. During the calculation, the stability of the corresponding solution is monitored and bifurcation points are detected and located. The continuation can be restarted from Hopf bifurcation and limit points to trace out the Hopf and limit point curves in a two dimensional parameter plane. These curves represent critical boundaries, which divide the parameter space into regions with qualitatively different patterns of behavior.

The methods are based on standard techniques, which are specially tailored to handle large sparse systems of differential algebraic systems (DAEs) with index 1 (see Mangold et al. [47], Kienle et al. [29]). For an introduction to the basic concepts of nonlinear system analysis using continuation methods the reader is referred to [38, 78].

In the first part of the work, focus is on the nucleation exponent b representing the physical system. As a base case the KCl - H_2O system is considered with parameters taken from Vollmer & Raisch [85] and given in Table C.1. In the second part of the work, the stability of the system is investigated with various operational parameters like fines and product cut size, fines dissolution rate and classified product removal rate.

4.1 Influence of the Nucleation Exponent

First, the influence of the nucleation exponent b is studied using model 1 for vanishing recycle ratios R_1, R_2 and τ according to Tab. C.1. This corresponds to a CMSMPR
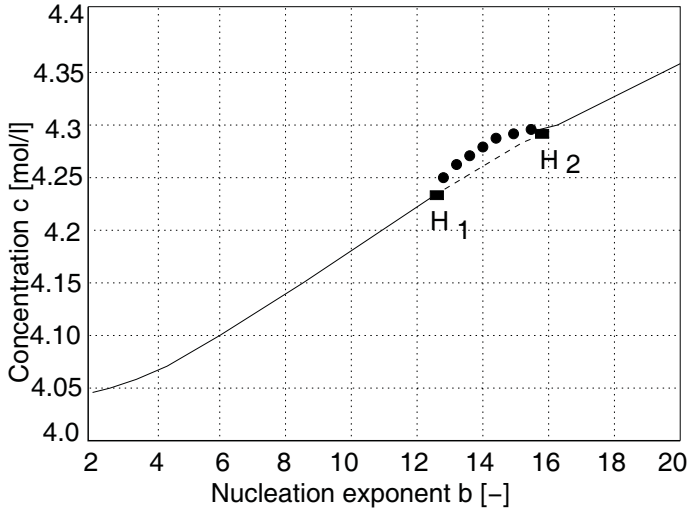
Figure 4.1: Bifurcation diagram concentration vs. nucleation exponent for $R_1, R_2 = 0, \tau = 300$ min. Solid line – stable steady state solutions, dashed line – unstable steady state solution, bullets – amplitude of periodic solutions, boxes – Hopf bifurcation points.

crystallizer without fines dissolution and product classification. The bifurcation diagram of the CMSMPR crystallizer is shown in Fig. 4.1. It shows a branch of steady state solutions represented by the solid and the dashed lines, respectively. For low and very high nucleation exponents the steady state solution is stable, which is indicated by the solid line. In between, the steady state solution is unstable, which is indicated by the dashed line.

Stability changes at two Hopf bifurcation points H_1 and H_2, where a conjugate complex pair of eigenvalues crosses the imaginary axis. These Hopf points give rise to a branch of periodic solutions indicated by the bullets in Fig. 4.1. They represent the amplitude, with which the crystallizer oscillates around the unstable steady state. Since R_1 and R_2 are equal to zero, these oscillations correspond to the so-called high order cycling [73]. It occurs in Fig. 4.1 for nucleation exponents between 12 and 16, which is much higher than in most physical systems. Some typical values of the nucleation exponent for different physical systems are given in Tab. 4.1 according to [60]. For the KCl - H_2O system a
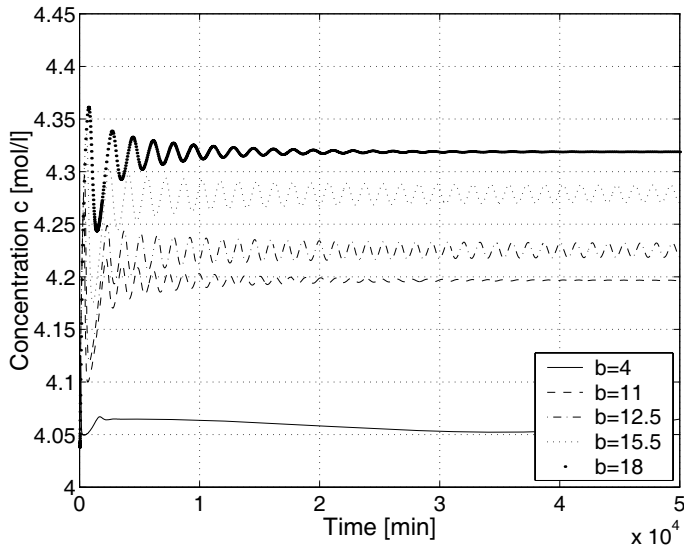
Figure 4.2: Dynamic transient behavior for different nucleation exponents in Fig. 4.1.

System	Mode of crystallization	Kinetic order
Calcium sulfate/phosphoric acid	Precipitation	2.6-2.8
Ammonium sulfate/water	Cooling	1.7
Ammonium alum/water	Cooling	2.1
Ammonium alum/water/ethanol	Salting out	1.0
Ammonium alum/water/methanol	Salting out	4.0
Sodium chloride/water/ethanol	Salting out	9.0
Ammonium alum/water/ethanol	Salting out	2.0
Potassium Chloride/water	Cooling	4.0
Cyclonite-water/nitric acid	Precipitation	1.0

Table 4.1: Kinetic order reported for various crystal systems [60].

value of $b = 4$ was reported. Hence, it is readily seen from Fig. 4.1 that for the KCl - H_2O system no instability occurs without product classification and fines dissolution.
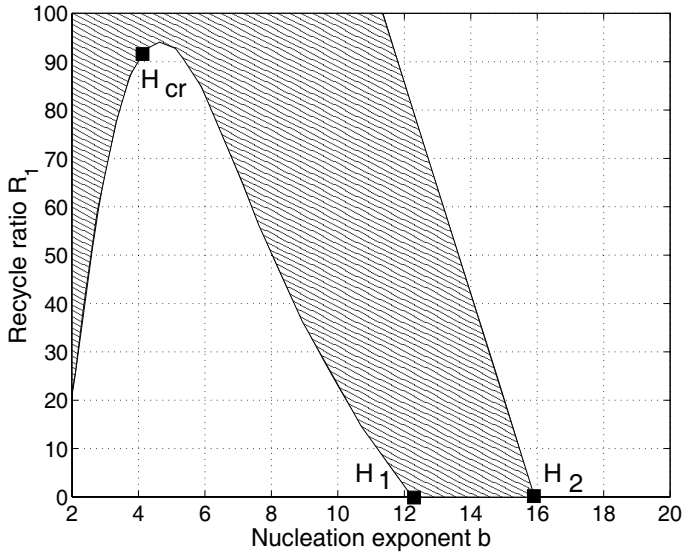
Figure 4.3: Instability region in the R_1/b-plane for $R_2 = 0, \tau = 300$ min.

The dynamic transient behavior for different nucleation exponents in Fig. 4.1 is shown in Fig. 4.2. The transient behavior shows the expected self sustained oscillations for nucleation exponents in the range of 12 to 16. As an initial condition for performing dynamic simulations shown in Fig. 4.2, the liquid is saturated and no crystals are present in the crystallizer.

Next, the influence of R_1, the recycle ratio of the fines dissolver, on the location of the Hopf points is investigated. For that purpose a two-parameter continuation is used to

(a) for $R_1 = 0$

(b) for $R_1 = 70$

(c) for $R_1 = 94$

(d) for $R_1 = 98$
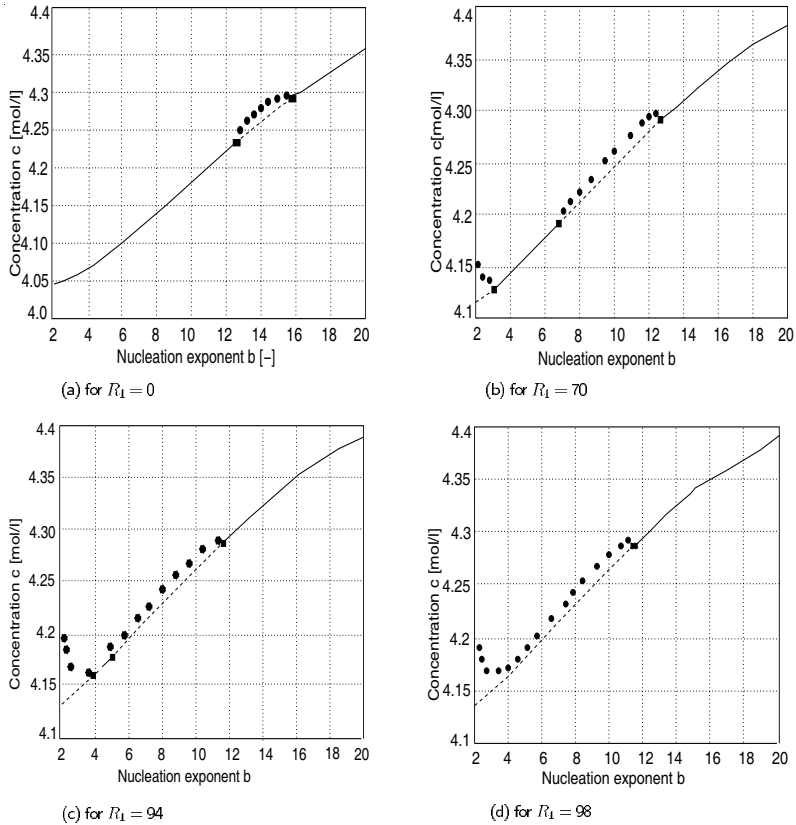
Figure 4.4: Bifurcation diagrams c/b for different values of R_1 in Fig. 4.3.

directly trace out the curves of Hopf bifurcation points in the R_1, b-plane starting at H_1 and H_2 for $R = 0$ in Fig. 4.1. The results are shown in Fig. 4.3. Oscillatory behavior occurs for parameter combinations within the shaded region of this figure. For $R_1 = 0$, instability again occurs for nucleation exponents in the range of 12 to 16. For decreasing nucleation exponents the instability region is shifted to higher recycle ratios R_1. At a value of $b = 5$ the instability region is shifted again to lower recycle ratios. Consequently, at recycle ratios of about between 20 and 90 oscillations can occur for either very high or low nucleation exponents. This is a surprising feature, which was previously not reported in the literature to the best of our knowledge. This is also illustrated in Fig. 4.4, which shows the corresponding bifurcation diagrams for different values of R_1 in Fig. 4.3. The first is identical with Fig. 4.1. For intermediate values of R_1 (next two diagrams in Fig. 4.4) three Hopf points with two branches of periodic solutions can be observed, one at low and one at high nucleation exponents. Beyond the critical point H_{cr} in Fig. 4.3, these two branches of periodic solutions merge and instability occurs over a wide range of b. This situation is shown in the fourth diagram in Fig. 4.4.

For the KCl - H_2O system the nucleation exponent b is equal to 4 and instability only occurs for very high recycle ratios R_1 close to 90 as can be directly seen from Fig. 4.3.
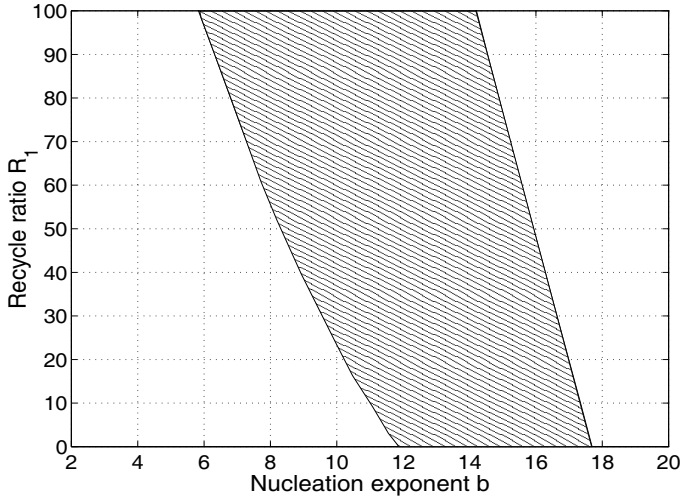
Figure 4.5: Instability region in the R_1/b-plane for $R_2 = 0, \tau = 400$ min.

Next, the influence of residence time τ and product recycle ratio R_2 is studied by means of instability regions in the R_1/b-plane for different values of τ, R_2. The influence of residence time is illustrated in Fig. 4.5. By comparison with Fig. 4.3, we find that the instability region is increased at higher residence time. Instability for small nucleation exponents disappears. Consequently, for the KCl - H_2O system $(b = 4)$, no instability occurs in the range of R_1 values plotted in Fig. 4.5.

At higher recycle ratios R_2, the instability region is shifted to the left as shown in Fig. 4.6 compared to Fig. 4.3. Consequently, instability will also occur at lower exponents and lower fines recycle ratios for crystallizers with classified product removal. This results is consistent with earlier observations by Randolph [72], Randolph & Larson [73], Kind & Nieken [34], Kind & Lieb [31]. For the KCl - H_2O system $(b = 4)$ instability now occurs also for much smaller values of R_1.
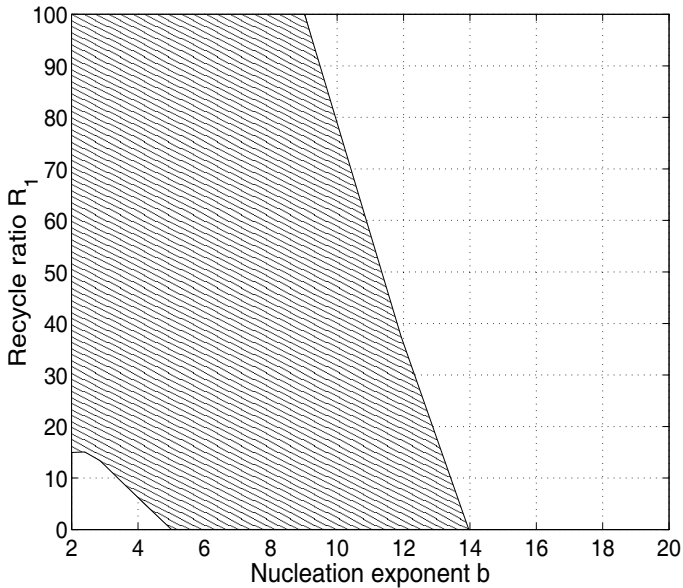
Figure 4.6: Instability region in the R_1/b-plane for $R_2 = 5, \tau = 300$ min.

4.2 Studies on the Stability of the KCl - H_2O System
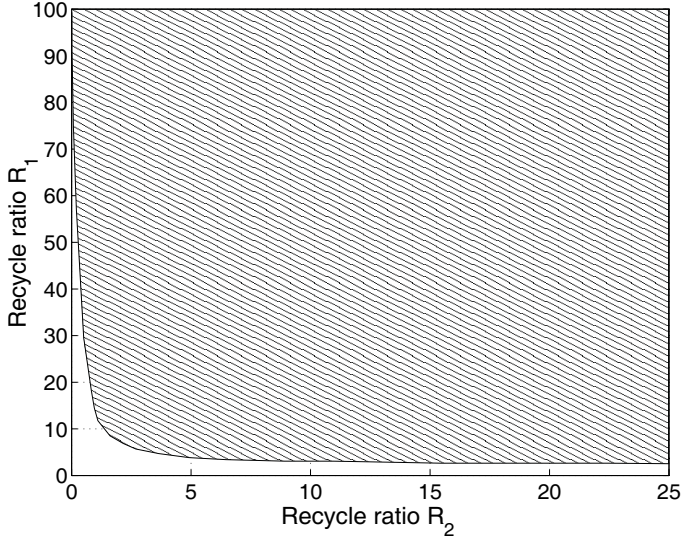
Figure 4.7: Instability region in the R_1/R_2-plane of the KCl - H_2O system ($b = 4$), for $\tau = 300$ min, L_f=0.2 mm and L_p=1 mm

Further insight into the influence of the recycle ratios R_1 and R_2 on the stability of the specific KCl - H_2O system with $b = 4$ is shown in Fig. 4.7. From Fig. 4.7 we conclude that without fines dissolution the crystallizer is stable for any ratio R_2. Instead, without product classification instability can occur only at large values of the fines recycle rate R_1 of about 90 (see also Fig. 4.3). Further, we find that at fines recycle rates R_1 greater than five, instability occurs also for rather small product recycle rates R_2.

It is important to note, that these results also depend on the product and the fines cut sizes L_p and L_f. The influence of the two cut sizes is illustrated for the KCl - H_2O system in Fig. 4.8, which should be compared to the base case in Fig. 4.7. The two diagrams on the left of Fig. 4.8 show the instability regions in the R_1/R_2 parameter plane for an increased (Fig. 4.8a) and a decreased (Fig. 4.8b) product cut size L_p compared to the base case in Fig. 4.7, whereas the two diagrams on the right show the instability regions for an
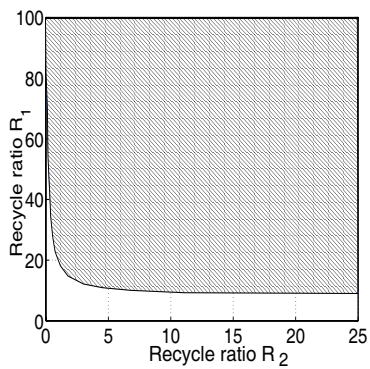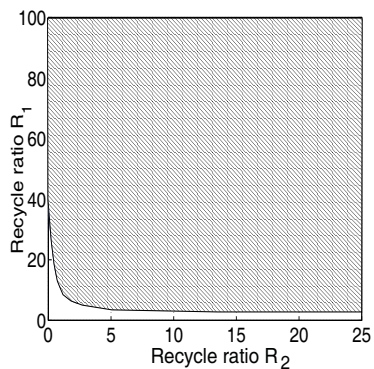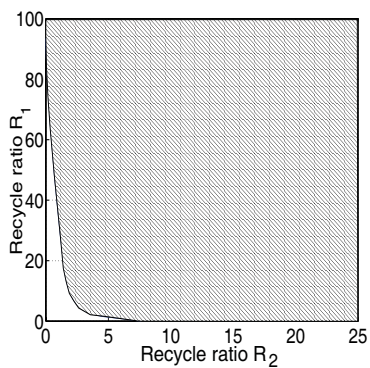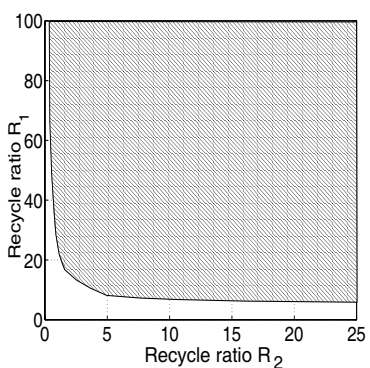
Figure 4.8: Instability regions in the R_1/R_2-plane for the KCl - H_2O system ($b = 4$), for $\tau = 300$ min and for different values of the product cut size L_p and the fines cut size L_f with reference to Fig. 4.6

increased (Fig. 4.8c) and a decreased (Fig. 4.8d) fines cut size L_f compared to the base case in Fig. 4.7. It is shown that the instability region is getting larger – i.e. also extends to lower recycle ratios R_1 – for a lower product cut size. In particular, for a lower product cut size oscillations are also possible without fines dissolution ($R_1 = 0$).

A reverse effect is found with regard to the fines cut size L_f in Figs. 4.8c, 4.8d. Here, the instability region increases with increasing fines cut size. In particular, for the higher fines cut size $L_f = 0.3$ mm in Fig. 4.8c oscillations are possible without product classification ($R_2 = 0$) at comparably low values of the fines recycle rate R_1 (≈ 40 compared to ≈ 90 in Fig. 4.7).

The influence of the product cut size on the nature of the oscillations is illustrated in Fig. 4.9 for $R_1 = 20$ and $R_2 = 5$ in Fig. 4.8a. Fig. 4.9 shows the mass density distribution at different characteristic times during one cycle of the oscillation which takes about 1100 min in the present case. In the beginning a large number of nuclei is formed due to high supersaturation. Then the nuclei start growing. Thereby supersaturation and hence the formation of new nuclei is decreased. Because of crystal growth the mass density distribution of the crystals increases and moves towards larger crystal sizes. As soon as the peak approaches the product cut size of 1.5 mm in Fig. 4.9, product is withdrawn and the peak is fading at lengths around the product cut size. Hence, the supersaturation in the liquid phase is increasing again and new nuclei are formed, which start to grow again.

Because the growth rate in model 1 does not depend on the crystal size, the time for the crystals to reach the product cut size is almost proportional to the cut size. Hence, the period of the oscillations is also almost proportional to the product cut size. In simulation studies we found cycle times of about 500 min, for $L_p = 0.5$ mm and 800 min, for $L_p = 1.0$ mm compared to 1100 min, for $L_p = 1.5$ mm in Fig. 4.9. The other parameters were the same in all three cases. In reality, the growth rate usually increases with increasing crystal length [73]. Hence, in practice the increase of cycle time with increasing product cut size is expected to be smaller.
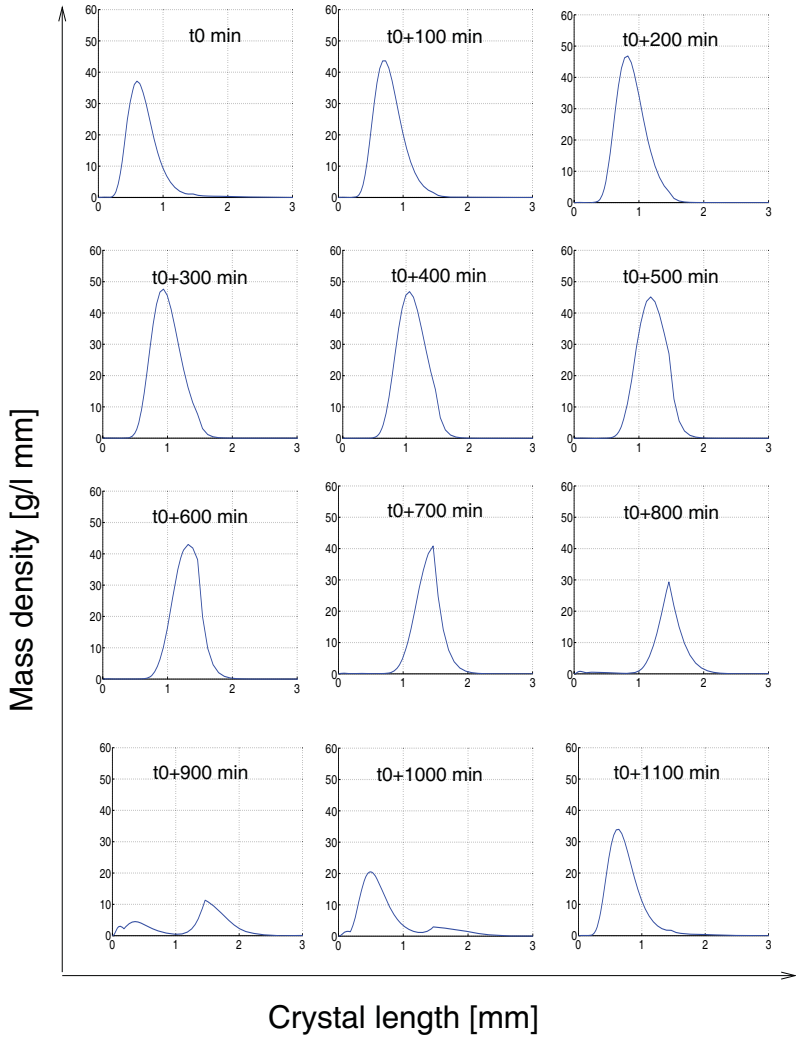
Figure 4.9: Periodic behavior of the mass density distribution of the KCl - H_2O system $(b = 4)$, for $\tau = 300$ min, $R_1 = 20$, $R_2 = 5$, $L_f = 0.2$ mm and $L_p = 1.5$ mm.

4.2.1 Comparison between Model 1 and Model 2

So far the influence of different operational parameters like fines cut size, product cut size, classified product removal rate and fines dissolution rate on the stability of the system is studied. Emphasis in this section is on stability of the KCl - H_2O system with fines dissolution and classified product removal with a particular classified product cut size and fines cut size. The predictions of model 1 will now be compared with the theoretical predictions of model 2 with complex kinetics involving breakage of crystals due to attrition with the stirrer.
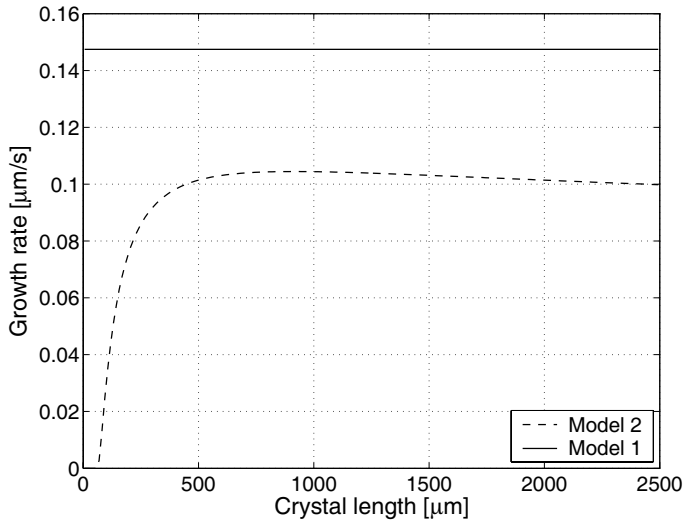
Figure 4.10: Comparison of growth rates for model 1 and model 2 at steady state for KCl - H_2O system.

It should be noted that the prediction of instability regions is done so far is for a DTB crystallizer of 10.5 litre volume and for a residence time of $\tau = 300$ min. However, due to non-availability of the crystallizer dimensions like the draft tube diameter d_{dt}, number of stirrer blades a_{st} etc which are necessary to predict the CSD for model 2, the crystallizer that has been used in the experiments for estimating growth rate parameters is considered. The physical, chemical and operational parameters are given in Appendix

B and C. As a first step it is good to compare the kinetics of two models. The growth rates of two models at steady state are shown in Fig. 4.10. Fig. 4.10 is a plot of growth rate versus crystal length. From Fig. 4.10, it is shown that the growth rate of model 1, which is size independent, has a steady state value of around 0.15 μm/s for all crystal lengths. For model 2, the curve shown in Fig. 4.10 indicates how the growth rate of the crystals changes with length. Fig. 4.10 shows that the growth rate is small for smaller crystal lengths and increases steadily as the length of the crystals increases and thereafter remains almost constant beyond some specific crystal length. As shown in Fig. 4.10, the growth rate of two models do not differ significantly and therefore the two models are reasonably comparable.

For studying the origin and parameter dependent behavior of the oscillations, a numerical bifurcation analysis of model 1 is done using the DIVA simulation environment [37]. Using the two parameter continuation method available in the DIVA simulation environment [47], a bifurcation diagram is obtained for the operating parameters R_1 and R_2 (Fig. 4.11) for a residence time of $\tau = 50$ min. The classified product size and fines cut size
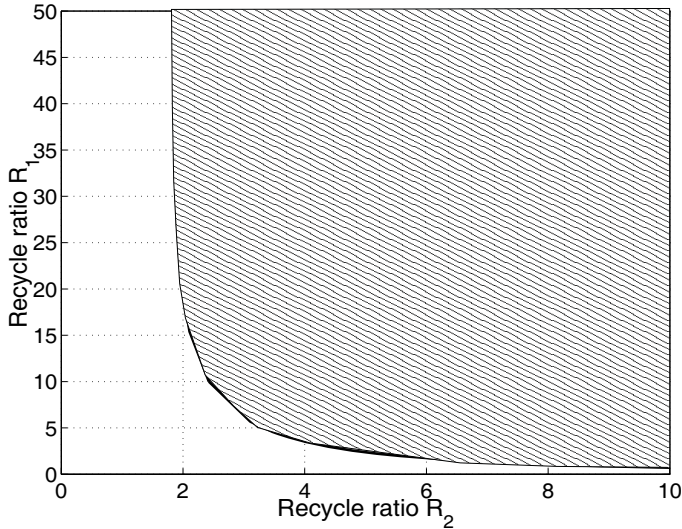
Figure 4.11: Instability region in the R_1/R_2 plane for the KCl - H_2O system predicted by model 1 for $\tau = 50$ min.

are $L_p = 1000\mu m$ and $L_f = 200\mu m$ respectively. The curve in Fig. 4.11 represents the locus of Hopf bifurcation points in the R_1/R_2 plane, where the system changes from stable to unstable. Oscillatory behavior occurs for the parameter combinations within the shaded region of Fig. 4.11. Without product classification i.e. $R_2 = 0$, the system is stable even for a high fines recycle ratio R_1. However, as the classified product recycle ratio R_2 is increased, the instability occurs for a high fines recycle ratio of $R_1 = 39$.

Further, the figure reveals that as the classified product removal rate is increased, the crystallizer tends to oscillate at low fines dissolution rates. Moreover, the system tend to oscillate with increasing fines dissolution rate and classified removal rate above $R_1 = 39$ as shown in Fig. 4.12. However, the industrial crystallizers are generally operated at recycle ratio R_1 not more than 30 [34, 31]. Here the shape of the Hopf bifurcation point curve must be noted, as it will be helpful for further analysis. Because, these results are produced with model 1, they are expected to be only qualitative in nature. In the following, they are compared with the results from model 2.
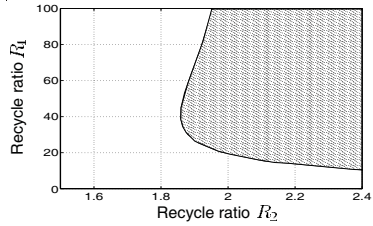
Figure 4.12: Instability region in the R_1/R_2 plane for the KCl - H_2O system predicted by model 1 for $\tau = 50$ min.

For that, a detailed crystallizer model having attrition, nucleation and size dependent growth rate is considered. Due to the complexity of model 2, it is very difficult to predict the instability region. Therefore, point wise dynamic simulation is carried out for model 2 in the instability and stability regions shown in Fig. 4.11. Several fines dissolution rates R_1 and classified product removal rates R_2 are chosen and the corresponding results are presented in Fig. 4.13. The ▲ points in Fig. 4.13 represent simulation results of the system that are stable, and the • points represent simulation results showing sustained oscillations. It is evident from Fig. 4.13, that the behavior predicted by model 2 is not in good agreement with that predicted by model 1 in some cases. The possible explanation could be due to inaccurate estimation of nucleation and growth rates for model 1. These rates were determined for a crystallizer of 10.5 litre volume with low residence time. It is known from literature that nucleation and growth rate might change with respect to the residence time, the hydrodynamic behavior, the type of stirrer etc. Therefore, effort has been made to predict the instability region for model 2 using point wise dynamic
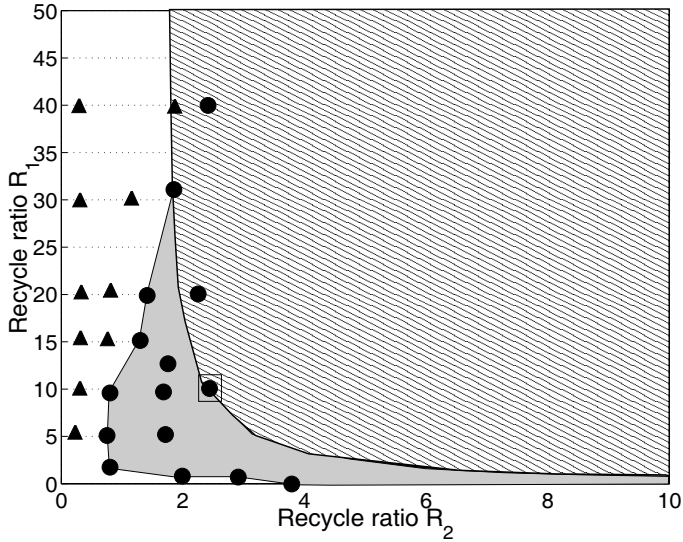
Figure 4.13: Comparison of instability regions of KCl - H_2O system predicted by model 1 with predictions by model 2 for $\tau = 50$ min with ▲ - stable solution and ● - periodic solution.

simulation. Because of high computational effort involved, it is very difficult to predict the whole instability region and therefore a rough estimation is presented in Fig. 4.13. The gray region which is partly overlapped by the shaded region predicted by model 1, represents the instability region predicted by model 2. From the figure it is shown that the instability region increases for model 2, however, the shape of the instability region is very similar to the one shown in Fig. 4.12.

To gain further insight into the dynamic behavior of the two models, dynamic simulations are performed for fines dissolution rate $R_1 = 10$ and a classified product removal rate $R_2 = 2.5$. Fig. 4.14 and Fig. 4.15 show the simulation results of the mass density distribution for model 1 and model 2 at different characteristic time during the cycle of oscillations. The period of the oscillation for model 1 is 5537 sec and for model 2 is 6500 sec. Since the figures are very similar to the one presented in the next section, a combined explanation is provided there. Compared to the period of the oscillations that is obtained
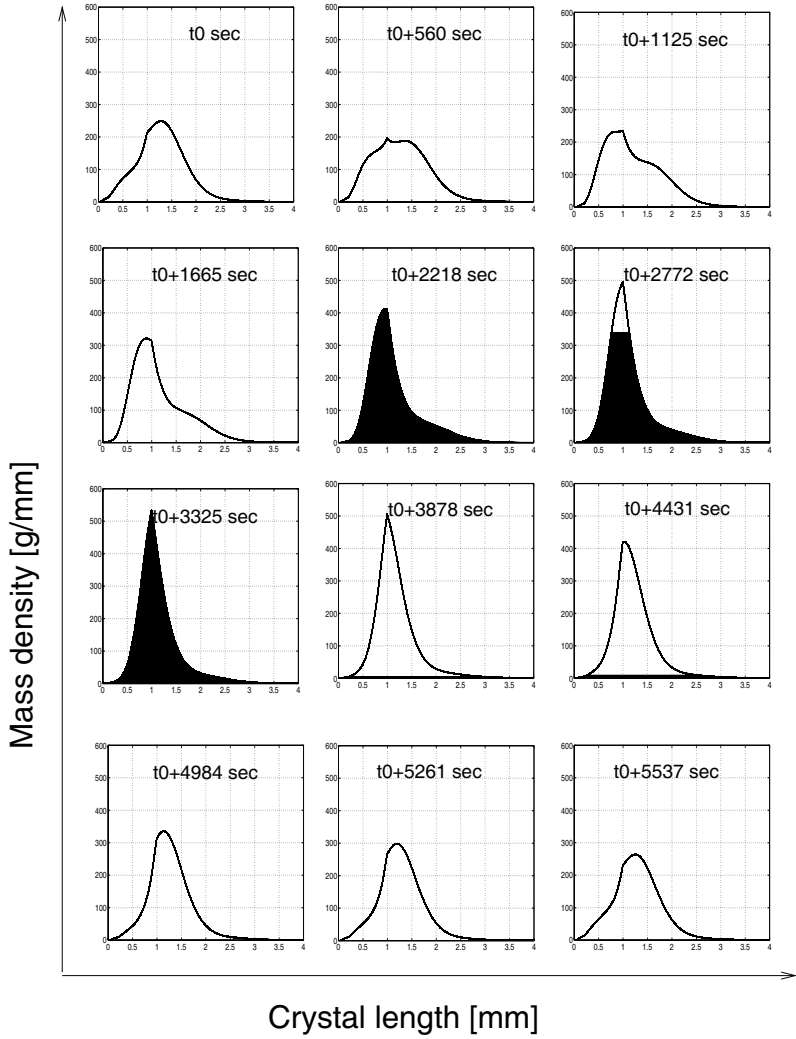
Figure 4.14: Periodic behavior of the mass density distribution of the KCl - H_2O system for model 1 for $R_1 = 10$, $R_2 = 2.5$, $L_p = 200$ μm, $L_f = 1000$ μm and $\tau = 50$ min.
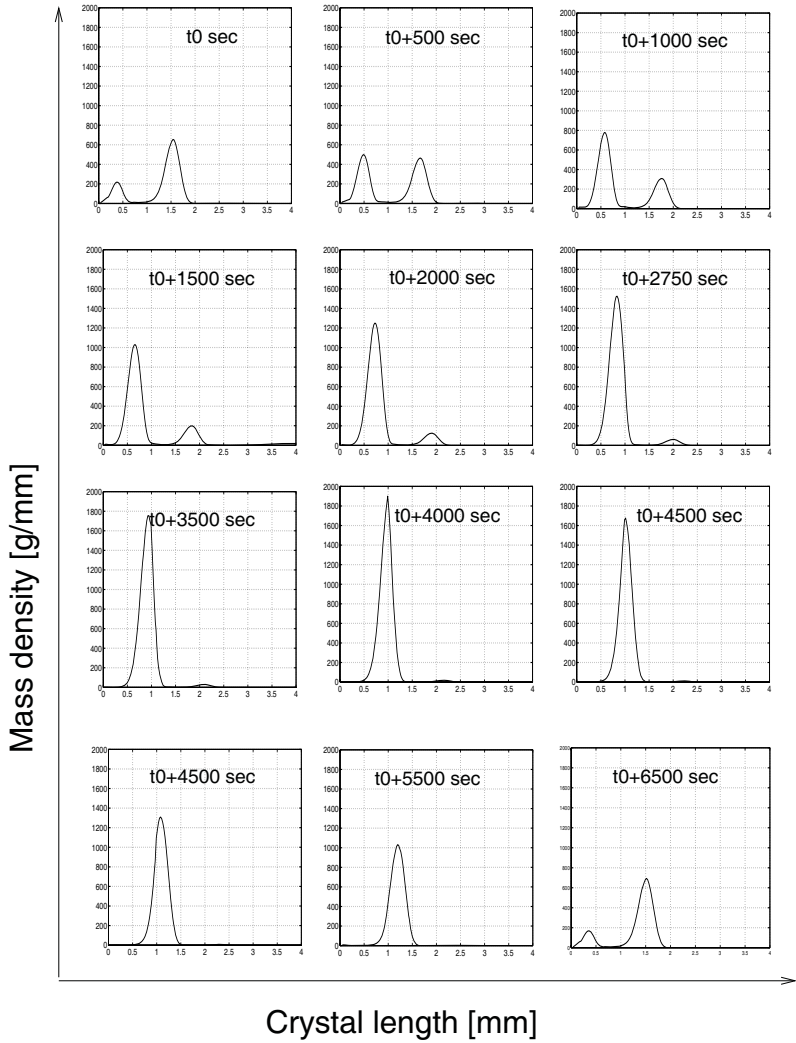
Figure 4.15: Periodic behavior of the mass density distribution of the KCl - H_2O system for model 2 for $R_1 = 10$, $R_2 = 2.5$, $L_p = 200$ μm, $L_f = 1000$ μm and $\tau = 50$ min.

with model 2, the time period of oscillations for model 1 is larger. The physical reason behind this is that the growth rate for model 1 is higher and crystals reach the product cut size faster than the crystals in model 2. Furthermore, attrition in model 2 has a large influence on the evolution of the mass density function in Fig.4.15.
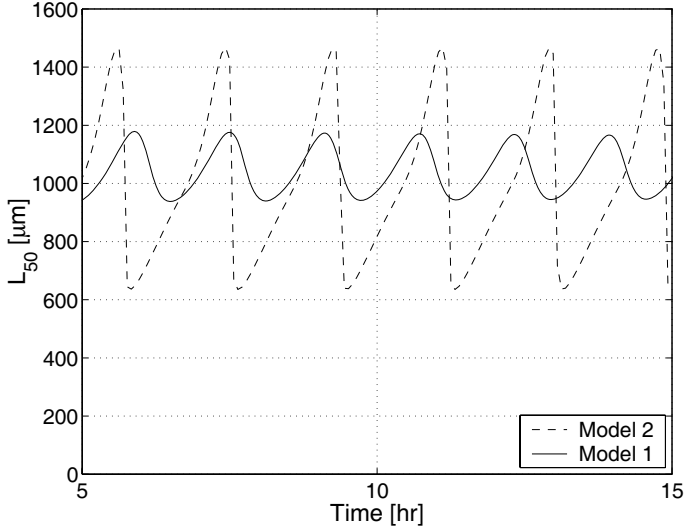
Figure 4.16: Comparison of L_{50} for particular operating parameters of the KCl - H_2O system for model 1 and model 2, for $R_1 = 10$, $R_2 = 2.5$, $L_p = 1000$ μm, $L_f = 200$ μm and $\tau = 50$ min.

The L_{50} of the two models are also compared in Fig. 4.16. The solid line in the figure represents L_{50} of model 1, and the dashed line represents L_{50} of model 2. From the figure, it is evident that the period of oscillation predicted by model 1 is smaller than that predicted by model 2. The physical explanation for this is that in model 1 the growth rate is a little larger than that in model 2, as discussed earlier. Also, the amplitude of the oscillations for model 1 is low as compared to model 2. This could be due to attrition which generates lot of small crystals, which in turn lead to large amplitude of oscillations.

4.3 Studies on the Stability of the $(NH_4)_2SO_4$ - H_2O System

In this section, the focus is on nonlinear oscillations of ammonium sulphate crystallization. This system has been studied intensively in the past and can be viewed as a standard test system for crystallization processes. The focus is on crystallizers with fines dissolution and classified product removal. Using methods from numerical bifurcation analysis, we investigate how stability in such a system depends on the various operational parameters, like cut sizes and recycle rates of fines dissolution and product classification.

Theoretical predictions of three different population models are compared with each other: (i) a model with simple kinetics and ideal fines classification (model 1), (ii) a model with complex kinetics involving breakage due to attrition and ideal fines classification (model 2), and (iii) a model with simple kinetics and non-ideal fines classification (model 3).

4.3.1 Comparison between Model 1 and Model 2

For the study of nonlinear oscillations, crystallization of an ammonium sulphate-water $((NH_4)_2SO_4$ - $H_2O)$ system in a 1100 litre DTB crystallizer is considered. The physical, chemical and operational parameters of this system for both models are taken from work by Mitrović [57], Kind & Lieb [31] (see Appendix C). It should be noted that the crystallizer considered here is actually operated in an evaporative mode, where a solvent is evaporated for creating supersaturation and the concentration of the feed is saturated at the operating temperature of the crystallizer. Instead of including the evaporation explicitly in the continuous phase balance for models 1 and 2, the driving force in terms of supersaturation can be created by adjusting the flow rate of the feed and feed concentration in such a way that a supersaturated liquid is fed accordingly. Moreover, it must be noted the parameters for model 1 have been estimated in a 1 litre DTB crystallizer [33].

For comparison of two models their kinetics is considered. At steady state the growth rate of two models is compared as a first step. The result is depicted in Fig. 4.17. The growth rate for model 1 is size independent. The steady state value for all crystals is 0.032 μm/s. In contrast, the growth rate for model 2 is size dependent. It is small for smaller crystals. As shown in Fig. 4.17, the growth rate increases with crystal length and thereafter remains
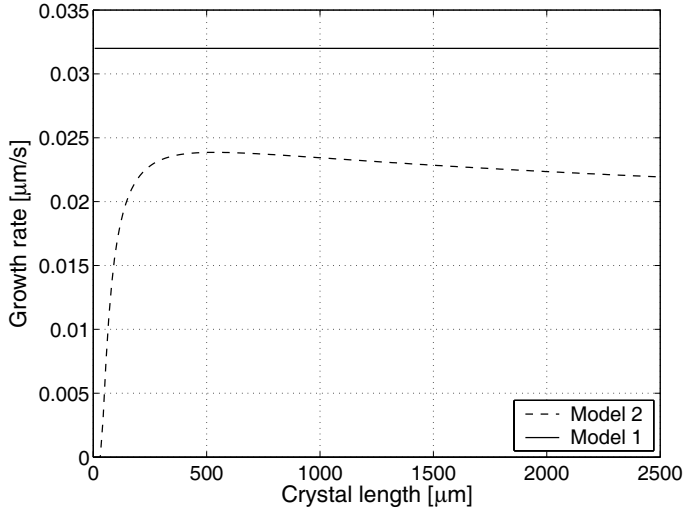
Figure 4.17: Comparison of growth rates of the $(NH_4)_2SO_4$ - H_2O system for model 1 and model 2 at steady state for $\tau = 75$ min.

almost constant beyond some specific length. In comparison with Fig. 4.10 for the KCl - H_2O system the growth rates difference between the two models is smaller.

Similar to Fig. 4.11, a bifurcation diagram Fig. 4.18 for model 1 is obtained for the operating parameters R_1 and R_2. This will be used to study the origin and parameter dependent behavior of the oscillations of the system. The other operating parameters pertaining to the Fig. 4.18 are for residence time $\tau = 75$ min, classified product cut size $L_p = 800$ μm and fines cut size $L_f = 300$ μm respectively. The system stability is represented by the locus of Hopf bifurcation points in the R_1/R_2 plane. This is depicted as curve in Fig. 4.18. The shaded region represents the oscillatory behavior of the system. For no classified product removal, the system is unstable for high recycle ratio of $R_1 = 73$. This value is an unrealistically high with respect to the operation of industrial crystallizers. Therefore, it is not shown in the figure. Further, the figure reveals that, as the classified product removal rate is increased, the crystallizer tends to oscillate at low fines dissolution rates. Since the nature of results that are produced by model 1 are qualitative and therefore, they will be compared with model 2.
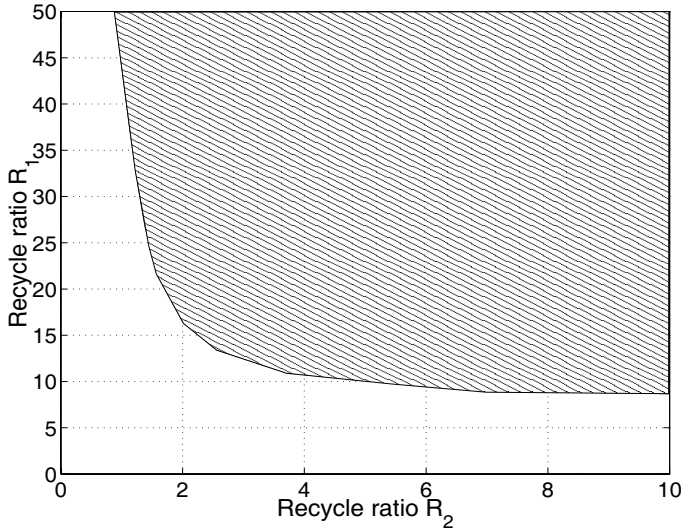
Figure 4.18: Instability region in the R_1/R_2 plane of the $(NH_4)_2SO_4$ - H_2O system predicted by model 1 for $\tau = 75$ min.

For model 2 point wise dynamic simulation is carried out for different parameter combinations of R_1 and R_2. This is done in the stability and instability region of Fig. 4.18. The results are depicted in Fig. 4.19. Simulation results of the system that are stable are represented as ▲ points in Fig. 4.19. Similarly, the ● points represents the system showing sustained oscillations. From Fig. 4.19, it is evident that the behavior of model 2 is in good agreement with the predicted behavior from model 1. These results for the $(NH_4)_2SO_4$ - H_2O system are in contrast to the previous section for the KCl - H_2O system. It is conjectured that this good agreement is due to much better agreement of the growth rates in Fig. 4.17 compared to Fig . 4.10.

Some of the results obtained by dynamic simulation for model 2 are shown in Figs 4.20, 4.21. Fig. 4.20 shows the progress of L_{50} with respect to time in the stability region near the locus of Hopf bifurcation points in the R_1/R_2 parameter plane of Fig. 4.19. For operating parameters $R_1 = 30$ and $R_2 = 1.0$, the system becomes stable around 90 hrs. However, for operating parameters $R_1 = 20$ and $R_2 = 1.2$, i.e. very near the locus of Hopf bifurcation point the system takes more than 90 hrs to become stable.
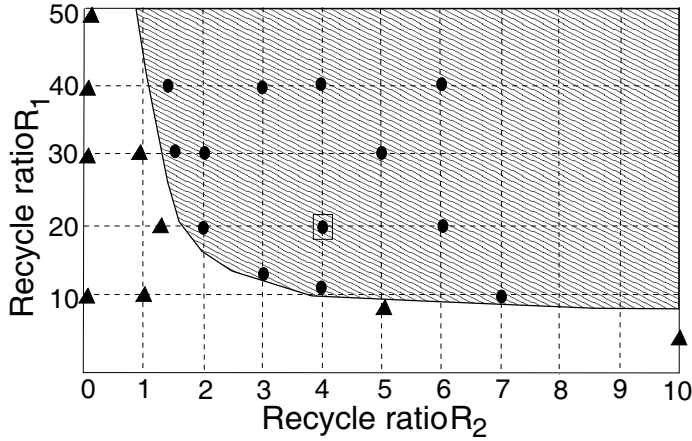
Figure 4.19: Comparison of instability regions of the $(NH_4)_2SO_4$ - H_2O system predicted by model 1 with predictions by model 2 for $\tau = 75$ min with ▲ - stable solution and • - periodic solution.

Similarly, Fig. 4.21 shows the progress of L_{50} with respect to time in the instability region near the locus of Hopf bifurcation points in the R_1/R_2 parameter plane of Fig. 4.19. For operating parameters $R_1 = 20$ and $R_2 = 2.0$, the system starts oscillating periodically after 20 hrs while for $R_1 = 30$ and $R_2 = 1.5$ the system oscillates periodically after 40 hrs. As expected if the operating parameters are near the locus of Hopf bifurcation points on the either side of the locus, it takes more time for the system to approach the attractor.

To gain further insight in the dynamic behavior of the two models, dynamic simulation are performed for a fines dissolution rate $R_1 = 20$ and a classified removal rate $R_2 = 4$. Fig. 4.22 shows the simulation result of the mass density distribution for model 1 at different characteristic times during the cycle of oscillations. In this figure, time advances from the top left to the bottom right in rows. In the beginning, there are a large number of nuclei due to high supersaturation represented by the first peak. A second peak represents some big crystals that are present in the crystallizer that are in the process being removed from the crystallizer. As time progresses, the crystals grow towards larger crystal lengths, and that is why the mass density function of the first peak increases towards larger crystal lengths. The second peak is slowly fading away as a result of product removal. As the crystals reach the product cut size of $L_p = 800$ μm, they are removed and the peak starts
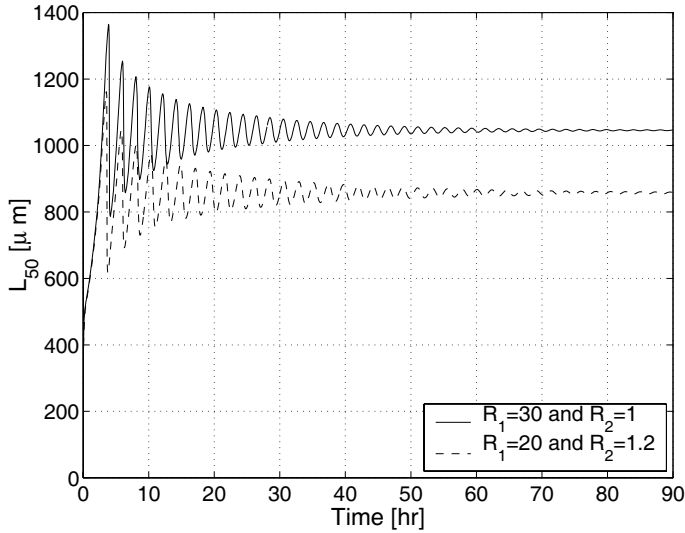
Figure 4.20: L_{50} for particular operating parameters of the $(NH_4)_2SO_4$ - H_2O system within the stability region predicted by model 2 for $\tau = 75$ min.

decreasing. The supersaturation increases, and again new nuclei are formed after one cycle. The time period of this oscillation is 7500 s.

A similar dynamic simulation is done for model 2 with the same initial conditions that were used for model 1. The mass density distribution is shown in Fig. 4.23 for the same operational parameters that were taken for the simulation of model 1. The dynamic behavior can be explained in the following way. Initially, crystals are present at smaller crystal lengths and larger crystal lengths. The smaller and larger crystals are formed as a result of the attrition process, which is represented by a bimodal distribution. In addition to this, there is a very small peak at very small lengths. These crystals are called crystals of zero growth rate, as explained in the previous section. As time progresses the small crystals grow towards larger crystal lengths as we can see that a small peak moves and grows larger. After some time, when the crystals grow, the attrition process becomes significant and large crystals break and change the shape of the distribution. Further, as time passes, the peak of the larger crystals decreases continuously as a result of attrition and classified product removal. Again supersaturation increases, and the small crystals
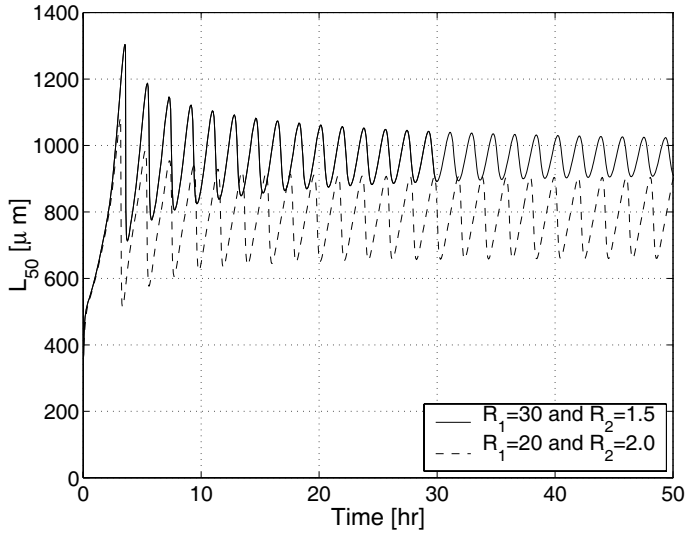
Figure 4.21: L_{50} for particular operating parameters of the $(NH_4)_2SO_4$ - H_2O system within the instability region predicted by model 2 for $\tau = 75$ min.

start growing. The period of these oscillations is 8000 s. Compared to the period of the oscillations that is obtained with model 2, the time period of oscillations for model 1 is smaller. The physical reason behind this is that the growth rate for model 1 is higher and crystals reach the product cut size faster than the crystals in model 2. Furthermore, attrition in model 2 has a large influence on the evolution of the mass density function in Fig.4.23.
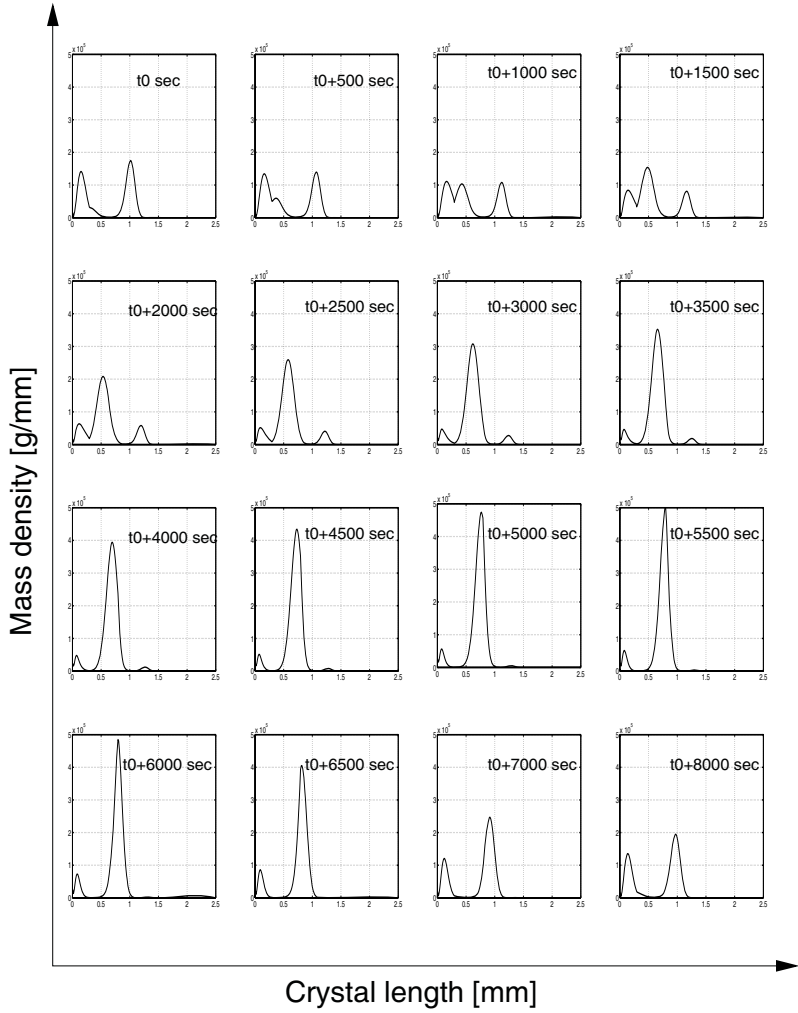
Figure 4.22: Periodic behavior of the mass density distribution of the $(NH_4)_2SO_4$ - H_2O system for model 1 for $R_1 = 20$, $R_2 = 4$, $L_p = 800\ \mu$m, $L_f = 300\ \mu$m and $\tau = 75$ min.
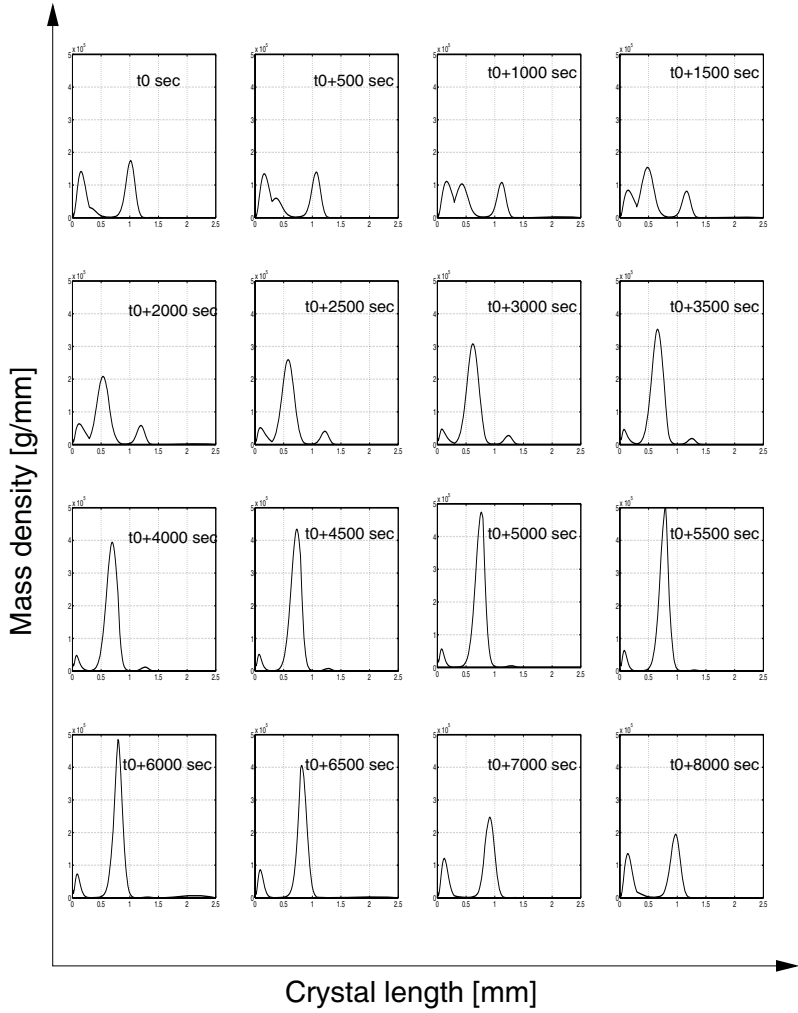
Figure 4.23: Periodic behavior of the mass density distribution of the $(NH_4)_2SO_4$ - H_2O system for model 2 for $R_1 = 20$, $R_2 = 4$, $L_p = 800 \ \mu$m, $L_f = 300 \ \mu$m and $\tau = 75$ min.
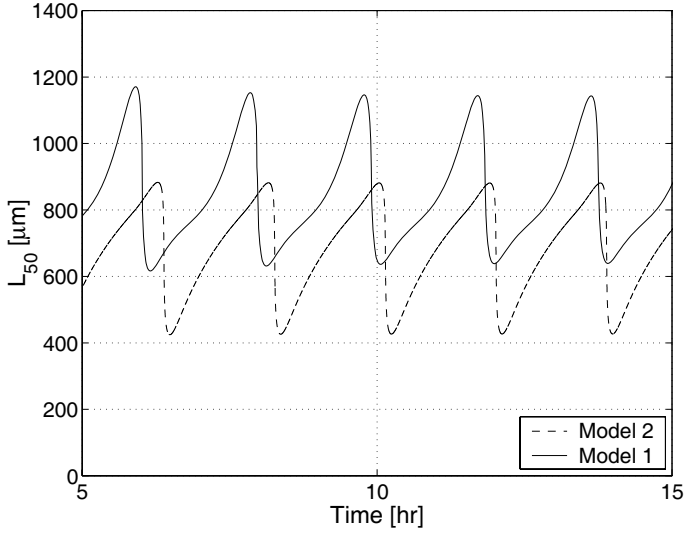
Figure 4.24: Comparison of L_{50} for particular operating parameters of the $(NH_4)_2SO_4$ - H_2O system for model 1 and model 2, for $R_1 = 20$, $R_2 = 4$, $L_p = 800$ μm, $L_f = 300$ μm and $\tau = 75$ min.

Moreover, the two models are compared with their mass median crystal length L_{50}. For parameter combination of $R_1 = 20$ and $R_2 = 4$, the L_{50} progression with time for model 1 and 2 is depicted in Fig. 4.24. The other operating parameters are $L_p = 800$, μm $L_f = 300$ μm and $\tau = 75$ min respectively. The Fig. 4.24 reveals the following things. Firstly, the L_{50} for model 1 (represented by solid line) is greater than model 2 (represented by dashed line). The reason is due to the growth rate of model 1 greater than model 2. In addition, the attrition is prevalent in model 2. Secondly, the time period of oscillation for mode1 1 is smaller than model 2. This is again due to faster growth rate of crystals for model 1 as was already discussed above.

4.3.2 Comparison between Model 1 and Model 3
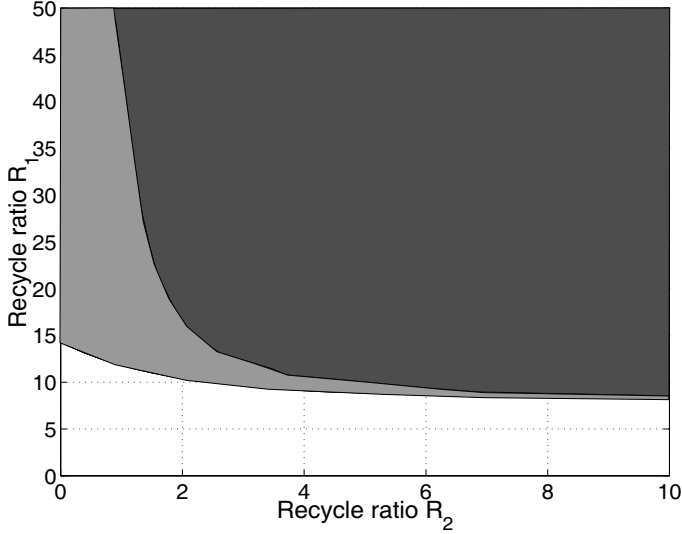
Figure 4.25: Comparison of two parameter plots of the $(NH_4)_2SO_4$ - H_2O system for model 1, and model 3 for $\tau = 75$ min.

Finally, in this section the influence of non-ideal fines classification as proposed in [57] is discussed. As explained in Chapter 2, it has been reported that in a specific DTB crystallizer there is a considerable temperature difference between the reflux stream of the fines entering the crystallizer and the crystallizer. As a result there is a possibility of large crystals in the settling zone getting dissolved. In other words, this is so a kind of classification. For convenience, we will call it non-ideal classification, and the classification function is given by equation (2.47). It is assumed that large crystals greater than $L_{fd} = 900 \; \mu$m are dissolved at rate $R_1 k_{fd}$. The instability region in the R_1, R_2 plane is determined for model 3 and compared that for model 1. The dark gray region in Fig. 4.25 represents the instability region for model 1 with ideal fines classification. The light gray region, which is overlapped by the dark gray region, represents the instability region for model 3 with non-ideal fines classification. From Fig. 4.25, we conclude, that non-ideal fines classification has a significant influence on the size and location of the instability region.

Without product classification at $R_2 = 0$, model 3 is getting unstable at $R_1 = 14$, whereas model 1 is getting unstable at $R_1 = 73$.

4.4   Summary and Conclusions

In this chapter the results of numerical bifurcation analysis of continuous crystallization processes were presented. Focus was on self-sustained oscillations, which may limit the product quality in practice significantly. It is shown that crystallizer stability critically depends on operating conditions and the physical parameters of the system considered. Compared to previous studies, special emphasis was on the influence of fines dissolution and classified product removal. These investigations can lead the way to process stabilization by means of suitable process design and control. Further, new surprising features were found, like the occurrence of two different periodic solution branches.

For the analysis in this work, similar models were used as in the literature [72, 73, 31, 57]. The stability of ammonium sulfate and potassium chloride crystallization with fines dissolution and classified product removal was studied by means of three different models. From the comparison of the different model predictions the following conclusions can be drawn:

- For the $(NH_4)_2SO_4$ - H_20 system the detailed kinetics (model 2) is surprisingly not that important. The model 1 with simple kinetics is able to predict the instability region in the space of adjustable operating parameters. However, the results for the KCl - H_20 system varies. There is a large deviation between predictions of model 1 and model 2. Therefore, it is conjectured that the parameters taken from the literature for the simple model 1 are not adequate to describe the situation considered in this work.

- Moreover, detailed kinetics make a big difference if we look at the mass density distribution (MDD), which is predicted by the different models and which is of major interest in view of product quality.

- From a comparison of two models with simple kinetics and ideal as well as non-ideal fines classification, it is found that non-ideal fines classification has a large impact on the size and location of the instability regions in the space of the adjustable operating parameters. A similar strong influence can be expected for the

product classification function. Hence, for a reasonable prediction of stability, detailed modeling of the product and the fines classification seems to be important. Furthermore, it can be concluded that the stability of crystallization processes can be directly manipulated by manipulating the fines and product classification.

4.5   Preliminary Results of Mandelic Acid/Water System

In this section, stability of a chiral system is investigated, i.e., crystallization of Mandelic acid from aqueous solution. Using model 1, some preliminary results of numerical bifurcation analysis with emphasis on fines dissolution and classified product removal, obtained via the DIVA simulation environment are presented. The physical, chemical and operational parameters of this system are given in Appendix C. It needs to be mentioned that the nucleation rate is not available in the literature. Therefore, as a first step the nucleation rate similar to that of the $(NH_4)_2SO_4$ - H_2O system is considered. The reason for taking the similar nucleation rate is due to the following: The crystal shape for both the systems is similar, i.e. orthorhombic. Therefore, the probability of crystals getting attrited with the stirrer could be the same, even though it also depends on the hardness of the crystal. Moreover, the metastable zone width for the $(NH_4)_2SO_4$ - H_2O is 1.8 K and for Mandelic Acid/Water System is 2.5 K respectively, which is quite close [30, 68].

A bifurcation diagram in R_1/R_2 plane is obtained for a residence time of $\tau = 50$ min using a two parameter continuation method available in DIVA. The classified product size and fines cut size are $L_p = 800\ \mu m$ and $L_f = 300\ \mu m$ respectively. Fig. 4.26 shows the curve of the Hopf points where the system changes from stable to unstable. The system oscillates within the shaded region shown in Fig. 4.26. Furthermore, the figure reveals that as the classified product recycle ratio R_2 is increased, the system tends to oscillate with increasing fines recycle ratio R_1. Surprisingly, this result is different to the systems that had been studied so far, where the system oscillates with increase in classified product removal and decrease of fines reflux ratio. However, to know the true qualitative behavior the system has to be investigated further with accurate nucleation rate.
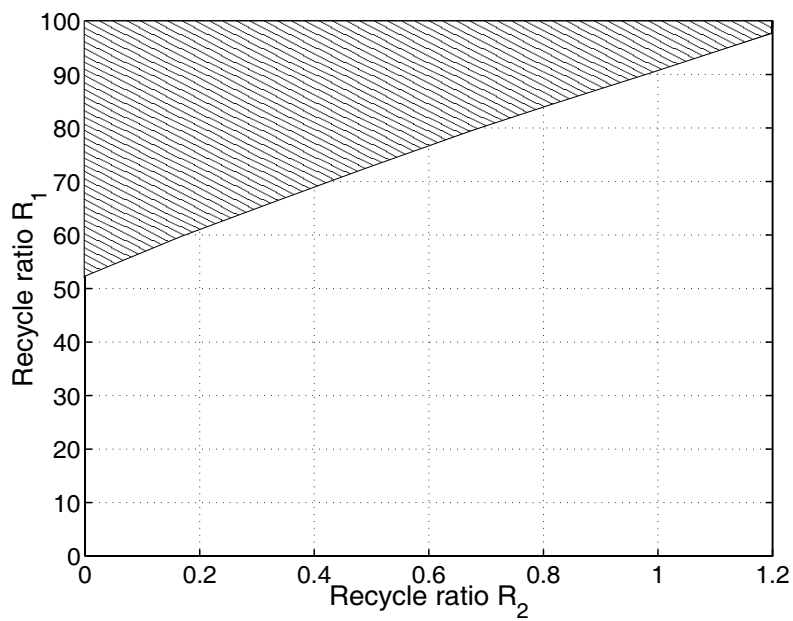
Figure 4.26: Instability region in the R_1/R_2 plane for the Mandelic acid/Water system predicted by model 1 for $\tau = 75$ min

Chapter 5

Summary and Future Work

5.1 Summary

Crystallization processes are one of the oldest unit operations used for separation and purification in chemical industry. However, the design and operation of crystallization processes still pose some problems. It has been reported that in a DTB continuous crystallizer, slow sustained oscillations occur in CSD under some operating conditions. This will result in a poor product quality, and severe production and yield losses. Moreover, it poses problems for further downstream processing of the product. During crystallization two significant kinetic processes, nucleation and growth rate, occur simultaneously. The rate equations of these kinetic processes are non-linear and can lead to self sustained oscillations. Analysis by previous researchers reveals two different explanations for this oscillation behavior, i.e high order cycling and low order cycling. High order cycling is induced due to the non-linearity of the nucleation rate and also at high nucleation exponents. Low order cycling occurs at low nucleation exponents, when the crystallizer is operated with classified product removal and fines dissolution. Fines dissolution is employed to the DTB continuous crystallizer for obtaining high supersaturation which will in turn lead to a coarse product. Classified product removal is the classification of coarse particles from the crystallizer contents. The net result is that a narrower CSD is produced. The goal of this thesis has been to study the influence of different parameters responsible for this instability using advanced numerical bifurcation analysis.

For doing the theoretical analysis a model is necessary to describe the crystallization process. A crystallization process comprises of a dispersed phase and a continuous phase. A

model was derived for a DTB continuous crystallizer in chapter 2 based on first principles. A PBE introduced by Hulburt & Katz [25] was derived for describing the evolution of the CSD in the dispersed phase. A mass balance equation was derived to describe the dynamics of the solute concentration in the continuous phase. Three models were used in this work to study the instability of crystallization processes. (i) A model with simple kinetics (model 1) (ii) a model with complex kinetics involving breakage of crystals due to attrition and ideal fines classification (model 2) and (iii) a model with simple kinetics and non-ideal fines classification (model 3).

In Section 2.4 of chapter 2, an overview pertaining to kinetics of crystallization processes was given. The expressions for the calculation of nucleation rate, growth rate and particular number flux due to attrition of crystals with the stirrer were also given. These kinetic expressions were incorporated into the population balance model to describe the crystallization process.

A description of the 20 litre DTB continuous crystallizer and necessary equipment which was used for determining the kinetic parameters for the size dependent growth rate of the KCl crystals in the KCl-H_2O system is given in Chapter 3. Experimental results were presented for different operating conditions and were compared with the results obtained from the numerical simulation using model 2. It was shown that the deviation of the simulations results with respect to experimental results was less than 10%.

For studying the instabilities in the crystallization process, two well known chemical systems i.e. KCl - H_2O and $(NH_4)_2SO_4$ - H_2O were considered. In Chapter 4, the non-linear behavior of the crystallization process was investigated with models derived in Chapter 2. As a first step a fairly simple model, i.e. model 1, was considered for the study. By means of numerical bifurcation analysis, regions in the parameter space of operating conditions and physical properties with periodic behavior were predicted by taking the KCl - H_2O system as a base case. First, the influence of the nucleation exponent, i.e. low order cycling for vanishing fines dissolution and classified product removal recycle ratios R_1 and R_2 was investigated. It was shown that the system is stable for low and high nucleation exponents and between $12 - 16$ nucleation exponents the system is unstable. Next, the instability region was predicted in fines dissolution recycle ratio R_1/ nucleation exponent b parameter plane. Further, it was shown that there is a strong influence on this instability region by the other operating parameters like residence time τ and recycle ratio of classified product removal R_2.

Finally, the influence of fines dissolution recycle ratio R_1 and classified product removal

R_2 on the stability of the two chemical systems, i.e. KCl-H_2O and $(NH_4)_2SO_4$-H_2O were investigated. However, it should be noted that the stability is also influenced by fines and classified product cut size. The predictions of the simple model were then compared with predictions of model 2 consisting of detailed kinetics. In the case of stability analysis for $(NH_4)_2SO_4$-H_2O system, it was shown that detailed kinetics are not important. On the contrary, it was shown that for the KCl-H_2O system detailed kinetics are important. It is conjectured that the parameters taken from the literature for the simple model 1 are not adequate to describe the situation considered in this work. Moreover, there is a quantitative difference between the model predictions in terms of MDD and mass median crystal size L_{50}. Finally, the influence of non-ideal classification induced due to a considerable temperature difference between fines dissolution reflux stream and the crystallizer on the stability of the system was investigated. It was shown that the system tends to oscillate at a fairly low recycle ratio R_1 as compared to a system with ideal fines classification.

5.2 Future Work

The ultimate aim is true *quantitative* prediction of the nonlinear dynamic behavior of crystallization processes. Therefore, the theoretical results that were presented so far have to be experimentally investigated. For this the pilot plant crystallizer (see Chapter 3) that was used to estimate the growth rate parameters have to be extended with a fines dissolution and classified product removal.This can be done in the following way.

5.2.1 Fines Dissolution

The pilot plant crystallizer can be extended with fines dissolver and product classifier in the following way. With respect to the DTB crystallizer depicted in Fig. 2.1, it was shown that fines are collected in the settling zone. This settling zone is quiet zone and is in the outer shell of the crystallizer. From the settling zone the fines along with solution is sucked by means of a pump to the heat exchanger for dissolution. In the heat exchanger undersaturated conditions are created so that fines get dissolved. The dissolved solution is then sent back to the crystallizer.

A similar kind of strategy can also be applied to the pilot plant crystallizer with certain limitations. With the pilot plant crystallizer it is difficult to have separate settling zone in
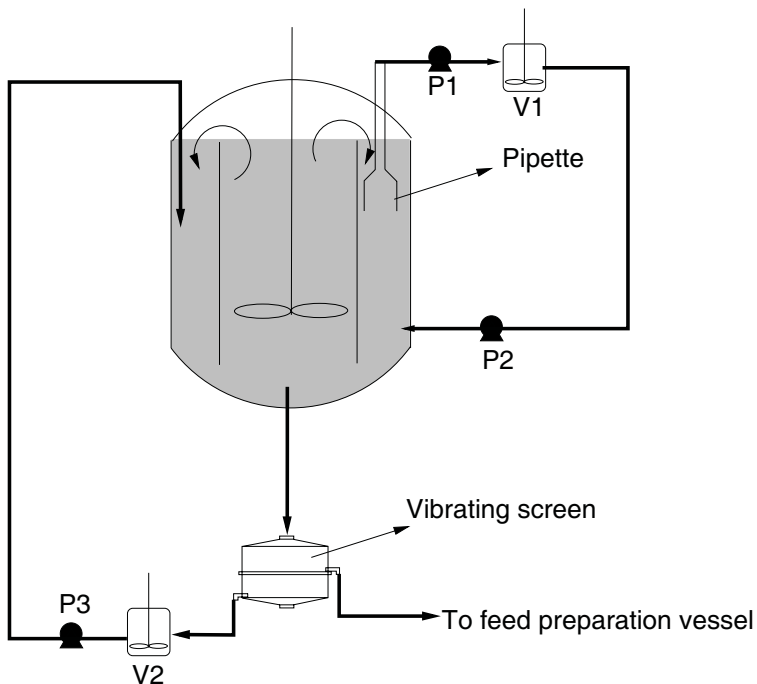
Figure 5.1: Simplified diagram of continuous crystallizer with fines dissolution and classified product removal.

the outer shell like the one depicted in Fig. 2.1. The settling zone can be created with pipette that is shown in the Fig. 5.1. As depicted in the figure, the pipette has a cylindrical type of opening at the bottom. The diameter of this opening is considerably greater than the diameter of the pipette pipe. By placing this pipette from the top inside the crystallizer, the fines are collected in the cylindrical opening. The slurry is then sucked by a vacuum pump P1 from the pipette. For fines dissolution, this is sent to a small double walled jacketed stirred tank V1. In the stirred tank undersaturated conditions have to be created for fines dissolution. This can be done by heating the stirred tank with hot water. Based on fines removal rate, pipettes with different diameter can be used. The fines size depends on fines removal rate. The heat supplied to the stirred tank also depends on fines removal rate. The solution can then feed back to the crystallizer by the pump P2.

5.2.2 Classified Product Removal

For classified product removal, different type of classifiers can be used. They are hydrocyclone, hydraulic classifier and vibrating screen. Based on the experimental investigations done by Gerla [20], the vibrating screen offers better separation efficiency than others. Therefore, it is recommended to employ a vibrating screen for the existing pilot plant crystallizer. Moreover, the option of classified product size can be changed by changing the screen size. The product classification can be done in the following way. The flow from bottom of the crystallizer is fed to the vibrating screen (see Fig. 5.1). The vibrating screen splits the flow into two. One is called product flow and other is recycle flow. The product flow consists of mostly coarse crystals and less amount of liquid. Whereas, the recycle flow consists of more liquid and small particles. The recycle flow is sent to a small recycle vessel V2. In the recycle vessel stirring tanks place to avoid any segregation of crystals. The slurry from the recycle vessel is then send back to the crystallizer by means of the pump P3. The product flow from the vibrating screen is sent back to the feed preparation vessel.

As a long term objective the control strategy proposed by Vollmer & Raisch [85] have to be experimentally investigated. The control is for stabilization of continuous crystallizer showing sustained oscillations for high fines removal rate. The feedback controller is designed using H_∞ theory. The measured variable for this controller is the overall crystal mass inside the crystallizer and manipulated variable is the fines removal rate.

Finally, it has been reported in literature that other particulate processes like polymerization [48], fermentation [93] and granulation [24] exhibit a similar type of oscillations. Therefore, a similar kind of approach in this thesis can be done in understanding the cyclic behavior of these processes.

Appendix A

Numerical Methods

A.1   Discretization Techniques

In this section, the numerical solution of the derived mathematical models will be addressed. Except for special cases, the population balance models cannot be solved analytically. Therefore, they have to be solved numerically. The given population balance is an Integro-partial differential equation (IPDE). For a numerical solution, the given population balance model has to be semi-discretized to a set of DAEs (Differential algebraic equations) along the property coordinate. For example, in this case the property coordinate is the characteristic crystal length L.

Many discretization schemes are published in literature [9, 4, 63, 59, 39, 40, 41]. However, these schemes are addressed specifically to the particular type of the problem. For example, Bennett & Rohani [4] discuss solving the population balance model for evaporative cooling crystallizers with a combined Lax-Wendroff/Crank-Nicholson method. The work shows that under normal growth conditions, the Lax-Wendroff and Crank-Nicholson methods, if applied separately, produces identical CSD for crystallizers with no fines dissolution. On the contrary, these methods become numerically unstable and shows oscillatory behavior when confronted with sharp changes in CSD i.e. with introduction of fines dissolution. For that a combined Lax-Wendroff/Crank-Nicholson method was proposed for stable, smooth and non-oscillatory dynamic results. However, this method had been tested for certain set of operating conditions and has to be tested for some more. Similarly, according to Motz et al. [59] other discretization methods from literature are not be considered in this work, since they to tend to oscillate or even show negative values of the

number density function F.

The discretization scheme used in this work is fairly simple and will not produce high accuracy results. This, however is not the objective of this work, since emphasis is rather on qualitative than on quantitative behavior. Using a method of lines discretization (MOL) [91] with a finite volume scheme, the population balance (2.12), (2.32) is converted to a set of ODEs (ordinary differential equations) (see Fig. A.1).
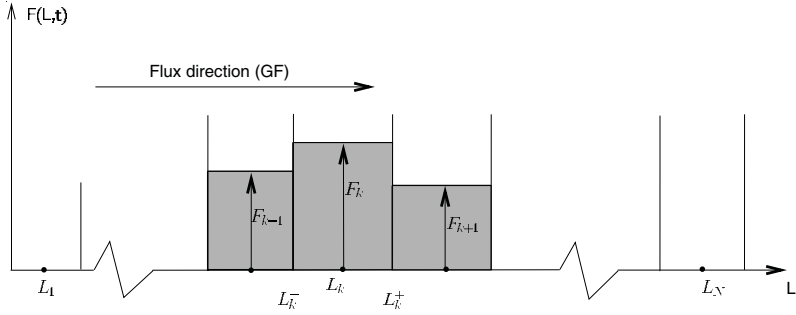
Figure A.1: Subdivision of the crystal length coordinate L into finite volumes taken from Motz et al. [59]

For model 2 a standard finite volume scheme [67, 59] with a piece-wise constant profile is used. An overview of the scheme is discussed in brief in the following. A general population balance equation is given by

$$\frac{\partial F(L,t)}{\partial t} + \frac{\partial GF(L,t)}{\partial L} = \sigma(F(L,t)) \tag{A.1}$$

In this equation (A.1), $GF(L,t)$ represents the flux in the direction of the internal coordinate L and $\sigma(F(L,t))$ represents sink and source terms due to population activity.

To derive the discretization equations, the domain of interest, i.e. crystal length L, is subdivided into N control volumes. For each control volume, a discretized number density function is derived. We focus our attention on the kth control volume, which has $k+1$ and $k-1$ as its neighbors. The lines at L_k^+ and L_k^- represent the faces of the kth control volume. The width of the volume is given by $\Delta L_k = L_k^+ - L_k^-$ for $k = 1, \cdots, N$.

The discretization point L_k is chosen in such a way that it is in the middle of the control volume and the value at the discretization point represents the value of the whole k^{th}

control volume except at $F(L_k^-, t)$ and $F(L_k^+, t)$. Therefore, the given PDE is integrated over each control volume

$$\int_{L_k^-}^{L_k^+} \frac{\partial F(L, t)}{\partial t} dL + \int_{L_k^-}^{L_k^+} \frac{\partial GF(L, t)}{\partial L} dL = \int_{L_k^-}^{L_k^+} \sigma(F(L, t)) dL \qquad \text{(A.2)}$$

As depicted in Fig. A.1, assuming that $F_k(L)$ is valid over the entire k^{th} volume, the equation reduces to

$$\frac{dF_k(t)}{dt} \Delta L_k + [(GF)_{L_k^+} - (GF)_{L_k^-}] = \sigma(F_k(t)) \Delta L_k \qquad \text{(A.3)}$$

For the calculation of the values of (GF) at the control volume boundaries, a piece-wise constant profile is assumed. For obtaining a numerically stable scheme, the values of GF have to be determined at each boundary volume. Depending on the flux direction the values of (GF) at the boundaries change. For a positive flux direction, i.e. growth of crystals, the value of (GF) at the kth control volume becomes

$$GF|_{L_k^+} = GF|_{L_k} \qquad \text{(A.4)}$$

For a negative flux direction, i.e. dissolution of crystals, the value of (GF) at the kth control volume becomes

$$GF|_{L_k^-} = GF|_{L_k} \qquad \text{(A.5)}$$

All integration terms are discretized according to the Riemann integration scheme, by using piece wise constant profile assumptions.

Because of the poor convergence of standard finite volume schemes with piece-wise constant profile, a higher order approximation is used for the calculation of the flux (GF) at the boundaries of control volumes for model 2. This higher order approximation was proposed by Vreugdenhil & Koren [88] and the method is called Robust upwind discretization method or finite volume with flux limiter. This method, in contrast to other schemes, is numerically stable, accurate and requires less discretization points.

With this method, the flux (GF) at the boundaries of the control volumes is calculated using a limiter function λ. For example, for a positive flux direction, the value of flux $GF|_{L_k^+}$ that is leaving the kth control volume (see Fig. A.1) is given by

$$GF|_{L_k^+} = GF|_{L_k} + \lambda(r_k^+)[GF|_{L_k} - GF|_{L_{k-1}}] \qquad \text{(A.6)}$$

In equation (A.6) the limiter function $\lambda(r_k^+)$ is dependent on the local upwind ratio r_k, which is the ratio of two consecutive gradients.

$$r_k^+ = \frac{GF|_{L_{k+1}} - GF|_{L_k} + \epsilon}{GF|_{L_k} - GF|_{L_{k-1}} + \epsilon} \qquad (A.7)$$

A division by zero is prevented by introducing a small number $\epsilon = 10^{-10}$. The limiter function is defined as

$$\lambda(r) = max(0, min(2r, min(\frac{1}{3} + \frac{2}{3}r, 2))) \qquad (A.8)$$

For a negative flux direction, the limiter argument is the upwind ratio of two preceding gradients and the scheme has to be reversed to handle the negative flux. The discretized IPDE is numerically solved using the simulation environment MATLAB [82].

A finite difference method with nonequidistant grid is used for model 1. Nonequidistant grid provides more grid points at smaller crystal lengths where a higher resolution of the solution is required. After discretizing the IPDEs, they are solved numerically using the DIVA simulation environment. A fixed grid is used in contrast to an adaptive grid to avoid any influence of the grid adaption on the stability of the solution.

A nonequidistant but fixed grid is used according to

$$L_i = L_{max} \left(\frac{i}{N} \right)^3, \qquad i = 0(1)N \qquad (A.9)$$

with maximum length of crystals L_{max} and a total number of grid points N. A suitable choice of L_{max} as well as a suitable choice for N will be discussed below. The solution of the obtained ODEs can be calculated using a standard ODE solver.

For the numerical solution of model 2 an equidistant grid is used. Owing to attrition of crystals in model 2 the length of the crystals is confined to a smaller domain and hence an equidistant grid can be used instead of the nonequidistant grid used in model 1 to obtain solutions with similar accuracy.

It is worth noting, that for $R_1, R_2 = 0$ the population balance model for model 1 can be converted to a set of ordinary differential equations by means of the method of moments

[1] [73]. This allows us to determine the numerical error, which was introduced by the discretization discussed above and select suitable values for the maximum crystal length L_{max} and the number of grid points N. If L_{max} is too small, a part of the crystal population is cut off. This acts like a classified product removal on the crystal population and may produce spurious instabilities [49]. Therefore, a rather large value of L_{max} of 60 mm is used here. For the selection of an appropriate number of grid points we focus on the Hopf points H_1 and H_2 in Fig. 4.1.

With the moments equations we find

$$b_{H_1} = 11.9033, \qquad b_{H_2} = 16.1052. \tag{A.11}$$

For the nonequidistant grid with 200 grid points we find

$$b_{H_1} = 12.2708, \qquad b_{H_2} = 15.8583 \tag{A.12}$$

and with 400 grid points we find

$$b_{H_1} = 12.0870, \qquad b_{H_2} = 15.9906. \tag{A.13}$$

The latter are slightly better. Consequently, in the intervals $\{11.9033, 12.2708\}$ and $\{15.8583, 16.1052\}$ the 'exact' solution of the moments equations will oscillate, whereas the approximate solution with 200 grid points will not oscillate. This is a similar effect as described in Motz et al. [59]. However, since we are mainly interested in the qualitative behavior and not so much in the exact location of the stability boundaries, a total number of 200 grid points is a good compromise between accuracy and efficiency and will be used throughout the work. It should be noted that with an equidistant grid much more grid points would be needed to get a similar resolution at small crystal lengths, which is also crucial for the accuracy of the solution.

---

[1]In context with population balance modeling, the so called moments of the size distribution μ_n is given by

$$\mu_n = \int_{L_0}^{L_\infty} F L^n dL \tag{A.10}$$

The moments μ_0, μ_1, μ_2, and μ_3 are respectively proportional to the total crystal suspension population, length, area, and mass.

Appendix B

Physical Properties

In this chapter, the physical properties of the Potassium Chloride-water system and the Ammonium Sulfate-water system are given. The data were taken from the following references [17, 18, 51, 6].

Description	Symbol	Value	Unit
General physical constants			
Ideal gas constant	R	8.314	$\frac{\text{J}}{\text{mol K}}$
Boltzmann's constant	k_B	$1.38 \cdot 10^{-23}$	$\frac{\text{J}}{\text{K}}$
Avagadro's number	N_A	$6.022 \cdot 10^{23}$	$\frac{1}{\text{mol}}$
Mechanical properties of Potassium Chloride crystals [14]			
Shear modulus	μ_{shear}	$9.44 \cdot 10^9$	$\frac{\text{N}}{\text{m}^2}$
Fraction resistance	$\frac{\Gamma}{K_r}$	2.16	$\frac{\text{J}}{\text{m}^2}$
Vickers hardness	H_V	$9.7 \cdot 10^7$	$\frac{\text{N}}{\text{m}^2}$
Physical properties of Potassium Chloride crystals [77], [8]			
Density of solute	ρ_A	1989	$\frac{\text{kg}}{\text{m}^3}$
Density of solvent	ρ_B	987	$\frac{\text{kg}}{\text{m}^3}$
Molecular weight of solute	M_A	$74.5 \cdot 10^{-3}$	$\frac{\text{kg}}{\text{mol}}$
Molecular weight of solvent	M_B	$18.015 \cdot 10^{-3}$	$\frac{\text{kg}}{\text{mol}}$
Volume shape factor	k_V	0.487	[-]
Dynamic viscosity	η_L	$0.737 \cdot 10^{-3}$	$\frac{\text{Ns}}{\text{m}^2}$

Description	Symbol	Value	Unit
Diffusion coefficient	D_{AB}	$0.83 \cdot 10^{-9}$	$\frac{m^2}{s}$
Physical properties related to crystal growth and nucleation [77]			
Molecule diameter	d_m	$3.962 \cdot 10^{-10}$	m
Heterogeneous nucleation factor	f_{het}	0.02	[-]
Integration reaction coefficient	k_r	$1.2 \cdot 10^{-5}$	$\frac{m^4}{mol\ s}$
Surface related energy	Γ_S	$4.0 \cdot 10^{-4}$	$\frac{J\ m}{mol}$

Table B.1: Physical properties of Potassium Chloride crystals

Description	Symbol	Value	Unit
Mechanical properties of Ammonium Sulfate crystals [14]			
Shear modulus	μ_{shear}	$8.90 \cdot 10^9$	$\frac{N}{m^2}$
Fraction resistance	$\frac{\Gamma}{K_r}$	2.8	$\frac{J}{m^2}$
Vickers hardness	H_V	$3.55 \cdot 10^8$	$\frac{N}{m^2}$
Physical properties of Ammonium Sulfate crystals			
Density of solute	ρ_A	1769	$\frac{kg}{m^3}$
Density of solvent	ρ_B	987	$\frac{kg}{m^3}$
Molecular weight of solute	M_A	$132.1 \cdot 10^{-3}$	$\frac{kg}{mol}$
Molecular weight of solvent	M_B	$18.015 \cdot 10^{-3}$	$\frac{kg}{mol}$
Volume shape factor	k_V	0.524	[-]
Dynamic viscosity	η_L	$2.1 \cdot 10^{-3}$	$\frac{Ns}{m^2}$
Diffusion coefficient	D_{AB}	$0.83 \cdot 10^{-9}$	$\frac{m^2}{s}$
Physical properties related to crystal growth and nucleation[77], [6]			
Molecule diameter	d_m	$6.0 \cdot 10^{-10}$	m
Heterogeneous nucleation factor	f_{het}	0.02	[-]
Integration reaction coefficient	k_r	$1.0 \cdot 10^{-5}$	$\frac{m^4}{mol\ s}$
Surface related energy	Γ_S	$1.22 \cdot 10^{-4}$	$\frac{J\ m}{mol}$

Table B.2: Physical properties of Ammonium Sulfate crystals

Appendix C

Operation and Simulation Conditions

Three models are used of continuous crystallizers in this work. The operational setup and simulation conditions for three chemical systems, i.e. Potassium chloride-water, Ammonium sulfate-water and Mandelic acid-water are complied in this chapter. These data are taken from different publications and simulations are performed with the different models based on these data. It should be noted that all the continuous crystallizers that are considered here, are initially started with a saturated liquid. Therefore, the initial condition for the continuous liquid phase for model 1, model 3 and model 2 is

$$c_0 = c_{sat} \qquad \& \qquad x_{L,A,0} = x_{L,A,sat} \tag{C.1}$$

Description	Symbol	Value	Unit
Growth rate constant	k_g	$3.0513 \cdot 10^{-2}$	$\frac{mm\ l}{min\ mol}$
Nucleation rate constant	k_b [a]	$8.357 \cdot 10^9$	$\frac{l^3}{min\ mol^4}$
Growth rate exponent	g	1	-
Nucleation rate exponent	b	4	-
Feed concentration	c_{feed}	4.4	$\frac{mol}{l}$
Saturation concentration	c_{sat}	4.0	$\frac{mol}{l}$
Volumetric shape factor	k_v	0.1112	-

Table C.1: Operating conditions and parameters of the KCl - H_2O for model 1

[a] please note that $k_b m_t$ in equation (2.50) is taken as k_b

Description	Symbol	Value	Unit
Total slurry volume	V	22.4E-03	m^3
Mole fraction of solute in feed	$x_{L,A,feed}$	8.69e-02	-
Mole fraction of solute in saturated liquid	$x_{L,A,sat}$	7.63e-02	-
Temperature inside the crystallizer	T	293.15	K
Pumping capacity	N_{pump}	0.3	-
Number of blades	a_{st}	3	-
Angle of blades	β_{st}	30	$^\circ$
Edge of the impeller	b_{edge}	0.002	m
Breadth of the impeller	b_{blade}	0.028	m
Impeller diameter	d_{st}	0.180	m
Draft tube diameter	d_{dt}	0.190	m
Impeller rotation speed	ω_{st}	400.0	$\frac{1}{min}$
Mean specific power input	ϵ	1.8	$\frac{W}{kg}$

Table C.2: Operating conditions and parameters of the KCl - H_2O for model 2

Description	Symbol	Value	Unit
Growth rate constant	k_g	$2.0 \cdot 10^{-5}$	$\frac{m}{s}$
Nucleation rate constant	k_b [a]	$5.12 \cdot 10^9$	$\frac{1}{kg\,s}$
Growth rate exponent	g	1	-
Nucleation rate exponent	b	2	-
Large crystal dissolution factor	k_{fd}	0.1	[-]
Feed concentration	w_{feed}	0.545	$\frac{kg}{kg}$
Saturation concentration	w_{sat}	0.5000	$\frac{kg}{kg}$
Density of solution	ρ_L	1252	$\frac{kg}{m^3}$
Volumetric shape factor	k_v	0.5238	-

Table C.3: Operating conditions and parameters of the $(NH_4)_2SO_4$ - H_2O for model 1

[a]The constant k_b and k_g are based on weight fraction of solute and therefore equation (2.32) becomes

$$\rho_L \frac{dc}{dt} = \frac{q(\rho_S - \rho_L w)}{V} + \frac{\rho_S - \rho_L w}{\epsilon} \frac{d\epsilon}{dt} + \frac{q\rho_L w_{feed}}{V\epsilon} - \frac{q\rho_S}{V\epsilon}(1 + k_v n_{LS}) \qquad (C.2)$$

Description	Symbol	Value	Unit
Total volume	V	1100 E-03	m^3
Mole fraction of solute in feed	$x_{L,A,feed}$	1.33E-01	–
Mole fraction of solute in saturated liquid	$x_{L,A,sat}$	1.02E-01	–
Temperature inside the crystallizer	T	323.15	K
Pumping capacity	N_{pump}	0.32	-
Number of blades	a_{st}	3	-
Angle of blades	β_{st}	25	$^\circ$
Edge of the impeller	b_{edge}	0.006	m
Breadth of the impeller	b_{blade}	0.18	m
Impeller diameter	d_{st}	0.485	m
Draft tube diameter	d_{dt}	0.5	m
Impeller rotation speed	ω_{st}	370.0	$\frac{1}{min}$
Mean specific power input	ϵ	2.3	$\frac{W}{kg}$

Table C.4: Operating conditions and parameters of the $(NH_4)_2SO_4$ - H_2O for model 2

Description	Symbol	Value	Unit
Growth rate constant	k_g	$9.0 \cdot 10^{-5}$	$\frac{m}{s}$
Nucleation rate constant	k_b	$5.12 \cdot 10^9$	$\frac{1}{kg\ s}$
Growth rate exponent	g	2.3	-
Nucleation rate exponent	b	2	-
Feed concentration	w_{feed}	0.2	$\frac{kg}{kg}$
Saturation concentration	w_{sat}	0.16	$\frac{kg}{kg}$
Density of solution	ρ_L	1037	$\frac{kg}{m^3}$
Density of crystals	ρ_S	1300	$\frac{kg}{m^3}$
Volumetric shape factor	k_v	0.43	-

Table C.5: Operating conditions and parameters of the $C_8H_8O_3$ - H_2O system for model 1 [46]

Bibliography

[1] Alopaeus, V., Koskinen, J., & Keskinen, K. I. (1999). Simulation of the population balances for liquid - liquid systems in a non ideal stirred tank. Part 1: Description and qualitative validation of the model. *Chemical Engineering Science*, **54**, 5887–5899.

[2] Barrett, P. & Glennon, B. (1999). In-line FBRM monitoring of particle size in dilute agitated suspensions. *Part. Part. Syst. Charact*, **16**, 207–211.

[3] Beer, W. F. & Mersmann, A. B. (1982). The influence of power input and suspension density on the crystallization kinetics of KCl in a continuous draft tube crystallizer. In *Proceedings of International Symposium on Industrial Crystallization 81*, Netherlands. North-Holland Publishing Company.

[4] Bennett, M. K. & Rohani, S. (2001). Solution of population balance equations with a new combined Lax-Wendroff/Crank-Nicholson method. *Chemical Engineering Science*, **56**, 6623–6633.

[5] Bequette, B. W. (1998). *Process Dynamics: Modeling, Analysis, and Simulation*. Prentice Hall, New Jersey.

[6] Bermingham, S. K., Neumann, A. M., Verheijen, P. J. T., & Kramer, H. J. M. (1999). Measuring and modeling the classification and dissolution of fine crystals in a DTB crystallizer. In *Proceedings 14th International Symposium on Industrial Crystallization*, Warwickshire, CV21, 3HQ, U. K. IChemE.

[7] Bermingham, S. K., Neumann, A. M., Verheijen, P. J. T., & Kramer, H. J. M. (2001). A predictive model framework for design purposes data quality (required) for parameter estimation. In *Proceedings 8th International Workshop on Industrial Crystallization*, pages 118–125. BIWIC.

[8] Broul, M., Sohnel, O., & Nyvlt, J. (1981). *Solubility in inorganic two-component systems*. Elsevier Scientific Publishing Company, Amsterdam Wiesbaden.

[9] Campos, F. B. & Lage, P. L. C. (2003). A numerical method for solving the transient multidimensional population balance equation using an Euler-Lagrange formulation. *Chemical Engineering Science*, **58**, 2725–2744.

[10] CILAS US, Inc (2000). Technical Manual. Madison. WI, USA.

[11] Dirksen, J. A. & Ring, T. A. (1991). Fundamentals of crystallization : Kinetic effects on particle size distribution and morphology. *Chemical Engineering Science*, **46**, 2389–2427.

[12] EEK, R. A. (1995). *Control and Dynamic Modelling of Industrial Suspension Crystallizers*. Ph. D. Thesis, T. U. Delft, Netherlands.

[13] Fakatselis, T. E. (1999). A review of crystallization theory applied to the draft tube baffle crystallizer. In *Proceedings* 14th *International Symposium on Industrial Crystallization*, Warwickshire, CV21, 3HQ, U. K. IChemE.

[14] Gahn, C. (1997). *Die Festigkeit von Kristallen und ihr Einfluss auf die Kinetik in Suspensionskristallisatoren*. Ph. D. Thesis, Lehrstuhl B für Verfahrenstechnik, T. U. München, Germany.

[15] Gahn, C. & Mersmann, A. (1995). The brittleness of substances crystallized in industrial processes. *Powder Technology*, **85**, 71–81.

[16] Gahn, C. & Mersmann, A. (1997). Theoretical prediction and experimental determination of attrition rates. *Trans IChemE*, **75**, 125–131.

[17] Gahn, C. & Mersmann, A. (1999a). Brittle fracture in crystallization processes. Part A: Attrition and abrasion of brittle solids. *Chemical Engineering Science*, **54**, 1273–1282.

[18] Gahn, C. & Mersmann, A. (1999b). Brittle fracture in crystallization processes. Part B: Growth of fragments and scale-up of suspension crystallizers. *Chemical Engineering Science*, **54**, 1283–1292.

[19] Gahn, C., Krey, J., & Mersmann, A. (1996). The effect of impact energy and the shape of crystals on their attrition rate. *Journal of Crystal Growth*, **166**, 1058–1063.

[20] Gerla, J. H. (1995). *Modeling, Measurement and Manipulation of Crystallizers*. Ph. D. Thesis, T. U. Delft, Netherlands.

[21] Gerstlauer, A., Mitrović, A., Motz, S., & Gilles, E. D. (2001). A population model for crystallization processes using two independent particle properties. *Chemical Engineering Science*, **56**, 2553–2565.

[22] Gerstlauer, A., Motz, S., Mitrović, A., & Gilles, E. D. (2002). Development analysis and validation of population models for continuous and batch crystallizers. *Chemical Engineering Science*, **57**, 4311–4327.

[23] Giulietti, M., Guardani, R., Nascimento, C. A. O., & Arntz, B. (2003). In-line monitoring of crystallization process using a laser reflection sensor and a neural network model. *Chemical Engineering Technology*, **26**, 267–272.

[24] Heinrich, S., Peglow, M., Ihlow, M., Henneberg, M., & Mörl, L. (2002). Analysis of the start-up process in continuous fluidized bed spray granulation by population balance modeling. *Chemical Engineering Science*, **57**(20), 4369–4390.

[25] Hulburt, H. M. & Katz, S. (1964). Some problems in particle technology, a statistical mechanical formulation. *Chemical Engineering Science*, **19**, 555–574.

[26] Jerauld, G. R., Vastis, Y., & Doherty, M. F. (1983). Simple conditions for the appearance of sustained oscillations in continuous crystallisers. *Chemical Engineering Science*, **38**(10), 1675–1681.

[27] John Garside, A. M. & Nyvlt, J. (1993). *Measurement of Crystal Growth and Nucleation Rates*. Institution of Chemical Engineers, U. K., second edition.

[28] Juzaszek, P. & Larson, M. A. (1977). Influence of fines dissolving on crystal size distribution in an MSMPR crystallizer. *AIChE J.*, **23**(4), 460–468.

[29] Kienle, A., Lauschke, G., Gehrke, V., & Gilles, E. D. (1995). On the dynamics of the circulation loop reactor- numerical methods and analysis. *Chemical Engineering Science*, **50**(15), 2361–2375.

[30] Kim, K. J. & Mersmann, A. (2001). Estimation of metastable zone width in different nucleation processes. *Chemical Engineering Science*, **56**, 2315–2324.

[31] Kind, M. & Lieb, A. (1999). Simulation study on the effect of classified product removal on the dynamic behavior of continuous crystallizers. In *Proceedings* 14th *International Symposium on Industrial Crystallization*, Warwickshire, CV21, 3HQ, U. K. IChemE.

[32] Kind, M. & Mersmann, A. (1983). Methoden zur Berechnung der homogenen Keimbildung aus wässrigen Lösungen. *Chemical Engineering Technology*, **55**, 720–721.

[33] Kind, M. & Mersmann, A. B. (1990). On supersaturation during mass crystallization from solution. *Chemical Engineering Technology*, **13**, 50–62.

[34] Kind, M. & Nieken, U. (1995). On the dynamic simulation of mass crystallization with fines removal. *Chemical Engineering and Processing*, **34**, 323–328.

[35] Kramer, H. J. M. & Jansens, P. J. (2003). Tools for design and control of industrial crystallizers - state of the art and future needs. *Chemical Engineering Technology*, **26**, 247–255.

[36] Kramer, H. J. M., Bermingham, S. K., & van Rosmalen, G. M. (1999). Design of industrial crystallizers for a given product quality. *Journal of Crystal Growth*, **198/199**, 729–737.

[37] Kröner, A., Holl, P., Marquardt, W., & Gilles, E. D. (1990). An open architecture for dynamic simulation. *Computers and Chemical Engineering*, **14**, 1289–1295.

[38] Kubicek, M. & Marek, M. (1983). *Computational Methods in Bifurcation Theory and Dissipative Structures*. Springer, New York.

[39] Kumar, S. & Ramakrishna, D. (1996a). On the solution of population balance equations by discretization - I. A fixed pivot technique. *Chemical Engineering Science*, **51**, 1311–1332.

[40] Kumar, S. & Ramakrishna, D. (1996b). On the solution of population balance equations by discretization - II. A moving pivot technique. *Chemical Engineering Science*, **51**, 1332–1342.

[41] Kumar, S. & Ramakrishna, D. (1997). On the solution of population balance equations by discretization - III. Nucleation, growth and aggregation of particles. *Chemical Engineering Science*, **52**, 4659–4679.

[42] Lakatos, B. G. (1994). Stability and dynamics of continuous crystallizers. *Computers and Chemical Engineering*, **18**(S), 427–431.

[43] Lakatos, B. G. & Sapundzhiev, T. J. (1993). Bifurcation and dynamic behavior of isothermal CMSMPR crystallizers. *Hungarian Journal of Industrial Chemistry*, **21**, 271–276.

[44] Lei, S.-J., Shinnar, R., & Katz, S. (1971). The stability and dynamic behavior of a continuous crystallizer with fines trap. *AIChE J.*, **17**(6), 1459–1470.

[45] Lieb, A. & Kind, M. (2002). Continuous crystallization of pentaerithritol from aqueous solution in a FC-crystallizer. In *Proceedings 9th International Workshop on Industrial Crystallization*. BIWIC.

[46] Lorenz, H., Sapoundjiev, D., & Morgenstern, A. S. (2002). Enantiomeric mandelic acid system - melting point phase diagram solubility in water. *Journal Chemical Engineering Data*, **47**, 1280–1284.

[47] Mangold, M., Kienle, A., Gilles, E. D., & Mohl, K. D. (1999). Nonlinear computation in DIVA -methods and applications. *Chemical Engineering Science*, **55**, 441–454.

[48] Melo, P. A., Evaristo C. Biscaia, J., José, & Pinto, C. (2003). The bifurcation behavior of continuous free-radical solution loop polymerization reactors. *Chemical Engineering Science*, **58**(13), 2805–2821.

[49] Menges, M. (1993). Modellierung und dynamische Simulation von Populationssystemen. Diploma Thesis, Universität Stuttgart, Germany.

[50] Mersmann, A. (1990). Calculation of interfacial tension. *Journal of Crystal Growth*, **102**, 841–847.

[51] Mersmann, A. (1995a). *Crystallization Handbook*. Marcel Dekker, Inc, New York.

[52] Mersmann, A. (1995b). General prediction of statistically mean growth rates of a crystal collective. *Journal of Crystal Growth*, **147**, 181–193.

[53] Mersmann, A. (1996). Supersaturation and nucleation. *Trans IChemE*, **74**, 812–820.

[54] Mersmann, A. & Bartosch, K. (1998). How to predict metastable zone width. *Journal of Crystal Growth*, **183**, 240–250.

[55] Mersmann, A., Angerhöfer, A., Gutwald, T., Sangl, R., & Wang, S. (1992). General prediction of median crystal sizes. *Seperation Technologies*, **2**, 85–97.

[56] Mersmann, A. B. & Kind, M. (1989). Parameters influencing the mean particle size of a crystalline product. *Chemical Engineering Technology*, **12**, 414–419.

[57] Mitrović, A. (2002). *Population Balance based Modeling, Simulation, Analysis and Control of Crystallization Process*. Ph. D. Thesis, Universität Stuttgart, Germany.

[58] Monnier, O., Klein, J.-P., Hoff, C., & Ratsimba, B. (1996). Particle size determination by laser reflection: Methodology and problems. *Part. Part. Syst. Charact*, **13**, 10–17.

[59] Motz, S., Mitrović, A., & Gilles, E. D. (2002). Comparison of numerical methods for the simulation of dispersed phase systems. *Chemical Engineering Science*, **57**, 4329–4344.

[60] Moyers, C. G. & Randolph, A. D. (1973). Crystal-size distribution and its interaction with crystallizer design. *AIChE J.*, **19**, 1089–1103.

[61] Myerson, A. S. (1990). *Handbook of Industrial Crystallization*. Butterworth-Heinemann, Linacre House, Jordan Hill, Oxford, U. K.

[62] Neumann, A. M., Bermingham, S. K., Kramer, H. J. M., & Rosmalen, G. M. V. (1999). The effect of the impeller speed on the product crystal size distribution (CSD) a 22 liter draft tube (DT) crystallizer. *Journal of Crystal Growth*, **198/199**, 723–728.

[63] Nicmanis, M. & Hounslow, M. J. (1998). Finite-element methods for steady state population balance equations. *AIChE J.*, **44**(10), 2258–2272.

[64] Nielsen, A. E. (1964). *Kinetics of Precipitation*. Pergamon Press, New York.

[65] Nyvlt, J. (1982). *Design of Crystallizers*. CRC Press Inc. Boca Raton, Florida.

[66] Nyvlt, J., Sohnel, O., Matuchova, M., & Broul, M. (1985). *The Kinetics of Industrial Crystallization*. Elsevier, Amsterdam.

[67] Patankar, S. V. (1980). *Numerical Heat Transfer and Fluid Flow*. Hemisphere Publishing Cooporation, Washington DC.

[68] Perlberg, A., Lorenz, H., & Morgenstern, A. S. (2003). Determination of a crystallization kinetics in chiral systems. In *Proceedings 10th International Workshop on Industrial Crystallization*. BIWIC.

[69] Ploss, R. & Mersmann, A. (1989). A new model of the effect of stirring intensity on the rate of secondary nucleation. *Chemical Engineering Technology*, **12**, 137–146.

[70] Ramakrishna, D. & Mahoney, A. W. (2002). Population balance modeling. Promise for the future. *Chemical Engineering Science*, **57**, 595–606.

[71] Ramkrishna, D. (2000). *Population Balances: Theory and Applications to Particulate Systems in Engineering*. Academic Press, New York.

[72] Randolph, A. D. (1980). CSD Dynamics, Stability and Control. *AIChE Symposium Series*.

[73] Randolph, A. D. & Larson, M. A. (1988). *Theory of Particulate Processes*. Academic Press, Inc, San Diego.

[74] Randolph, A. D., Beckman, J. R., & Kraljevich, Z. I. (1977a). Crystal size distribution dynamics in classified crystallizer: Part I. Experimental and theoretical study of cycling in a potassium chloride crystallizer. *AIChE J.*, **23**(4), 500–510.

[75] Randolph, A. D., Beckman, J. R., & Kraljevich, Z. I. (1977b). Crystal size distribution dynamics in classified crystallizer: Part II. Simulated control of crystal size distribution. *AIChE J.*, **23**(4), 510–520.

[76] Ruf, A., Worlitschek, J., & Mazzotti, M. (2000). Modeling and experimental analysis of PSD measurements through FBRM. *Part. Part. Syst. Charact*, **17**, 167–179.

[77] Sangl, R. (1991). *Mechanischer Abrieb von Kristallen als Beitrag zur sekundären Keimbildung*. Ph. D. Thesis, Lehrstuhl B für Verfahrenstechnik, T. U. München, Germany.

[78] Seydel, R. (1994). *Practical Bifurcation and Stability Analysis – From Equilibrium to Chaos*. Springer, New York.

[79] Sherwin, M. B., Shinnar, R., & Katz, S. (1967). Dynamic behavior of the well-mixed isothermal crystallizer. *AIChE J.*, **13**(6), 1141–1154.

[80] Tadayyon, A. & Rohani, S. (1998). Determination of particle size distribution by Par-Tec 100: Modeling and experimental results. *Part. Part. Syst. Charact*, **15**, 127–135.

[81] Takiyama, H. & Matsuoka, M. (2001). Design of seed crystal specifications for start-up operation of a continuous MSMPR crystallizer. *Powder Technology*, **121**, 99–105.

[82] The Math Works, Inc (2000). Using Matlab, Version 6. Natwick. MA, USA.

[83] Ulrich, J. & Strege, C. (2002). Some aspects of the importance of metastable zone width and nucleation in industrial crystallizers. *Journal of Crystal Growth*, **237/239**, 2130–2135.

[84] Verkoeijen, D., Pouw, G. A., Meesters, G. M. H., & Scarlett, B. (2002). Population balances for particulate processes - a volume approach. *Chemical Engineering Science*, **57**, 2287–2303.

[85] Vollmer, U. & Raisch, J. (2001). H_∞ control of continuous crystallizer. *Control Engineering Practice*, **9**(8), 837–845.

[86] Vollmer, U. & Raisch, J. (2002). Population balance modeling and H_∞ controller design for a crystallization process. *Chemical Engineering Science*, **57**(20), 4401–4414.

[87] Volmer, M. (1939). *Kinetik der Phasenbildung*. Ph.D. thesis, Theodor Steinkopff Verlag, Dresden.

[88] Vreugdenhil, C. B. & Koren, B. (1993). *Numerical Fluid Mechanics*, volume 45. Friederich Vieweg and Sohn Verlagsgesellschaft mbH, Braunschweig, Wiesbaden.

[89] Wang, S. & Mersmann, A. (1992). Initial size dependent growth rate dispersion of attrition fragments and secondary nuclei. *Chemical Engineering Science*, **47**, 1365–1371.

[90] Westhoff, G. M., Rijt, J. V. D., Kramer, H. J. M., & Jansens, P. J. (2003). Modeling growth rate dispersion in industrial crystallizers. *Chemical Engineering Technology*, **26**, 286–291.

[91] Wouwer, A. V., Saucez, P., & Schiesser, W. E. (2001). *Adaptive Method of Lines*. CRC Press, Boca Raton, Florida.

[92] Yu, K. M. & Douglas, J. M. (1975). Self-generated oscillations in continuous crystallizers. *AIChE J.*, **21**(5), 917–924.

[93] Zhu, G.-Y., Zamamiri, A., Henson, M. A., & Hjortsϕ, M. A. (2000). Model predictive control of continuous yeast bioreactors using cell population balance models. *Chemical Engineering Science*, **55**(24), 6155–6167.